INVESTIGATION OF DYNAMIC BEHAVIOR OF BACK TO BACK REINFORCED SOIL RETAINING WALLS WITH FINITE ELEMENT AND ARTIFICIAL NEURAL NETWORK

by

Tahir Erdem Öztürk

B.S., Civil Engineering, Boğaziçi University, 2003

M.S., Civil Engineering, Boğaziçi University, 2005

Submitted to the Institute for Graduate Studies in
Science and Engineering in partial fulfillment of
the requirements for the degree of
Doctor of Philosophy

Graduate Program in Civil Engineering

Boğaziçi University

2012

ACKNOWLEDGEMENTS

I owe special thanks to Prof. Dr. Erol Güler for his helpful guidance throughout this thesis.

I have very much benefited from the discussions with Prof. Dr. Derin Ural from Istanbul Technical University and Dr. Uğur Ayan from TUBITAK Marmara Research Center. And also I would wish to thank to Prof. Dr. Sabri Altıntaş and Prof. Dr. Cem Avcı for their valuable suggestions throughout the preparation of this thesis.

I extend my gratitude to Ayşe Aydın for her technical helps for my thesis preparation.

Heartfelt thanks to my friends Abdullah Cengiz, Yusuf Eşidir, Emrah Kılıç, Elif Çiçek and Dilan Ezgi Nalcı due to their motivational support.

I am grateful for the moral support that my family provided during my study. Additionally, the helping hand of an old civil engineer my father Hüzeyfe Öztürk when I needed contributed much to not only my study but also my life.

ABSTRACT

INVESTIGATION OF DYNAMIC BEHAVIOR OF BACK TO BACK REINFORCED SOIL RETAINING WALLS WITH FINITE ELEMENT AND ARTIFICIAL NEURAL NETWORK

Back-to-back Mechanically Stabilized Earth (MSE) wall are commonly used for bridge approach embankments. By the means of not only aesthetically pleasing appearance but also satisfactory performance under seismic loading reinforced soil retaining structures are becoming widely used in Turkey.

In this study, a parametric study of seismic response analysis of reinforced soil retaining structures was performed using a finite element analysis with commercial Finite Element software, Plaxis. The aim of the study is to determine the influence of reinforcement length, reinforcement spacing, wall height and facing type on seismic-induced permanent displacements. Permanent displacements under earthquake loading conditions associated with different L/H ratios and reinforcement spacing for 5 m to 9 m height walls are investigated. In order to investigate dynamic behavior of the walls harmonic motions with 5 seconds duration have been applied. The motion had three different levels of Peak Ground Accelerations, namely 0.2 g, 0.4 g and 0.6 g.

Artificial Neural Network (ANN) conducted in this study was applied for the first time in literature to estimate the deformations of retaining walls under dynamic loads. Although developing an analytical model is feasible in some simplified situations, most manufacturing processes are complex, ANN has been applied successfully in many non-linear geotechnical engineering problems in order to make reliable predictions and to check whether the range of classical design results are within reasonable outcomes.

ÖZET

SONLU ELEMAN VE YAPAY SİNİR AĞI İLE SIRT SIRTA DONATILI İSTİNAT DUVARLARININ DİNAMİK DAVRANIŞALARININ İNCELENMESİ

Sırt sırta donatılı istinat duvarları köprü yaklaşım dolgularında yaygın olarak kullanılır. Sadece estetik görünüşleri değil sismik yükler altındaki başarılı performanslarının da sayesinde donatılı zemin istinat yapıları Türkiye'de yaygın olarak kullanılır hale gelmiştir.

Bu çalışmada donatılı zemin istinad yapılarının sismik tepki analizleri, sonlu elemanlar yöntemi ile hesap yapan Plaxis programı kullanılarak yapılmıştır. Donatı uzunluğu, donatı aralığı, duvar yüksekliği ve yüzey elemanı tipi gibi parametrelerin depremde oluşan kalıcı yer değiştirmelere olan etkilerinin incelenmesi amaçlanmıştır. Farklı L/H oranları ve donatı aralıklarının deprem yüklemesi durumundaki kalıcı yer değiştirmelere olan etkisi, 5 m, 6 m, 7 m, 8 m ve 9 m'lik duvar yükseklikleri için araştırılmıştır. Duvarının dinamik davranışı araştırmak için tepe ivme değerleri sırası ile 0.2 g, 0.4 g ve 0.6 g olan 5 saniyelik üç farklı harmonik hareket uygulanmıştır.

Literatürde ilk kez bu çalışmada Yapay Sinir Ağı, istinat duvarlarının dinamik deformasyon analiz tahmininde kullanılmıştır. Bazı basitleştirilmiş durumlarda bir analitik veya deneysel model geliştirilmesi uygulanabilir olmasına rağmen, birçok üretim süreci karmaşıktır. Yapay Sinir Ağı pek çok doğrusal olmayan Geoteknik Mühendisliği problemlerinde ön kestirimde bulunmak ve klasik analiz sonuçlarının makul aralıkta kalıp kalmadığını kontrol etmek için başarıyla uygulanmıştır.

TABLE OF CONTENTS

LIST OF FIGURES

LIST OF TABLES

LIST OF SYMBOLS

$a(t)$	Ground acceleration with time t (m/s^2)
a_{cs}	Minimum peak connection strength (N/m)
a_u	Minimum peak interface shear strength (N/m)
B_f	Footing width (m)
$B'f$	Equivalent footing width (m)
c	Soil cohesion (N/m^2)
c_f	Foundation soil cohesion (N/m2)) capacity design (dimensionless)
C_{ds}	Coefficient of direct sliding (dimensionless)
C_i	Coefficient of interaction of anchorage (pullout) capacity design (dimensionless)
e	Eccentricity (m)
f_g	Ground motion predominant frequency
f_l	Wall fundamental frequency
F_{dtyni}	Dynamic reinforcement load (component) in reinforcement layer i (N/m)
F_i	Total reinforcement load in reinforcement layer i (N/m)
F_{stai}	Static reinforcement load (component) in reinforcement layer i (N/m)
FS_{bc}	Factor of safety against bearing capacity failure (dimensionless)
FS_{cs}	Factor of safety against connection failure (dimensionless)
FS_{gl}	Factor of safety against global stability failure (dimensionless)
FS_{os}	Factor of safety against reinforcement tensile over-stress (dimensionless)
FS_{ot}	Factor of safety against base overturning (dimensionless)
FS_{otc}	Factor of safety against crest toppling (dimensionless)
FS_{oti}	Factor of safety against internal overturning for conventional SRW structures (dimensionless)

FS_{otl}	Factor of safety against local overturning for reinforced SRW structures (dimensionless)
FS_{po}	Factor of safety against pullout (dimensionless)
FS_{sc}	Factor of safety against interface shear failure (dimensionless)
FS_{sl}	Factor of safety against base sliding (dimensionless)
FS_{sli}	Factor of safety against internal sliding (dimensionless)
g	Gravitational constant (m/s^2)
h	Height at back of reinforcement soil zone used in external stability calculations (m)
h_{IR}	Height from toe of wall to line of action of inertial force PIR (m)
h_{zi}	Height of soil at back of reinforced soil zone used in internal sliding calculations (dimensionless)
h_{β}	Height from base of wall to center of gravity of wedge of soil above reinforced soil zone (m)
H	Vertical wall height measured at face of wall (m)
H_{emb}	Embedment depth of wall (m)
H_f	Leveling pad thickness (m)
H_h	Hinge height of facing column (m)
H_w	Height of facing unit (m)
k_h	Horizontal seismic coefficient (dimensionless)
$k_h(ext)$	Value of k_h used for all external stability calculations and internal sliding calculations for reinforced SRW structures (dimensionless)
$k_h(int)$	Value of k_h used for all internal and facing stability calculations for reinforced SRW structures (dimensionless)
k_v	Vertical seismic coefficient (dimensionless)
K_A	Static earth pressure coefficient calculated using Coulomb earth pressure theory (dimensionless)
K_{AH}	Horizontal component of static earth pressure coefficient calculated using Coulomb earth pressure theory (dimensionless)
K_{AE}	Dynamic earth pressure coefficient calculated using Mononbe-Okabe (M-O) method (dimensionless)

K_{AEH}	Horizontal component of dynamic earth pressure coefficient calculated using Mononbe-Okabe method (dimensionless)
L_{Ai}	Anchorage length of reinforcement layer i (m)
L_g	Distance from the toe of a SRW unit to the center of gravity of the unit (including contribution of granular soil infill volumes if applicable)
L_i	Total length of reinforcement layer i beginning at face of wall (m)
L_{min}	Base width of reinforced soil zone plus facing column $\leq$ H (m)
L_w	Width of facing column (toe to heel dimension of SRW unit) (m)
M_o	Driving moment taken about toe of wall (N-m/m)
$M_o(z)$	Driving moment over depth z (N-m/m)
M_r	Resisting moment taken about toe of wall (N-m/m)
$M_r(z)$	Resisting moment due to weight of facing column over depth z (N-m/m)
m	Ratio of moment arm of dynamic active earth force to wall height (dimensionless)
N	Number of reinforcement layers (dimensionless)
$N_c, N\gamma, N_q$	Bearing capacity coefficients (dimensionless)
N_h	Integer number of standard SRW units comprising hinge height of facing column (dimensionless)
N_w	Total number of standard SRW units in facing column (dimensionless)
N_z	Integer number of facing units above the target point of rotation at depth z (dimensionless)
P_A	Static active earth force (N/m)
P_{AH}	Horizontal component of static active earth force (N/m)
P_{AE}	Dynamic earth force (N/m)
P_{AEH}	Horizontal component of (total) dynamic active earth force (N/m)
$P_{AEH}(z)$	Horizontal component of (total) dynamic active earth force acting over depth z (N/m)

P_{IR}	Horizontal inertial force due to the reinforced soil mass used in external stability factor of safety calculations (N/m)
q_a	Applied foundation bearing stress (N/m^2)
q_{ult}	Ultimate bearing capacity of the foundation soil (N/m^2)
RF_{CR}	Creep reduction factor (dimensionless)
R_S	Base sliding resistance at bottom of reinforced soil zone including facing column for reinforced SRW structures (N/m)
R_{SW}	Base sliding resistance at bottom of facing column for conventional SRW structures (N/m)
$R_S(z)$	Internal sliding resistance at depth z below the crest of the wall (N/m)
S_{vi}	Contributory area corresponding to reinforcement layer i (m^2/m)
$T_a(dyn)$	Allowable tensile load for the reinforcement under seismic loading (N/m)
T_{ci}	Peak connection capacity corresponding to reinforcement layer i
$T_{pull}i$	Peak anchorage (pullout) capacity corresponding to reinforcement layer i (N/m)
$V_u(z)$	Peak interface shear capacity at interface located at depth z below crest of wall (N/m)
W	Weight of active earth wedge behind retaining wall weight of
W_A	Weight of static internal failure wedge (AASHTO/FHWA method) (N/m)
W_h	Weight of facing column at base of wall using hinge height (N/m)
W_i	Total weight of the reinforced soil zone extending from the back weight of the facing column to length L$_{min}$ beyond the face of the wall and having constant height H (N/m)
$W'i$	Reduced weight of the reinforced zone extending from the back of the facing column to length 0,5H beyond the face of the wall and having constant height H used to calculate inertial force PIR or PIR (z) (N/m)
W_w	Total weight of facing column (N/m)

W_r	Total weight of reinforced sol zone (= W_w + W_i + Wβ) (N/m)
W_β	Weight of the wedge of soil in the slope above the crest of the wall at height H (N/m)
W'_β	Reduced weight of the wedge of soil in the slope above the crest of the wall at height H used to calculate inertial force PIR or PIR (z) (N/m)
X_h	Horizontal distance from the toe of the facing column to the center of gravity of the facing column corresponding to the hinge height weight W_h (m)
X_i	Horizontal distance from the toe of the facing column to the center of gravity of the reinforced soil zone corresponding to the weight W_i (m)
X_w	Horizontal distance from the toe of the facing column to the center of gravity of the facing column corresponding to the weight W_w (m)
X_β	Horizontal distance from the toe of the facing column to the center of gravity of the wedge of soil corresponding to the weight W_β (m)
y_i	Vertical distance from point of rotation on wall face to reinforcement layer I (m)
$y_{dyn}(z)$	Moment arm between the point of rotation at depth z and the centroid of the dynamic earth pressure distribution (m)
z	Depth from crest of wall (m)
z_i	Depth from crest of wall to reinforcement layer i (m)
z_{idyn}	Moment arm between the point of rotation at depth z and the line of action of the dynamic earth force increment (m)
z_{vi}	Distance from the crest of the wall to the middle of the contributory area S_{vi} (m)
αAE	Orientation of failure plane from horizontal using M-O method (°)
β	Backslope angle (°)

δ	Mobilized interface friction angle (°)
δ_w	Mobilized interface friction angle at the back of wall facing column (°)
Φ	Peak friction angle of soil (°)
Φ_b	Peak friction angle of retained (backfill) soil (°)
Φ_{cv}	Residual (constant volume) friction angle of soil (°)
Φ_d	Peak friction angle of drainage (leveling pad) soil (°)
Φ_f	Peak friction angle of foundation soil (°)
Φ_r	Peak friction angle of reinforced (infill) soil (°)
γ	Unit weight of soil (N/m^3)
γ_b	Unit weight of retained (backfill) soil (N/m^3)
γ_f	Unit weight of foundation soil (N/m^3)
γ_r	Unit weight of reinforced (infill) soil (N/m^3)
γ_w	Unit weight of SRW units (N/m^3)
λ_{cs}	Slope of peak connection strength failure envelope (°)
λ_u	Slope of peak interface shear strength failure envelope for SRW units(°)
μ_b	Masonry friction reduction factor (dimensionless)
σ_{vi}	Average overburden pressure acting over anchorage length LAi (N/m^2)
θ	Seismic inertia angle (°)
ω	Wall inclination angle (positive in a clockwise direction from the vertical) (°)

LIST OF ACRONYMS/ABBREVIATIONS

AI	Arias Intensity
ANN	Artificial Neural Network
ASI	Acceleration Spectrum Intensity
$AASMOD$	Algorith Adaptive Spline Modeling of Observation
CAV	Cumulative Absolute Velocity
EPA	Effective Peak Acceleration
$EPDM$	Ethlene Propylene Diene Monomer
FEA	Finite Element Analysis
FEM	Finite Element Method
$FHWA$	Federal Highway Administration
IM	Intensity Measures
LEM	Linear Elastic Model
$LMBNN$	Levenberg-Marquardt Back Propagation Algorithm
$NCMA$	National Concrete Masonry Association
MAE	Mean Absolute Error
MCM	Mohr Coulomb Model
MSE	Mechanically Stabilized Earth
MBW	Modular Block Wall
MLP	Multilayer Perceptrons
$M-O$	Mononbe-Okabe (pseudo-static earth pressure theory)
PGA	Peak Ground Acceleration
PGV	Peak Ground Velocity
$RMSE$	Root Mean Squared Error
$RS-RW$	Reinforced Soil Retaining Wall
SRW	Segmental Retaining Wall
VSI	Velocity Spectrum Intensity

1. INTRODUCTION

1.1. General

Back-to-back Mechanically Stabilized Earth (MSE) walls are commonly used for bridge approach embankments. Due to their cost effectiveness and increasing acceptance, large number of reinforced soil retaining structures are being designed and constructed throughout the world and also in Turkey. In order to gain better insight of mechanism affecting the behavior of such structures, engineering approaches are turning to numerical experiments (simulation analysis). Currently the most popular numerical analysis technique is the finite element method for both static and dynamic loading conditions. This powerful analytical tool holds much promise for simulating the behavior of reinforced soil retaining structures, especially under dynamic stress conditions which are considered to be very sophisticated.

Artificial Neural Network was used for the first time in literature to estimate the deformation of retaining walls under dynamic loading conditions. Although developing an analytical or empirical model is feasible in some simplified situations, most manufacturing processes are complex, and therefore, models that are less general, more practical, and less expensive than the analytical models are of interest. ANN has been applied successfully in many non-linear geotechnical engineering problems in order to make reliable predictions and to check whether the range of results obtained from classical design procedures had given reasonable outcomes.

Current conceived and executed numerical experiments offer the possibility to improve the understanding of the effects of dynamic loading on reinforced soil retaining structures and to demonstrate the influence of the component properties such as reinforcement length, vertical spacing of the reinforcement along the wall, and facing type on the system response to seismic loading.

Plaxis v.11.0 software program was used in the analysis of seismic response of

reinforced soil walls. It is a finite element package specifically intended for deformation analysis and stability in geotechnical engineering projects. Geotechnical applications require advanced constitutive models for the simulation of the nonlinear and time dependent behavior of soils. The modeling of the soil itself is an important issue; many geotechnical engineering projects involve the modeling of the structures and the interaction between the structures and the soil. In this finite element simulation, a two-dimensional plain strain model is used for structures with a (more or less) uniform cross-section and corresponding stress-state and loading scheme over a certain length perpendicular to the cross-section.

One of the key research areas of earthquake engineering field is the assessment of the capacity of a strong ground motion to damage structures, thus establishing a proper and objective measure of earthquake intensity. Defining the severity of a seismic excitation has become an important task in earthquake engineering field. Many ground motion intensity parameters have been proposed to relate the seismic damage to the intensity of the ground motions. Recently, evaluation of the seismic performance of structures under seismic excitations, where excitation is represented by a ground motion intensity parameter, has gained a wide popularity.

Numerical simulations were carried out to investigate the influence of reinforcement length, facing type, and vertical spacing of the reinforcement on the seismic response of 5 to 10 m high reinforced soil retaining walls under three different harmonic motions which have different intensity measures (IM).

The important point of the seismic evaluation of the seismic response of the structure is the selection of ground motion IM. The commercial software SeismoSignal constitutes an easy and efficient way to process strong-motion and to obtain all IM.

1.2. Organization of the Thesis

The study is presented in the thesis in the following order:

- Chapter 1 Introduction to the subject, scope and objective of the study
- Chapter 2 Literature review, description of geosynthetic reinforced retaining walls and Seismic Analysis Approaches
- Chapter 3 Description of Artificial Neural Network and application of ANN in Geotechnical Problems
- Chapter 4 Description of strong-ground motion and Intensity Measures (IM)
- Chapter 5 Numerical modeling of back-to-back Mechanically Stabilized Earth (MSE) wall with the Plaxis program
- Chapter 6 Validation analysis of numerical model
- Chapter 7 Results of finite element analysis
- Chapter 8 ANN Model analysis and results
- Chapter 9 Conclusions

2. LITERATURE REVIEW

2.1. Reinforced Soil Structures

2.1.1. Reinforced Soil Principles

Reinforced Soil Retaining Structures are composite construction materials in which the strength of engineering fill is enhanced by the addition of tensile reinforcement in the form of both steel strips and geosynthetic fabrics or grids. The basic mechanism of Reinforced Soil Structures involves the generation of frictional forces between the soil and the reinforcement. These forces are manifested in the soil in a form of analogous to an increased confining pressure which enhances the strength of composite.

Additionally the reinforcement has ability to unify a mass of soil that would otherwise part along the failure surface. The beneficial effects of soil reinforcement derive from

- The soils increased tensile strength.
- The shear resistance developed from the friction at the soil-reinforcement interfaces (Das, 1994).

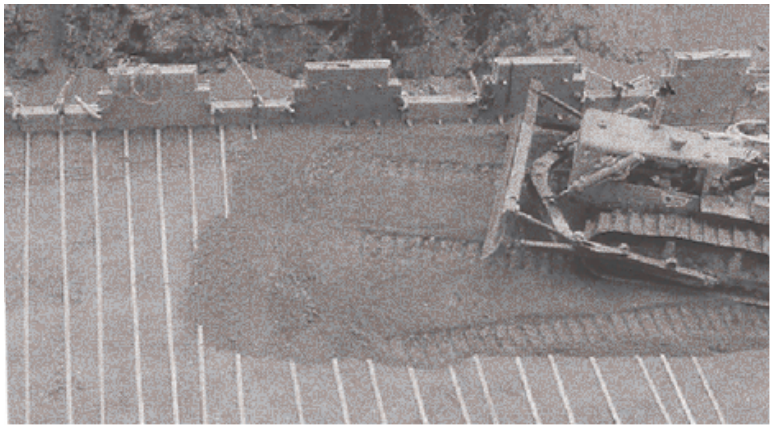

Figure 2.1. The components of reinforced soil retaining wall.

A reinforced soil mass is somewhat analogous to reinforced concrete in that the mechanical properties of the mass are improved by reinforcement placed parallel to the principle strain direction to composite for soils lack of tensile resistance. The composite material has the following characteristics:

- Stress transfer between the soil and reinforcement takes place continuously along the reinforcement.
- Reinforcements are distributed throughout the soil mass with a degree of regularity and must not be localized.

Stresses are transferred between soil and reinforcement by friction (Figure 2.2) and/or passive resistance (Figure 2.3) depending on reinforcement geometry.

Friction develops at locations where there is a relative shear displacement and corresponding shear stress between soil and reinforcement surface. Reinforcing elements where friction is important should be aligned with the direction of soil reinforcement relative movement. Examples of such reinforcing elements are steel strips, longitudinal bars in grids, geotextile and some geogrid layers.

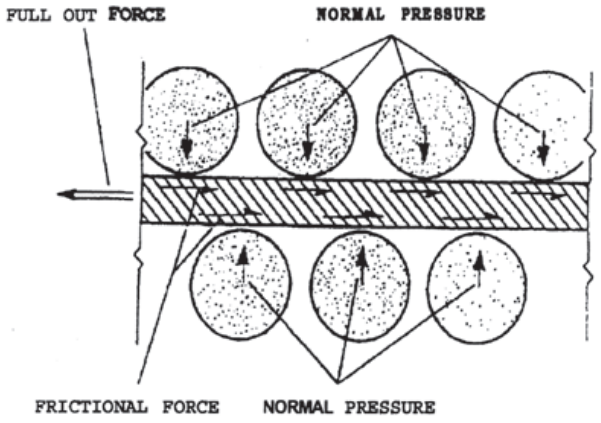

Figure 2.2. Stress transfer mechanism of soil reinforcements.

Passive resistance occurs through the development of bearing type stresses on "transverse" reinforcement surfaces normal to the direction of soil reinforcement rela-

tive movement. Passive resistance is generally considered to be the primary interaction for rigid geogrids, bar mat, and wire mesh reinforcements. The transverse ridges on "ribbed" strip reinforcement also provide some passive resistance.

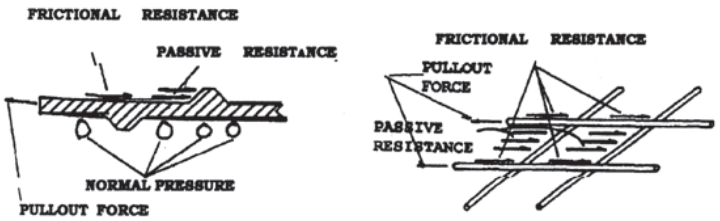

Figure 2.3. Soil passive resistance in reinforcements.

The contribution of each transfer mechanism for a particular reinforcement will depend on the roughness of the surface (skin friction), normal effective stress, grid opening dimensions, thickness of transverse members, and elongation characteristics of the reinforcement. Equally important for interaction development are soil characteristics, including grain size, grain size distribution, particle shape, density, water content, cohesion, and stiffness (FHWA, 1996).

2.1.2. Back to Back Reinforced Wall

For reinforced walls which are built back-to-back as indicated in Figure 2.4, two cases can be considered.

Case I, the overall base width is large enough so that each wall behaves and can be designed independently. In particular, there is no overlapping of the reinforcements. Theoretically, if the distance, D, between the two walls is shorter than

$$D = H_1 tan(45^o - \varphi/2) \tag{2.1}$$

then the active wedges at the back of each wall cannot fully spread out and the active thrust is reduced. However, it is assumed that for values of

$$D > H_1 tan(45^o - \varphi/2) \approx 0.5 H_1 \tag{2.2}$$

full active thrust is mobilized.

Case II, there is an overlapping of the reinforcements such that the two walls interact. When the overlap, L_R, is greater than 0.3 H_2, where H2 is the shorter of the parallel walls, no active earth thrust from the backfill needs to be considered for external stability calculations. For intermediate geometries between Case I and Case II, the active earth thrust may be linearly interpolated from the full active case to zero. For Case II geometries with overlaps greater than 0.3 H2, L/H ratios for each wall as low as 0.6 may be considered.

Considering this case, designers might be tempted to use single reinforcements connected to both wall facings. This alternative completely changes the strain patterns in the structure and results in higher reinforcement tensions such that the design method in this manual is no longer applicable. In addition, difficulties in maintaining wall alignment could be encountered during construction, especially when the walls are not in a tangent section.

Based on a performance review, back-to-back walls with overlapping reinforcements may be designed for static load conditions with a distance between parallel facing as low as L/H = 0.6, where H is the height of each wall, and for conditions where the seismic horizontal accelerations at the foundation level is less than 0.05 g. For walls in more seismically active areas (up to 0.19 g) a distance of 1.1H1 is presently recommended. For walls subjected to significant seismic loading (up to 0.40 g) successful performance has been observed when the distance between parallel facings was at least $1.2H_1$.

Justification of narrower back-to-back distances ($< 1.1H_1$) between faces in seismically active areas require a more detailed analysis be performed to include effects

of potential non-uniform distribution of seismic and inertial forces within the wall, as suggested by numerical studies and not provided for in the present design methodology (FHWA, 2001).

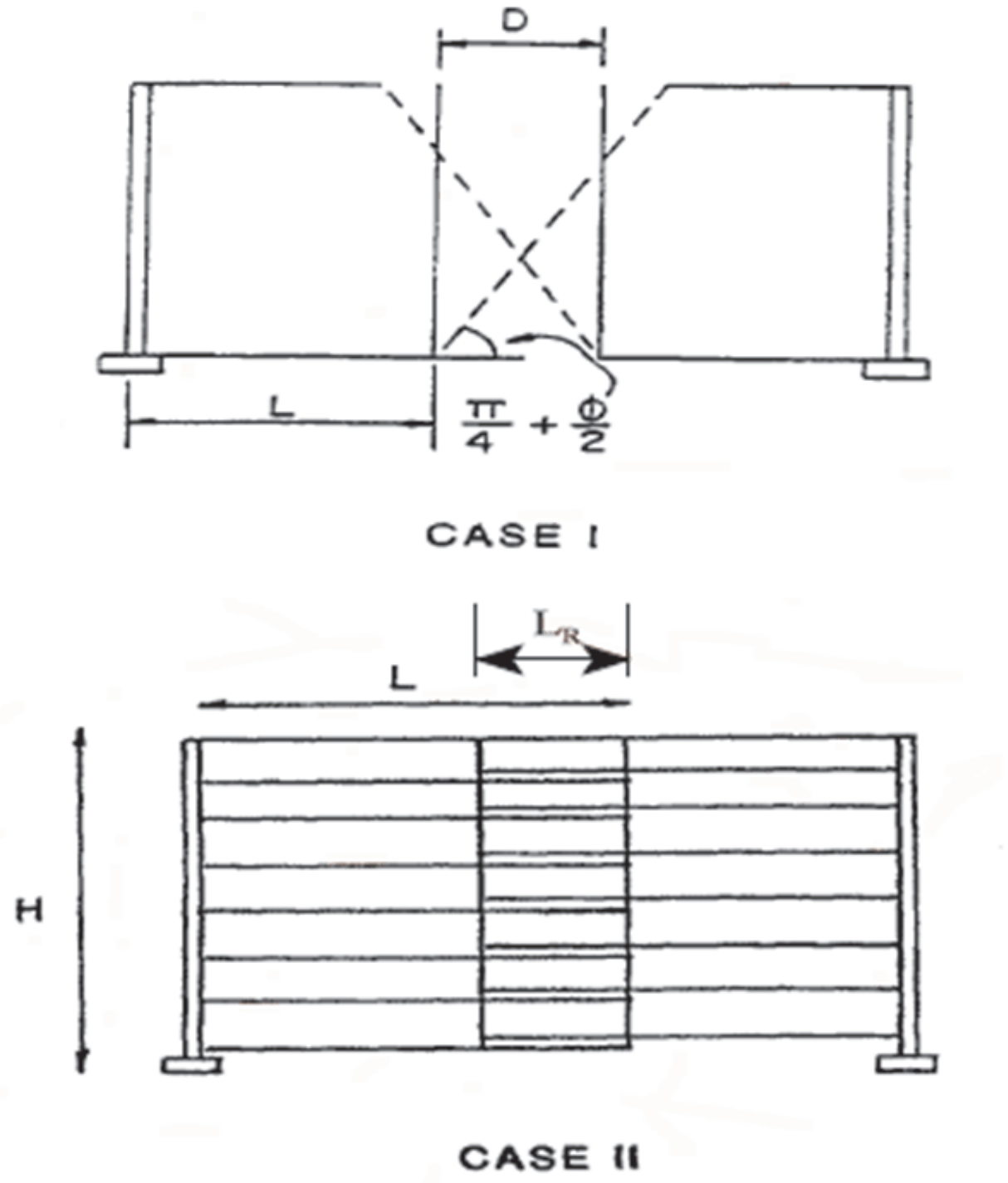

Figure 2.4. Back to back wall.

2.2. The Elements of Reinforced Soil Structures

The major components comprising a reinforced soil wall are; the backfill soil, the reinforcement, the facing units and foundation soil. In the above these components are examined briefly.

2.2.1. The Backfill Soil

Reinforced Soil Walls require high quality backfill for durability, good drainage, constructability, and good soil reinforcement interaction which can be obtained from well graded, granular materials. Many reinforced soil systems depend on friction between the reinforcing elements and the soil. In such cases, a material with high friction characteristics is specified and required. Some systems rely on passive pressure on reinforcing elements, and, in those cases, the quality of backfill is still critical. These performance requirements generally eliminate soils with high clay contents.

From a reinforcement capacity point of view, lower quality backfills could be used for Reinforced Soil structures; however, a high quality granular backfill has the advantages of being free draining, providing better durability for metallic reinforcement, and requiring less reinforcement. There are also significant handling, placement and compaction advantages in using granular soils. These include an increased rate of wall erection and improved maintenance of wall alignment tolerances.

The selection criteria of reinforced backfill should consider long-term performance of the completed structures, construction phase stability and the degradation environment created for the reinforcements. Much of our knowledge and experience with Reinforced Soil Structures today has been with select, cohesionless backfill. But researches are being carried out into the possibility of using cohesive soils as a backfill material. As clay is probably the most common soil encountered in the United Kingdom and also in Taiwan, encouraging results from such research would be of interest (Smith and Pole, 1980). In his research Simons pointed out that the tests were conducted at a very high rate of shear with failure resulting in less than 10 minutes under undrained

conditions at the higher clay contents. It was argued that in the field the generation of pore water pressures could be controlled by construction rate and provision of suitable drainage layers. Combining this with an effective stress analysis, rather than somewhat conservative total stress analysis, Simon saw no reason why cohesive fill should not be used successfully (Ingold, 1982).

2.2.2. Reinforcement

We can distinguish the reinforcement element into two main types:

- *Metallic Reinforcements:* Typically it is made of mild steel. The steel is usually galvanized or may be epoxy coated. The steel behaves as inextensible reinforcement; deformation of the reinforcement at failure is much less than the deformability of the soil. The geometry of the steel reinforcement is linear unidirectional.
- *Nonmetallic (Geosynthetic) Reinforcements:* Generally polymeric materials consisting of polypropylene, polyethylene, or polyester are used. The deformation of the reinforcement at failure is comparable to or even greater than the deformability of the soil (FHWA, 2001).

2.2.3. Facing Unit

At a free boundary of Reinforced Soil Structures, it is necessary to provide some form of barrier so that the soil is contained. This skin can be either flexible or stiff but it must be strong enough to hold back the local soil and to allow attachment of the reinforcement. The types of facing elements used in the different Reinforced Soil Walls systems control their aesthetics because they are the only visible parts of the completed structure. A wide range of finishes and colors can be provided in the facing. In addition, the facing provides protection against backfill sloughing and erosion, and provides in certain cases drainage paths. The type of facing influences settlement tolerances. Major facing types are:

- *Segmental precast concrete panels:* The precast concrete panels have a minimum

thickness of 140 mm and are of a cruciform, square, rectangular, diamond, or hexagonal geometry. Temperature and tensile reinforcement are required but will vary with the size of the panel. Vertically adjacent units are usually connected with shear pins. Precast elements can be cast in several shapes and provided with facing textures to match environmental requirements and blend aesthetically into the environment. Retaining structures using precast concrete elements as the facings can have surface finishes similar to any reinforced concrete structure.

- *Dry cast modular block wall (MBW) units:* These are relatively small, squat concrete units that have been specially designed and manufactured for retaining wall applications. The mass of these units commonly ranges from 15 to 50 kg, with units of 35 to 50 kg routinely used for highway projects. Unit heights typically range from 100 to 200 mm for the various manufacturers. Exposed face length usually varies from 200 to 450 mm. Nominal width (dimension perpendicular to the wall face) of units typically ranges between 200 and 600 mm. Units may be manufactured solid or with cores. Full height cores are filled with aggregate during erection. Units are normally dry-stacked (i.e. without mortar) and in a running bond configuration. Vertically adjacent units may be connected with shear pins, lips, or keys. Recently introduced dry cast segmental block MBW facings raise some concerns as to their durability in aggressive freeze-thaw environments because their water absorption capacity can be significantly higher than that of wet-cast concrete. Historical data provide little insight as their usage history is less than a decade. Further, because the cement is not completely hydrated during the dry cast process, (as is often evidenced by efflorescence on the surface of units), a highly alkaline regime may establish itself at or near the face area, and may become an aggressive aging media for some geosynthetic products potentially used as reinforcements. Freeze-thaw durability is enhanced for products produced at higher compressive strengths and/or sprayed with a posterection sealant.

Figure 2.5. Modular block facing with geogrid reinforcement.

- *Geosynthetic Facing:* Various types of geotextile reinforcement are looped around at the facing to form the exposed face of the retaining wall. These faces are susceptible to ultraviolet light degradation, vandalism (e.g. target practice) and damage due to fire. Alternately, a geosynthetic grid used for soil reinforcement can be looped around to form the face of the completed retaining structure in a similar manner to welded wire mesh and fabric facing. Vegetation can grow through the grid structure and can provide both ultraviolet light protection for the geogrid and a pleasing appearance.

2.2.4. Foundation Soil

To determine the characteristics of foundation soils, boring may have to be conducted to understand better the geological conditions of the foundation. The standard penetration test is used to obtain the strength of the foundation. The depth of investigation should be extended up to a firm soil layer that does not exhibit sign of instability, settlement and liquefaction. For the sites where potential problems have been revealed during pre-investigation, sounding, sampling and soil testing are required to obtain additional information (Rimoldi, 2002).

The determination of engineering properties for foundation soils should be focused on establishment of bearing capacity, settlement potential, and position of ground water levels. Major foundation weakness and compressibility may require the consideration of ground improvement techniques to achieve the adequate bearing capacity, or limiting total or differential settlement (FHWA, 2001).

2.3. Seismic Analysis Approach

Analytical and numerical approaches for the seismic analysis of reinforced walls, slopes and embankments can be divided into the following categories:

- Pseudo-static methods,
- Displacement methods,
- Dynamic finite element/finite difference methods.

2.3.1. Pseudo-static Analysis

The method that is most commonly used for the seismic analysis and design of GRS walls is the pseudo-static method in which pseudo-static forces related to the ground acceleration are added to the conventional static limit equilibrium analysis. In doing this, mostly the Mononobe-Okabe approach, which is an extension of the classical Coulomb wedge analysis, is used. For granular soils, PAE, the total active earth force applied by the backfill soil against the facing column is calculated as follows (Seed and Whitman, 1970):

$$P_{AE} = \frac{1}{2}(1 \pm k_v)K_{AE}\gamma H^2 \tag{2.3}$$

where

γ = unit weight of the soil

H = height of wall

K $_{AE}$= total earth pressure coefficient

$$K_{AE} = \frac{cos^2(\phi + \psi - \theta)}{cos\theta cos^2\psi cos(\delta - \psi - \theta)[1 + \sqrt{\frac{sin(\phi+\delta)sin(\phi-\beta-\theta)}{cos(\delta-\psi+\theta)cos(\psi+\beta)}}]^2} \tag{2.4}$$

where

ϕ = peak soil friction angle

ψ = wall face inclination (ψ shown in the figure is positive)

δ = mobilized interface friction angle at the back of the wall

β = backslope angle (from horizontal)

θ = seismic inertia angle

$$\theta = tan^{-1}(\frac{k_h}{1 \pm k_i}) \tag{2.5}$$

where k_h and k_v are horizontal and vertical seismic coefficients.

Seed and Whitman (Seed and Whitman, 1970) decomposed the PAE in Equation 2.3 into static component PA and incremental dynamic component ΔP_{dyn}:

$$P_{AE} = P_A + \Delta P_{dyn} \tag{2.6}$$

or

$$(1 \pm k_1 K_{AE} = K_A + \Delta K_{dyn} \tag{2.7}$$

where

- K_A= static active earth pressure coefficient
- ΔK_{dyn}= incremental dynamic active earth pressure coefficient

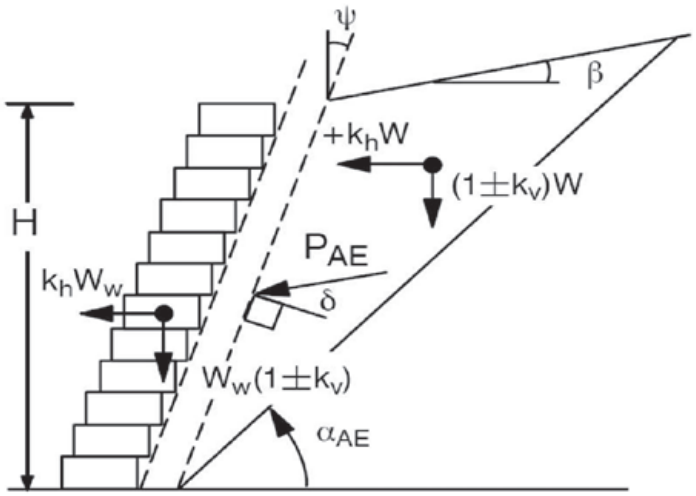

Figure 2.6. Force diagram for Pseudo-static analysis (Bathurts and Alfaro, 1996).

Closed-form approximate solutions for α_{AE} developed by (Okabe, 1924) and (Zarrabi, 1979) are given below. These were shown to result in excessive reinforcement lengths, so in practice, the orientation of the internal failure plane for reinforcement design is found using static load conditions (i.e. $k_h = k_v = 0$) (Bathurst *et al.*, 2002).

$$\alpha_{AE} = \phi - \theta + tan^{-1}[\frac{-A_\alpha + D_\alpha}{E_\alpha}] \tag{2.8}$$

where

- $A_\alpha = tan(\phi - \theta - \beta)$
- $D_\alpha = \sqrt{A_\alpha[A_\alpha + B_\alpha][B_\alpha C_\alpha + 1]}$
- $E_\alpha = 1 + [C\alpha(A_\alpha + B_\alpha)]$
- $B_\alpha = \frac{1}{tan(\phi - \theta + \psi)}$
- $C_\alpha = tan(\delta + \theta - \psi)$

Bathurst and Cai (Bathurst and Cai, 1995) proposed the active earth pressure distribution shown in Figure 2.7 for external, internal and facing stability calculations of GRSW with segmental facing upon reviewing the literature for conventional gravity retaining walls. Without seismic effects, the distribution becomes the triangular static distribution due to soil weight.

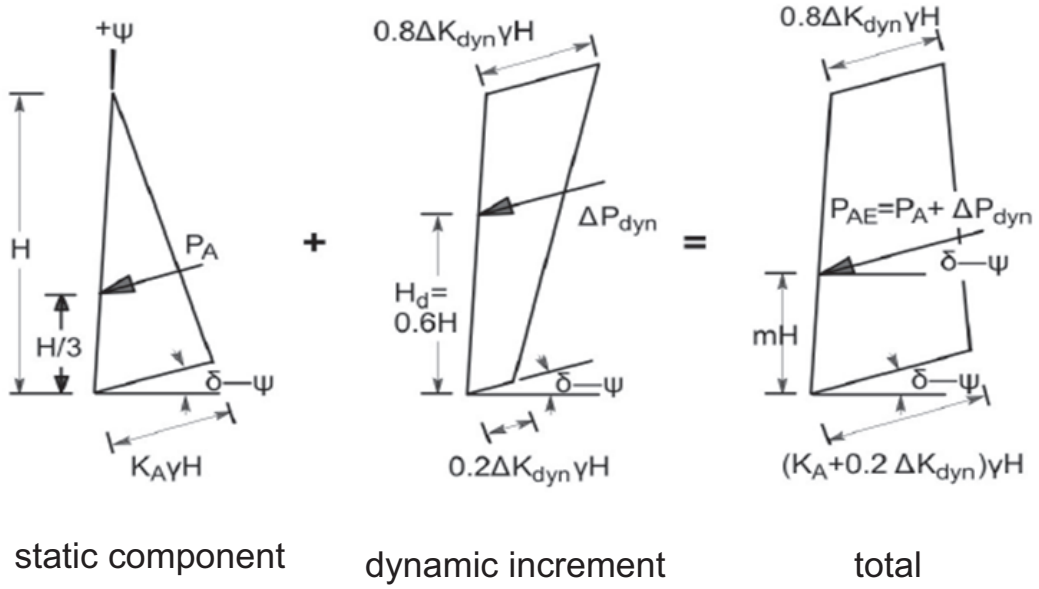

Figure 2.7. Calculation of total earth pressure due to soil self-weight (Bathurst and Cai,1995).

$$k_h = \frac{a_h}{g}(1.45 - \frac{a_h}{g}) \tag{2.9}$$

where a_h= horizontal peak ground acceleration.

For the vertical seismic coefficient k_v, Seed and Whitman (Seed and Whitman, 1970) and Wolfe *et al.*, (Wolfe *et al.*, 1978) suggested that ignoring k_v is acceptable in pseudo- static analysis. For sites close to the epicenter, vertical accelerations may become significant, so the decision should be made with care.

FHWA guidelines (Elias and Christopher, 1999) restrict the use of pseudo-static methods to sites with ah lower than 0.29 g. For larger accelerations, structural displacements may exceed the acceptable values, so at least a sliding block analysis is required.

External stability calculations are similar to those for conventional gravity retaining walls. Factors of safety against base sliding and overturning for the reinforced soil zone together with the facing column are calculated using the forces and geometry shown in Figure 2.8. PIR is the horizontal inertial force. There are various suggestions for the value of PIR, but in all cases it is taken lower than khWR in order not to be too conservative.

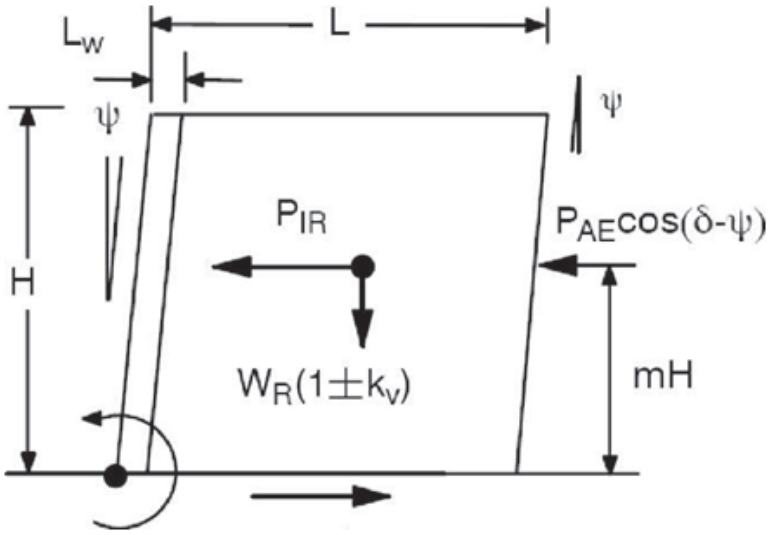

Figure 2.8. Forces and geometry for external stability calculations (Bathurst *et al.*, 2002).

For internal stability calculations, each reinforcement layer is required to carry the part of the assumed internal pressure distribution applied to the area S_v in Figure 2.9. Tensile strength, facing connection strength and pullout capacity of the reinforcement layer should be adequate. Various methods used are presented in the following figures.

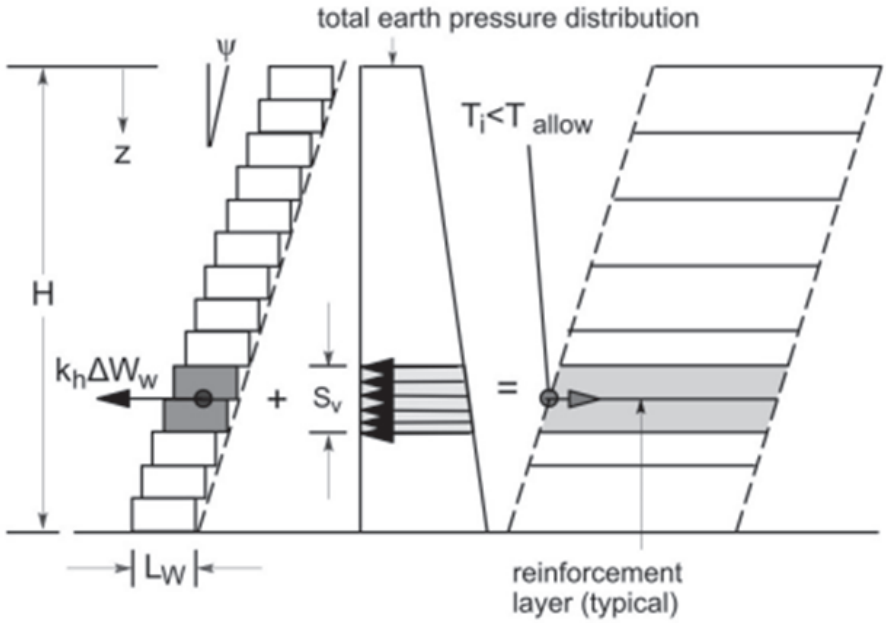

Figure 2.9. Reinforcement tensile load calculation using Bathurst and Cai method (Bathurst and Alfaro, 1996).

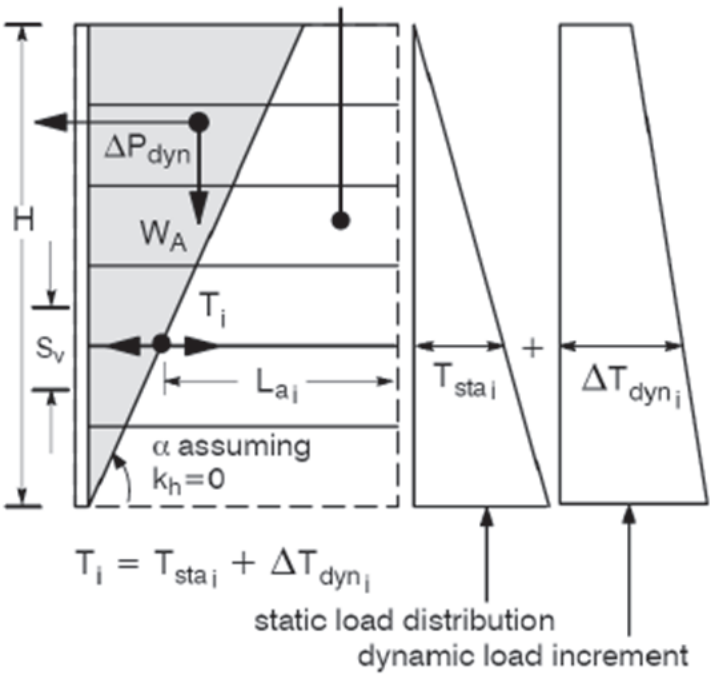

Figure 2.10. Reinforcement tensile load calculation using FHWA method, which utilizes Rankine earth pressure theory (Bathurst and Alfaro, 1996).

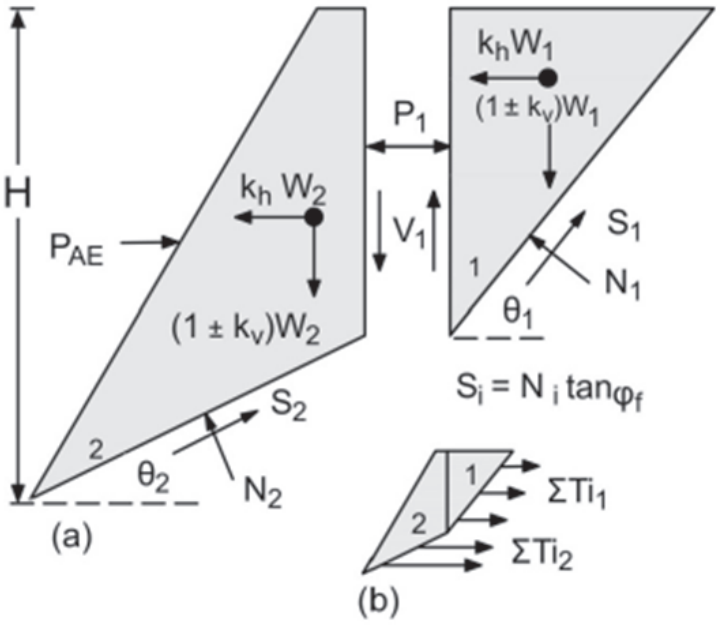

Figure 2.11. Two-part wedge analysis: (i) free-body diagram (ii) with reinforcement forces (Bathurst and Alfaro, 1996).

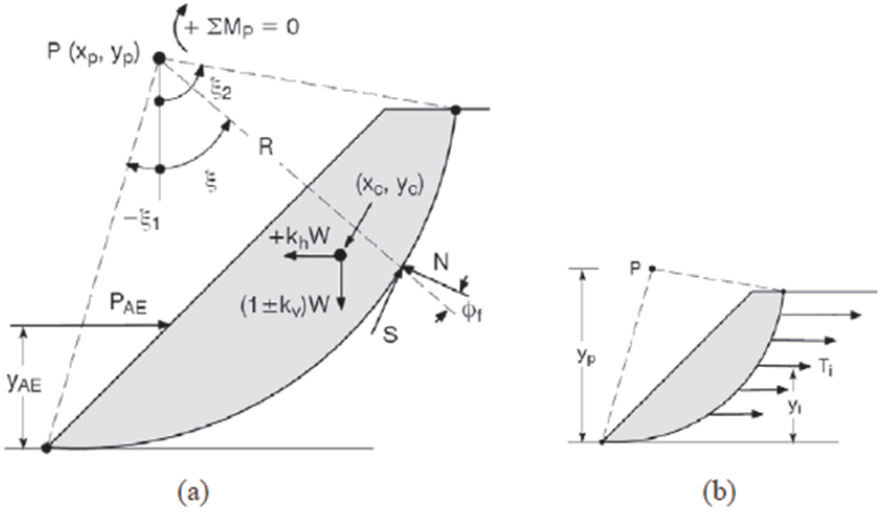

Figure 2.12. Log-spiral analysis: (i) free-body diagram (ii) with reinforcement forces (Bathurst and Alfaro, 1996).

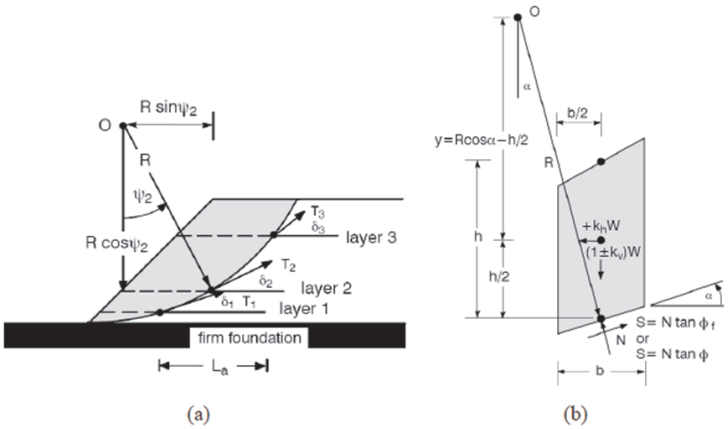

Figure 2.13. Circular slip analysis: (i) circular slip geometry (ii) method of slices (Bathurst and Alfaro, 1996).

2.3.2. Newmark Displacement Method

As with all limit-equilibrium methods of analysis, pseudo-static approaches cannot explicitly include wall or slope deformations. This is an important shortcoming since failure of geosynthetic-reinforced soil walls, in particular, may be manifested as unacceptable movement without structural collapse. The permanent displacement of a geosynthetic-reinforced soil structure due to horizontal sliding/shear mechanisms can be estimated using one of the two general approaches, as described below.

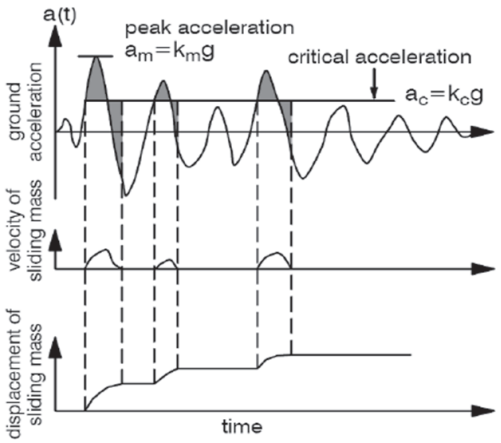

Figure 2.14. Calculation of permanent displacements (unidirectional displacement) using Newmark's method.

For a given input acceleration time history, Newmark's double integration method for a sliding mass can be used to calculate permanent displacement (Newmark, 1965). According to Newmark's theory, a potential sliding body is treated as a rigid-plastic monolithic mass under the action of seismic forces. Permanent displacement of the mass takes place whenever the seismic force induced on the body (plus the existing static force) overcomes the available resistance along, a potential sliding/shear surface. Newmark's method requires that the critical acceleration, k_c, to initiate sliding or shear failure be determined for each translation failure mechanism. The value of k_c can be determined by searching for values of k_h that give a factor of safety of unity in pseudo-static factor of safety expressions. The critical acceleration is then applied to the horizontal ground acceleration record at the site and double integration is performed to calculate cumulative displacements, as illustrated in Figure 2.14 where g is the gravitational constant, a(t) is the horizontal ground acceleration function with time t, $a_m = k_m$ g is the peak value of a(t), and $a_c = k_{cg}$ is the critical horizontal acceleration of the sliding block. For a given ground acceleration time history and a known critical acceleration of the sliding mass, the earthquake-induced displacement is calculated by integrating those portion of the acceleration history that are above the critical acceleration and those portions that are below until the relative velocity between the sliding mass and the sliding base reduces to zero.

A number of researchers have postulated that the critical acceleration value to initiate slip should be based on the peak shearing resistance of the soil (e.g. ϕ_{peak}) but thereafter residual strength values should be used (e.g. Elms and Richards, 1990; Chugh, 1995). Alternatively, conservative estimates of seismic-induced displacements should be based on residual strength values if a single value of ϕ is adopted to simplify analyses.

If the input acceleration data at a site are specified by characteristic parameters such as the peak ground acceleration and the peak ground velocity, then empirical methods that correlate the expected permanent displacement to the characteristic parameters of the earthquake, and a critical acceleration ratio for the structure, are required. Alternatively, if the tolerable permanent displacement of the structure is

specified, based on serviceability criteria, the wall can then be designed using an empirical method so that, expected permanent displacements do not exceed specified values. Newmark's sliding block theory has been widely used to establish empirical relationships between the expected permanent displacement and characteristic seismic parameters of the input earthquake by integrating existing acceleration records. The critical acceleration ratio, which is the ratio of the critical acceleration, k_c g, of the sliding block to the peak horizontal acceleration, k_m g, of the earth-quake, has been shown to be an important parameter that affects the magnitude of the permanent displacement. Thus, the seismic displacement of a potential sliding soil mass computed using Newmark's theory has been traditionally correlated with the critical acceleration ratio k_c/k_m, and other representative characteristic seismic parameters, such as the peak ground acceleration, k_m g, the peak ground velocity, V_m, and the predominant period, T, of the acceleration spectrum (e.g. Newmark, 1965; Sarma, 1975; Franklin and Chang, 1977).

Cai and Bathurst, (1996b) have reformulated a number of existing displacement methods based on non-dimensionalized displacement terms that are common to the methods, and divided them into two separate categories based on the characteristic seismic parameters referenced in each method. Example relationships between the dimensionless displacement term, d/ν^2 m/k_m g), where d is the actual expected permanent displacement, and the critical acceleration ratio are shown in Figure 2.15. Other curves are available in the literature but it should be noted that any empirical curve will be influenced by the earthquake data that is used to establish the curve and the interpretation of the original data.

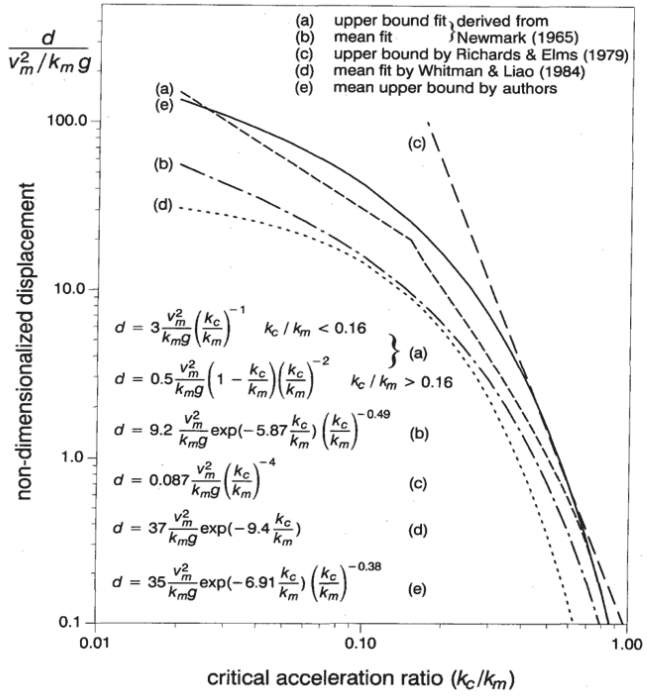

Figure 2.15. Nondimensionalized displacement in terms of $d/(v_m^2/k_m\ g)$ versus critical acceleration ratio k_c/k_m (after Cai and Bathurst, 1996a).

2.3.3. Dynamic Analysis Using Numerical Techniques

2.3.3.1. The Finite Element Method:. The advantages offered by numerical techniques (e.g. the possibility of implementing complex models for the involved materials) make this choice a very promising method for the design and analysis of geosynthetic reinforced soil walls and slopes. Various programs based on finite element method or finite difference method are available or being developed, and many studies involving the comparison of numerical analysis results with the results of physical tests are conducted. Some of the major studies showing the power of numerical techniques are alluded below.

Fujii *et al.*, (Fujii *et al.*, 2006) aimed to simulate results from a series of dynamic centrifuge tests on GRS segmental walls using finite element analyses with the program FLIP. In total, thirteen test cases with different input wave forms and amplitudes were analyzed.

El-Emam *et al.*, (El-Emam *et al.*, 2004) reported the results of numerical modeling of 1-m high shaking table tests that investigated full-height panel face GRS walls with different toe boundary conditions using the finite difference-based program FLAC. The numerical models were found to give reasonably accurate predictions of the experimental results (wall facing displacements, reinforcement loads and measured toe loads) despite the complexity of the physical models under investigation.

Bathurst and Hatami (Bathurst and Hatami, 1998a) reported the results of a numerical parametric study of an idealized 6-m high GRS wall with a full-height rigid facing and six layers of reinforcement. They showed that the magnitude and distribution of reinforcement loads was sensitive to the stiffness of the reinforcement materials used.

2.3.3.2. Previous Studies on Seismic Analysis of RS-RWs with FEM:. The force mobilized in the reinforcement layers and the stress distribution in the soil within a reinforced soil system may be expected to depend on interaction between the facing, the reinforcement and the soil. It might be also be hypothesized that the nature of the interaction may change with changes in the physical properties of these materials. In principle, these effects could be studied by construction of a larger number of full scale field tests, but the cost involved is so high that this is not practical. Numerical "experiments" or simulations with computer based finite element analysis provide an alternative and cost effective means of performing such a study. (Rowe and Ho, 1997) With respect to above description researchers have been using finite element (also finite difference method) analysis to demonstrate the reinforced soil wall behaviour approximately thirty years since then.

The study which was conducted by Richardson and Lee may be the first about the seismic design of reinforced soil retaining walls. They examined a small laboratory scale wall subjected to horizontal sinusoidal seismic loading with a shaking table. The modal walls and box was constructed of 19 mm plywood and was 760 mm wide. Most of the walls were constructed 300 mm high and the backfill extended about 910 mm

behind the wall to the rigid back of the backfill box. The box was rigidly mounted on a shaking table driven by 5 ton hydraulic ram which could be controlled to any regular sinusoidal varying time and frequency deformation pattern. The tests showed that wall was responded to input vibrations like a nonlinear damped elastic system.

Also a limited number of finite element analyses were performed to aid in interpreting the data from the laboratory tests. The Berkeley's computer program QUAD-4, which includes strain dependent modules and damping, was modified to include elastic tension - compression bar element for the reinforcement. The 300 mm x 910 mm long sand box was modeled by 64 elements. The density of the soil and stiffness of reinforcement bar elements were made to actual values and the maximum acceleration was the same as used in the comparative tests. The writers made some observations about the behaviour of reinforced soil wall with respect to testing and modeling procedure. But finally they made a conclusion that considerably more works are required to better define and understand most aspects of the behaviour of reinforced walls under seismic loading (Richardson and Lee, 1975).

One of the main studies on seismic design of reinforced soil retaining wall was made by (Segrestin and Bastick, 1988). The dynamic study was carried out using the SUPERFLASH program. Their results are close to given an agreement between the experimental results which were examined before by different researchers. They modeled two different height walls 6 m and 10.50 m respectively. The lengths and number of strips were similar. In the study the authors used mild steel to model reinforcement. As an important implementation they stated that the results of this research can not be applicable for other reinforcement materials having totally different elasticity modulus. Two different typical accelerograms were applied to the models, San Francisco (1957) earthquake and (San Fernondo, 1971) earthquake records. The predominant frequency was 8 Hz.

Segrestin concluded that response of wall had sensitivity to the maximum acceleration value for using base excitation. There is also very marked reduction in dynamic forces as a function of foundation stiffness for a given seismic motion. There is ten-

dency in the distribution of dynamic forces for lower reinforcement to be relatively more affected. In the study of Segrestin and Bastick the most important result might be that they determined an empirical equation for an estimation of the average maximum horizontal acceleration in the reinforced wall, which is currently used in many reinforced soil retaining wall design manuals (Segrestin and Bastick, 1988).

In the related research Brinkgreve and Yogendrakumar studied at dynamic response analysis of reinforced soil retaining walls with two different finite element programs which were based on two different methods of analysis for response of wall under dynamic loading. The first method was an iterative equivalent linear approach, QUAD-4B and the second was incremental elastic approach, implemented in TARA-3. The predicted capability of the two methods of analysis were evaluated by comparing the computed time histories of horizontal acceleration and dynamic forces in the reinforcement layers with the field test data of full scale instrumented reinforced soil wall with metallic strips. The field test data was obtained by subjecting the instrumented wall to seismic excitation generated by buried explosives denoted by delays. The wall was 6.1 m in height and reinforced with metallic strips of 4.88 m long, placed with equal vertical spacing of 0.76 m.

The measuring device was directly attached to steel strips. The writers made a comparison between the finite element programs QUAD-4B and TARA-3, on the measured responses. The results computed by TARA-3 demonstrated that the nonlinear incremental elastic methods of analysis implemented in the program results in good agreement between actual and predicted responses of a reinforced soil retaining wall under blast loading (Brinkgreve and Yogendrakumar, 1992).

Due to the lack of knowledge about dynamic behaviour of geosynhtetic reinforced retaining structures, researchers focused on this subject. The study of Bathurst and Cai made one the first main research in geosynhtetic reinforced soil retaining walls. The writers have modeled dynamic response of geosynhtetic reinforced soil retaining wall that is constructed with dry stacked modular concrete blocks as facing system by finite element program TARA-3. Their constitutive model represents nonlinear

cyclic load response of both the soil and the reinforcement element. The finite element mesh included 650 elements and 657 nodes for 4.2 m high wall and comparison 16 concrete masonary units, a uniform granular backfill and five layers of high density polypropylene geogrid reinforcing extending 2.5 m into backfill soil. It is obvious that by the time the inventions in computer technology resulted that more finer meshes with much finer finite element meshes with more lement and detailed modeling. For the base reference acceleration (time history) (El-Centro, 1940) earthquake was used. The peak accelerations were 0.125 g and 0.25 g. They have highlighted the results of analysis, influence of dynamic loading or wall displacements, tensile forces developed in the reinforcement and acceleration response over the height of the wall (Bathurst and Cai, 1995).

A study with a very wide content was done by Bathurst and Hatami on seismic response analysis of geosynhtetic reinforced soil retaining walls. The authors mentioned that carefully conceived and executed numerical experiments offer possibility to improve the understanding of the effects of dynamic loading on reinforced soil structures and to demonstrate the influence of the primary component properties (reinforcement stiffness, number of reinforcement layers, base condition, wall geometry and facing type) on the system response to the earthquake. Their numerical experiments were carried out to investigate the influence of reinforcement stiffness, reinforcement length and toe restraint condition an the seismic response of an idealized six meter high geosynhtetic reinforced soil retaining wall constructed with a very stiff continuous facing panel with two dimensional, explicit, dynamic finite difference program (FLAC). The wall was subjected to base excitation using a variable amplitude harmonic motion with frequency close to the fundamental frequency of the structure. The frequency of the applied input base acceleration is representative of a typical predominant frequency of medium to high frequency content earthquakes (Bathurst and Hatami, 1998b).

In the same study also a second parametric analysis were carried out with a range of material damping ratios, variable width of numerical grid and different far-end truncated boundary conditions to investigate the effect of these model parameters on the predicted wall response. The responses of the wall to a scaled earthquake record

with the same peak acceleration as the reference harmonic motion was investigated.

In the results the writers concluded that wall displacements and reinforcement loads accumulated during base shaking. The magnitude of permanent wall displacement diminished with increasing reinforcement stiffness and increasing reinforcement length. The greatest influence on wall response is the choice of the base input record applied to the structure. The difference between the frequency of the base excitation record and the fundamental frequency of the model is the most important factor determining wall response to seismic excitation. They recommended that it may be prudent to select a numerical grid width that will capture the volume of the yielded soil in the retained soil zone predicted by pseudostatic methods (Bathurst and Hatami, 1998c).

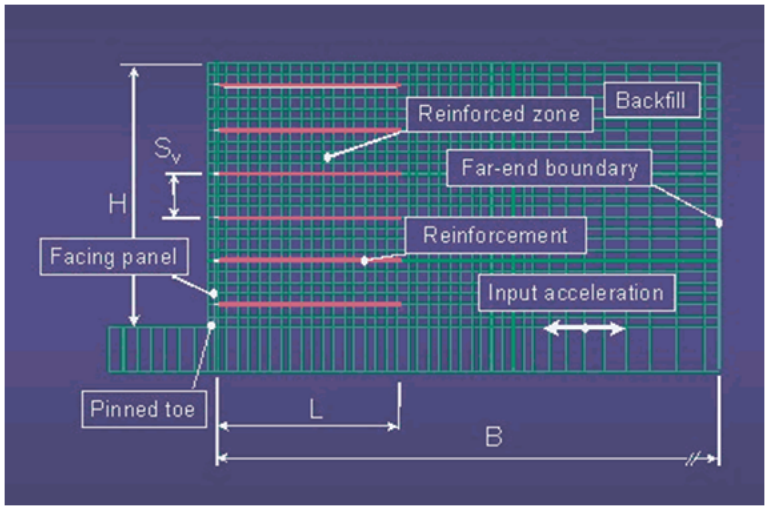

Figure 2.16. The finite difference model of reinforced soil retaining wall (Bathurst and Hatami, 1998c).

2.4. Performance of Reinforced Soil Structures during Recent Earthquakes

Largely qualitative observations of the performance of reinforced slopes and walls in USA, Japan and Turkey suggest that those structures perform well during seismic events when located on competent foundation soils and above water table. The relatively flexible nature of reinforced soil walls constructed with extensible and inextensible reinforcement is routinely cited as the reason for good performance of those structures during seismic event (Bathurst and Alfero, 1997).

In the below paragraphs the performance of the reinforced soil structures during Loma Prieta 1989 USA, Northridge 1994 USA, Grant Hanshin Kobe 1995 Japan, Ji-Ji 1999 Taiwan, and Kocaeli 1999 Turkey earthquakes will be reviewed from the observations of the researchers.

The performance of five reinforced slopes and walls that experienced the Loma Prieta earthquake of 1989 was evaluated by Collin in 1992. Two of these slopes were summarized as: A 3 m high geogrid wrap face wall with 4H:1V sloping backfill above the top of the wall located 11 km from the epicenter and estimated horizontal acceleration at the site was 0.4 g . Although their originals design in corporated a maximum horizontal acceleration of $0.1 - 0.2$ g, no cracks were observed on top of wall. Nearby this a 15 m high geogrid reinforced slope with a slope angle of 1H:1V was located 26 km from the epicenter and estimated horizontal acceleration of the site was 0.4 g. The face of the slope showed no sign of sloughing or damage. The performance of five reinforced soil slopes subjected to the Loma Prieta earthquake has shown that these structures can withstand severe ground motions (Collin *et al.*, 1992).

White and Holtz, (1997) reported the performance of seven geosynthetic reinforced slopes and wall allow which experienced significant to moderate shaking during Northridge, California earthquake 1994. The performance of the seven geosynthetic reinforced slopes and wall shaken in the Northridge earthquake was adequate particularly when compared to the performance of other structures in the immediate vicinity (White and Holtz, 1997). Similar performances were observed in Northridge earthquake with extensible reinforced walls (Reinforced Earth) as reported by Frankenberger. The structures include 21 Reinforced Earth walls supporting rail line, highways, freeways an on/off ramps, city street, refinery oil storage tanks, housing development and bridge abutments. The distance of the structures were from earthquake epicenter, range from 13 to 83 km. In this area, ground accelerations ranged from 0.46 to 0.66 g horizontal and 0.1 to 0.29 g vertical. Regardless of the wall locations relative to the epicenter, all structures have remained fully intact and structurally sound well (Frankberger, 1996).

The performance of geogrid reinforced soil walls during the Great Hanshin (Kobe)

earthquake in 1995 was reviewed by Tatsuoka, Koseki and Tateyama. In compression with other reinforced retaining structures as masonary leaning type and gravity type unreinforced concrete retaining walls showed very low stability against the strong seismic shaking. A number of geogrid reinforced soil retaining walls with full height rigid facing that are constructed in 1992 at Tanata, did not collapse despite the fact that the site was located in the one of the most severely shaken and seriously damaged areas. Tanata wall was located on the south slope of the existing embankment of JR Tohkaido railway line and was constructed to increase the number of railway trucks from four to five. The wall was 305 m in total length with a maximum height of 6 m. In the area surrounding Tanata side where seismic intensity of 7 was estimated that this wall experienced the highest seismic load among other modern retaining walls (Tatsuoka *et al.*, 1995, 1997).

Also researchers Nishimura and his colleagues report the findings of the onsite investigation of geogrid reinforced soil walls stricken by Kobe earthquake. They investigated ten geogrid Reinforced soil retaining walls, nearby the hypocenter where a seismic intensity of 6 to 7 was recorded. They found that although the earthquake caused some settlement and cracks in the foundation, the wall themselves were almost free of deformation (Nishimura *et al.*, 1996).

The performance of several modular block reinforced soil retaining walls a on reinforced slopes at the vicinity of the fault of Ji-Ji earthquake of Taiwan in 1999 was evaluated by Ling, Leschinsky and Chou. Reinforced soil retaining walls and reinforced slopes have gained wide popularity in Taiwan over recent years because many of large scale housing and industrial development sites located on the slopes and hillsides. Taiwan has a geotechnical conditions that rendered a less conservative and more challenging design comparing to North America, Europe and Japan. The Ji-Ji earthquake caused some damages to reinforced soil retaining walls in Taiwan. The writers gave attention on the cracks behind the wall indicated that few of the structures suffered compound failure or did not have adequate global stability. The lack of seismic design consideration could be a major cause of failures in the earthquake (Ling *et al.*, 2001).

Figure 2.17. Tanata Wall and the around structures after Kobe Earthquake.

And also following the August 1999 Kocaeli Earthquake (Mw:7.4) the authors Martin and Olgun performed field investigation in the affected area to document the performance of improved soil sites and mechanically stabilized embankments. The reinforced Earth system at Arifiye Bridge Overpass was constructed of steel strips and compacted select backfill, performed well despite being shaken with ground acceleration more than 0.3 g and being subjected to fault related ground displacement of 350 cm that occurred almost adjacent to the wall. An unreinforced earth embankment about 250 m from the wall suffered heavy damage, settling more than 1 m. The maximum permanent lateral movement of the wall facing panels was about 10 cm and this occurred at about one third of the wall height above the base. The settlement along the centerline of the double wall system was estimated at 25-30 cm primarily to lateral bugling of the system. The results suggested that well-designed conventionally constructed walls and with good foundation, tend to perform well under strong ground shaking (Olgun and Martin, 2002).

3. ARTIFICIAL NEURAL NETWORKS

3.1. Introduction

Artificial neural networks (ANNs) are a mode that tries to hit off the function of the human intelligence and nerve set-up. ANNs covers significant functional relations among the data in spite of their unknown and physical meaning which is difficult to explain. These are one of efficient methods which need prior knowledge about the nature of the relations through the data. ANNs are very suitable in order to build the elaborate situation of most geotechnical engineering materials that demonstrate extreme variability. They have an advantage over traditional modeling because there is not a necessity making theory about what kind of efficient rules regulate the problem in hand could be.

(Zurada, 1992) and (Fausett, 1994) described that ANNs consist of a number of artificial neurons known as 'processing elements' (PEs), 'nodes' or 'units'. For multi-layer perceptrons (MLPs), which is the most commonly used ANNs in Geotechnical engineering, processing elements in are situated as an input layer, an output layer and one or more intermediate layers called hidden layers (Figure 3.1)

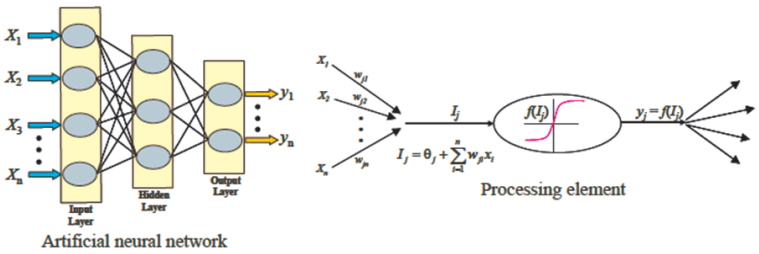

Figure 3.1. Typical structure and operation of ANNs.

With the help of weighted connections, that determine the strength of the connections between interconnected neurons, processing element is fully or partially connected to many other processing elements. These other processing elements receive weighted inputs which can be summed, added or subtracted. In consequence of enumeration

which is elapsed through transfer function in order to make the output of the processing element (Equation 3.1 and Equation 3.2 illustrated in Figure 3.1).

$$I_j = \theta_j \sum_{i=1}^{n} w_{ji} X_i \tag{3.1}$$

$$y_j = f(I_j) \tag{3.2}$$

where,

I_j = the activation level of node j;
w_{ji} = the connection weight between nodes j and i;
x_i = the input from node i, i = 0, 1, ..., n;
θ_j = the bias or threshold for node j;
y_j = the output of node j; and
f(.) = the transfer function.

The dissemination of data in MLPs begins at the input layer where the input data are submitted. During the process each input are weighted, summed and elapsed through a transfer function to make the nodal output. If the network cannot find a set of weights, that perform the input-output mapping, it will be still regulating its weights on presentation of a set of training. This process is called as 'learning' or 'training'

The learning of ANNs phenomena is based on supervised and unsupervised. If the network is only submitted with the input incentive and there are no acceptable outputs this is unsupervised learning. In this case network regulates the connection weights according to the input properties. According to supervised learning, the network is compared with acceptable output, and an error is counted up for connection weights

between the model inputs and outputs.

In accordance with feedback between processing elements, feed-forward and feedback networks belong to ANNs. In feed forward networks, the feedback between the processing elements are in the forward way only, whereas, in feedback networks, connections between processing elements are in both the forward and backward ways.

The ANN modeling philosophy is similar to a number of conventional statistical models in the sense that both are attempting to capture the relationship between a historical set of model inputs and corresponding outputs. For example, suppose a set of x-values and corresponding y- values in 2 dimensional space, where y= f(x). The objective is to find the unknown function f, which relates the input variable x to the output variable y. In a linear regression model, the function f can be obtained by changing the slope tanφ and intercept β of the straight line in Figure 3.2(a), so that the error between the actual outputs and outputs of the straight line is minimized. The same principle is used in ANN models. ANNs can form the simple linear regression model by having one input, one output, no hidden layer nodes and a linear transfer function (Figure 3.2(b)). The connection weight w in the ANN model is equivalent to the slope tanφ and the threshold θ is equivalent to the intercept β, in the linear regression model. ANNs adjust their weights by repeatedly presenting examples of the model inputs and outputs in order to minimize an error function between the historical outputs and the outputs predicted by the ANN model.

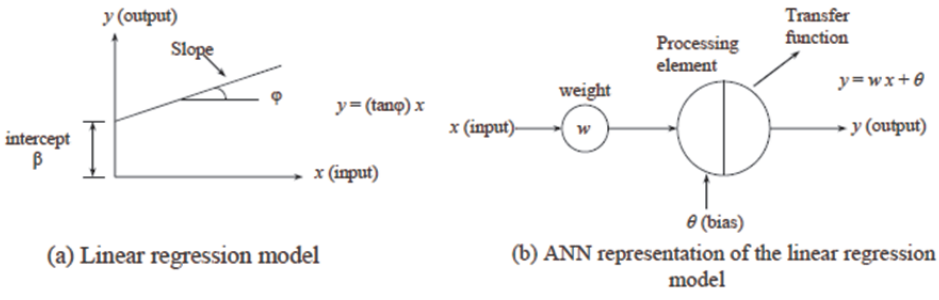

Figure 3.2. Linear regression versus ANN models.

ANN doesn't require the nature of the non- reality, that occur as a relationship

between x and y. The degree of non-linearity can be also replaced easily by varying the transfer function and the number of hidden layer nodes. In order to solve the highly non-liner problems ANNs can deal with by changing the transfer function or network structure, and the type of non-linearity can be replaced by changing the number of hidden layers and the number of nodes in each layer.

3.2. Artificial Neural Networks in Geotechnical Engineering

Starting from 1990s, ANNs have been used productively for solving major particular problems in geotechnical engineering. It find place in lots of literature sources that ANNs have been widely used for prescreening the axial and lateral load (Goh, 1994a; Chan, *et al.*, 1995; Das and Basudhar, 2006; Ahmad, *et al.*, 2007; Goh, 1996b; Lee and Lee 1996; Nawari, *et al.*, 1999; Rahman, *et al.*, 2001; Shahin, 2008; Hanna, *et al.*, 2004) ground anchors (Rahman, *et al.*, 2001; Shahin and Jaksa, 2004; Shahin and Jaksa, 2005a; Shahin and Jaksa, 2006).

Classical constitutive modeling is unable to imitate the situation of geomaterials because of formulation complexity, and undue empirical options (Adeli, 2001). According to this, many researchers (Basheer, 1998; Basheer, 2000; Basheer, 2002; Basheer and Najjar, 1998; Ellis, *et al.*, 1992; Ellis, *et al.*, 1995; Fu, *et al.*, 2007; Ghaboussi and Sidarta, 1998; Habibagahi and Bamdad, 2003; Shahin and Indraratna, 2006; Sidarta and Ghaboussi 1998; Tutumluer and Seyhan 1998; Zhu *et al.*, 1998a; Zhu *et al.*, 1998b; Zhu *et al.*, 1996) claimed that constitutive modeling is based on the elasticity and plasticity theoretician, and suggest neural networks as a dependable and practical disjunctive to modeling the constitutive monotonic and hysteretic behavior of geomaterials.

Mineralogy, fabric, and pore water control geotechnical properties of soils but it is difficult to find out interactions of these factors by traditional statistical methods due to their interdependence (Yang and Rosenbaum, 2002). In order to estimate several soil properties including the pre-consolidation pressure (Celik and Tan, 2005), shear strength and stress history (Kurup and Dudani, 2002; Lee *et al.*, 2003; Penumadu, *et al.*, 1994; Yang and Rosenbaum, 2002), swell pressure (Erzin, 2007; Najjar, *et al.*,

1996a), compaction and permeability (Agrawal, *et al.*, 1994; Goh, 1995b; Gribb and Gribb, 1994; Najjar, *et al.*, 1996b; Sinha and Wang, 2008), soil classification (Cal, 1995) and soil density (Goh, 1995b), methodologies have been developed which are based on the application of ANNs.

To prevent damage caused by failure of soils such as in liquefaction, there are different types ANNs being aware of many applications in geotechnical engineering include retaining walls (Goh *et al.*, 1995; Kung *et al.*, 2007), dams (Kim and Kim, 2008), blasting (Lu, 2005), mining (Rankine and Sivakugan, 2005; Singh and Singh, 2005), geo-environmental engineering (Shang, *et al.*, 2004), rock mechanics (Gokceoglu, *et al.*, 2004), site characterization (Basheer, *et al.*, 1996; Najjar and Basheer, 1996; Rizzo and Dougherty, 1994; Rizzo *et al.*, 1996; Zhou and Wu, 1994), tunnels and underground openings (Benardos and Kaliampakos, 2004; Lee and Sterling 1992; Moon, *et al.*, 1995; Neaupane and Achet, 2004; Shi, *et al.*, 1998; Shi 2000; Yoo and Kim, 2007). During earthquake liquefaction very often occurs and makes big damage to most civil engineering objects. Liquefaction is a well-known phenomenon and a lot of researchers (Agrawal, *et al.*, 1997; Ali and Najjar, 1998; Baziar and Ghorbani, 2005; Goh, 2002; Goh, 1994b; Goh, 1996a; Goh *et al.*, 1995; Hanna, *et al.*, 2007; Javadi, *et al.*, 2006) suggested using ANNs in order to prevent this type of damage like liquefaction and protect environment. This has attracted many researchers (Ural and Saka, 1998; Young-Su and Byung-Tak, 2006) to investigate the applicability of ANNs for predicting liquefaction.

3.3. Modeling Issues in Artificial Neural Networks

ANN models should be designed in a systematic way in order to show good results. Data division and pre-processing, the choice of suitable network architecture, careful selection of some internal parameters that control the optimization method, the stopping criteria and model validation - these are main principals in order to improve performance in a systematic manner.

3.3.1. Determination of Model Inputs

The main point in progress ANN models is to choose the model input variables with important influence on model performance and appropriate subset of input variables can sufficiently make better performance (Faraway and Chatfield, 1998). The network size is increased because of some amount of input variables and the same time it reduces processing speed and decrease the efficiency of the network (Lachtermacher and Fuller, 1994). Some options were suggested in order to choose input variables. One option is suitable input variables can be chosen beforehand (Goh 1994b; Najjar, *et al.*, 1996b); second option is to choose the network with appropriate work and prepare a lot of neural networks with different combinations of input variables. There can be other variant when separate networks are trained and if one of them shows good result it can be saved, connecting the variable that performs the best with each of remaining variables. This process is called a step-wise technique and it was described by (Maier and Dandy, 2000). Useful methods in searching the selection of input variables with the help of genetic algorithm that selects appropriate set of input variables. (Kavli, 1993) also suggests to algorithm adaptive spline modeling of observation data (ASMOD) for making parsimonious neurofuzzy networks that have great influence on the outputs.

All these options are modal based and this is their big gap because input parameters are subordinated to the error of a trained model which is not a function of the inputs, but also model structure and calibration. To solve this problem and make contribution to ANN models, utilization can be used for model-free options using correlation or mutual information, which belong to means linear or non- linear dependence measures.

3.3.2. Division of Data

ANNs also like convention statistical models are trying to make less error between model outputs and some measured values of specific data set. It have many numbers of model parameters (connection weight) if the number of degrees of the model is big comparing with the number of data points, the model cannot be suitable in general

situation, but can learn the idiosyncrasies of the specific data points used for calibration that leads to 'memorization', rather than 'generalization'. The main aim of ANNs is to non-linearly interpolate (generalize) in high-dimensional space between the data used for calibration (Minns and Hall, 1996; Tokar and Johnson, 1999). Appropriate data usually are split up into two subsets: an independent validation set for evaluation of model act in an environment and a training set to create the neural network model. Mixing of the above data division method is cross-validation (Stone, 1974) in which the data are split up into three sets: training, testing, and validation. To set the connection weights and at the same time adjusts the act of the model at different levels of training and find out when to pack up training in order to elude from over-fitting - this process is used by training set. The validation covers the evaluation of the trained network in the deployed environment. Using training, testing and validation the scientist tried to find out the most suitable correlation of the data (Shahin *et al.*, 2004b) and according to this investigation the best result was received when 20% of the data were used for validation and the other data were split up into 70% for training and 30% for testing.

Sometimes the leave-k-out method is used (Masters, 1993) because data can be too petty to work with model training and it is complicated to gather more data for validation. Therefore this leave-k-out method restrains little part of the data for validation and other part of the data for training. Then the trained network act is evaluated by validation set.

The division of data into their subsets can have important influence on the results obtained (Tokar and Johnson, 1999). In order to create best ANN model all samples that are included into the data should be a part of calibration set. For instance, if there are extreme data points in available data the model can't show good result the reason is that validation data will check not model's interpolation capability, but extrapolation. It is difficult to estimate the generalization capability of the model when all samples are included into the validation data. When the cross-validation is used as the stopping criterion, the results, received from testing set, must be presented by training set because testing set shows when to stop training. Different data subsets (e.g. training, testing and validation) must be similar in order to show that every

subset displays the same statistical population. Masters (1993) supported that data is used for calibration and validation have same statistical properties. In order to make less difference between standards divisions of the data in the training, testing and validation sets (Bowden *et al.*, 2002) used a genetic algorithm.

In order not to make complicateions in the process of division the data for training, testing and validation (Kocjancic and Zupan, 2000 and Bowden, *et al.*, 2002) suggested a self-organizing map (SOM). This map means to collect high-dimensional input and output data in two-dimensional space and split up appropriate data in such way that values of each cluster are shown in a different data subset. But there is a drawback of this system because of lack of guidelines for determining the optimum size and shape of the SOM and it can have big influence on the received results (Cai, *et al.*, 1994). Because the size of the SOM reflects cluster variation and if map large or small it makes difficult to select representative subsets. To avoid the size of clusters problem, a data division approach was suggested by (Shahin, 2004b). He explained that data division can work in a systematic way with the help of fuzzy clustering technique.

3.3.3. Data Pre-Processing

Before to be used to the ANN, the data is pre-processed in order to verify whether every variable was maintained while the training process (Maier and Dandy, 2000). Data scaling, transformation and normalization are variations of pre-processing and also can make faster a learning process (Masters, 1993). It is important to enlarge the output data because they must be corresponding to scope of the transfer functions used in the output layer (e.g. between -1.0 to 1.0 for the transfer function and 0.0 to 1.0 for the sigmoid transfer function). Concerning to the input data, it is not essential to be scaled because researches demonstrated that in spite of new or transformed data the model parameters were the same (Faraway and Chatfield, 1998).

3.3.4. Determination of Model Architecture

In ANN model progress the network architecture is very significant because of detailed choice of the quantity of layers and nodes in each of these. As concerns MLPs input and output variables are supported by two layers. There was discussion emerged about the function and influence of one hidden layer. On one hand one hidden layer is important to connect any continuous process, operating a sigmoidal activation function and this can solve problems of any surface of practical interest (Hecht-Nielsen, 1989) and on the other hand (Flood, 1991) claimed that there are so many variants in order to solve problem with surface, so that it is not enough using a sigmoidal network using one hidden layer, it doesn't provide the flexibility needed to model complex functions in many situations. (Lapedes and Farber, 1988) suggested two hidden layers such that one is used to determine the local features of the input patterns and the second hidden layer is useful for the global features of the training patterns. Though, according to (Masters, 1993) using two hidden layer slows down training process.

The quantity of nodes in the input and output layers is limited by quantity of model inputs and outputs. In order to know the number of nodes and in each hidden layer, trial-and-error procedure is used in geotechnical engineering problems. Big number of connection weights can bring to over fitting and inappropriate generalization (Maren *et al.*, 1990, Masters 1993). Therefore, availability of the quantity of minimum number of hidden nodes is much better because of (i) induces the network to reach good results of generalization; (ii) shrink the estimated time which is needed for training; (iii) analyzation of trained network is easier than before and solve the problem of over fitting. Some approaches are suggested for single hidden layer networks in order to get the acceptable number of hidden layer nodes. First approach is to take the number of hidden nodes to be 75% of the number of input units (Salchenberger *et al.*, 1992). Second approach offers to approve an upper bound and strat working from this bound. A third is to the quantity of hidden nodes ought to be located among the medium and number of the nodes in the input and output layers (Berke and Hajela, 1991). According to research, the complication surface of a network is because of one hidden layer. The rule of geometric pyramid states that the quantity of nodes is reduced from the

input layer towards the output layer. This rule is used for networks with two hidden layers (Nawari *et al.*, 1999).

Connection between the quantities of hidden nodes to the quantity of available training patterns is another way to obtain appropriate quantity of hidden nodes in order to perform well done model generalization (Maier and Dandy, 2000). There are rules-of-thumb that combine training patterns with the quantity of connection weights. Some researchers suggested different theories, (Rogers and Dowla, 1994) insist on less number of weights than the quantity of training patterns. (Masters, 1993) claimed that at least 2 minimum ratio is appropriate for the number of training patterns to the number of connection weights and 4 minimum ratio for the most favorable training patterns size to the number of connection weights. Hush and (Horne, 1993) contradicted saying that minimum ratio ought to be at least 10, even 30 doesn't cause overfitting.

For proper network architecture, (Ghaboussi and Sidarta, 1998) offered the adaptive method of architecture, to start from arbitrary and small number of nodes in the hidden layers. In the process of training, new nodes are connected with the hidden layers and new connection weights are generated in order get knowledge base that was not highlighted in old connection weights. In order to reach these results, some training interacts with new-made connection weights only, but old connection weights are stopped and this process is repeated. In the end of training, additional hidden nodes are used as much it needs and proper network architecture is appointed automatically. Bayesian approaches, noticed by (Kingston *et al.*, 2008), clearly can find out the proper quantity of hidden nodes, combining connection weight and an examination of the correlation structure. (Millert, 1989) insisted on genetic algorithm which offered optimal variants in order to get proper neural network architecture. The adaptive spline modeling of observation data (ASMOD) (Kavli, 1993) algorithm is good method in order to determine appropriate architecture of B-spline neurofuzzy network. To determine an appropriate architecture of ANNs, (Fahlman and Lebiere, 1990) suggested Cascade-Correlation as a constructive method. At first the neural network is trained working with Fahlman's quickprop algorithm not including hidden nodes with direct combination of the input layer and the output layer. Hidden nodes are used one or

few and at the same time give a connection to new hidden nodes as well as from the original inputs. During this process new hidden nodes are joined the network the input connection is frozen and output connections with the help of quickprop algorithm are trained. This procedure is over when there is no good result. Cascade - Correlation method identifies that adding a new single-nodes layer to the network and every time a new node is added - shows the method in which the hidden nodes are connected. This scheme was made in order to present the smallest map that can easily outline input-output connection and this is has a number of benefits: better generalization ability (Castellano *et al.*, 1997) and higher processing speed (Bebis and Georgiopoulos, 1994). But the automatic approaches in order to determine optimal network architectures can be presumed because they do not highlight the question of overfitting and can be presumed (Masters, 1993).

3.3.5. Model Optimization

"Training" or "learning" is model, optimizing the connection weights whose purpose is to determine a global compromise about the problem of a highly non-linear optimization (White 1989). There are some optimization methods simulated annealing and genetic algorithms (Hassoun, 1995). They are used to choose appropriate weight combination of feed-forward MLP neural networks. These methods have benefits as they are able to avoid local minima in the error surface and then find out proper solution of the problem. As a result, the model performance criteria will rule which training algorithm is most appropriate. If there is no problem in training speed, the back-propagation algorithm, which is based on first-order gradient descent, can't be used successfully (Breiman, 1994). Another variant is Least Mean Squared or Normalized Least Mean Squared learning rules used by updated weights of B-spline neurofuzzy networks (Brown and Harris, 1994).

3.3.6. Stopping Criteria

The training process are under supervision of stopping criteria that obtain information about appropriate or not model training and can stop the training process

(Maier and Dandy, 2000). There are several ways in order to stop training process: after performance of stable quantity of training records; when there is or not particularity of training error; when no sufficient changes happen in training error. As a result these stopping criteria processes can cause the model stopping in advance or over-training. In order to avoid this type of problem (Stone, 1974) suggested the cross-validation to escape from over fitting. Cross-validation technique demands split data into three sets; training, testing and validation, as it was highlight before. To regulate the connection weight training set is used. Determination the ability of the model to generalization, appropriate quantity of hidden layer nodes and proper meaning of the internal parameters (learning rate, momentum term and initial weights) are under supervision of testing set. Training and testing are closely connected to each other because of the incensement the error of the testing the training is stopped. And validation set estimates the efficiency of training set when it was done. According to stopping criteria of cross-validation, it demands the data to be split into only two sets; a training set to model scheme; and validation to test in order to check ability of the in the deployed environment. The process of model's work ought to connect model qualities with a number of training data and model error; this is the main point of stopping criteria.

3.3.7. Model Validation

Since training set of model has been finished effectively it must be validated. The aim of validation is to check the capacity of the model to generalize the limits set by to training data. If this type of procedure is appropriate, the model is considered robust that it can be generalized.

The coefficient of correlation, r, the root mean squared error, RMSE, and the mean absolute error, MAE, are the main criteria that are often used to evaluate the prediction performance of ANN models. The coefficient of correlation is a measure that is used to determine the relative correlation and the goodness-of-fit between the predicted and observed data. (Smith, 1986) suggested the following guide for values of $|r|$ between 0.0 and 1.0:

- $|r|$ > strong correlation exists between two sets of variables;
- $0.2 < |r| < 0.8$ correlation exists between the two sets of variables; and
- $|r| < 0.2$ weak correlation exists between the two sets of variables.

A well known measure of error is the RMSE and contributes to the fact that unlike all errors the large errors get more attention. But both RMSE, and MAE are needed during output data are smooth or ongoing. (Twomey and Smith, 1997). ANNS must be distributed throughout and present their ability they should give plausible prognosis according to relationship modeled and robusted under different circumstances. When ANNs are checked for errors, it can give prognosis for identical cases that are in training data and they will be reliable after data's appropriate estimation (Kingston *et al.*, 2005b).

The robustness of ANNs was used in prognosis the adjustment of shallow foundations on granular soils. (Shahin *et al.*, 2005c) discovered that good work of ANN models on the data that are used for model calibration and validation doesn't mean that the models will work properly in a robust fashion. (Shahin *et al.*, 2005c) suggested providing analysis to check the reaction of ANN's outputs to changes in its inputs. In order to obtain the model robustness the model prognosis must be examined whether they are in good relationship with known underlying physical processes. Also (Shahin *et al.*, 2005c) said that the connection weights can be considered as part of the interpretation of ANN model behavior. (Olden *et al.*, 2004) supported connection weigh approach because it is best way to number ANN input.

4. STRONG GROUND MOTION AND INTENSITY MEASURES

4.1. Introduction

In estimating strong-motion characteristics for seismic design, there is a need to define the parameters that reflect the destructive potential of the motion. The main target of engineering seismology is to provide quantitative estimates of expected levels of seismic ground-motion as the basic input to earthquake-resistant design, the evaluation of collateral seismic damages, such as liquefaction and landslides. This always requires characterizing the complex nature of strong-motion accelerograms by using simple parameters and the development of predictive relationships for these parameters. The first strong-motion accelerograms were obtained in the Long Beach earthquake of 1933. Since then, a lot of parameters have been defined in order to characterize outstanding features of the ground motion. Increasing numbers of parameters have been recently defined for this goal, plenty of them of increasing complexity. However, according to a great deal of academic researches done in this field, there is generally considerable ambiguity or conflict about the definition of even the simplest strong-motion parameters (Bommer and Martinez-Pereira, 2000).

How useful a strong-motion parameter is depends primarily on its purpose of use. There are a few parameters that can be used in earthquake-resistant design. In theory, any parameter can be used for the purposes of seismic risk assessment. In this case, the usefulness of the parameter will directly depend on the degree to which it is a measure of the effect of the motion. Researchers have shown that very few parameters, if any, can be sufficient in characterizing the nature of strong motion in isolation and many, by themselves, tell nothing about the effect of the shaking. It is also shown that there is a strong possibility to identify lower bound values for damage to occur in spite of the generally poor correlation between simple strong-motion parameters and damage levels (Bommer and Martinez-Pereira, 2000).

4.2. Description of the Intensity Measures

The main elements of earthquake engineering field and structural dynamics are ground motion time history records of acceleration, velocity and displacement. Those time series compromise a lot of information about the strong ground motion. Among those information included in time history record, amplitude, frequency content and duration characteristics of the strong ground motion are the most crucial ones for engineering purposes (Kramer, 1996). Several ground motion parameters, as an intensity measure, have been defined in the literature to reflect these characteristics. While some of them require some computational effort, others can be easily extracted from ground motion time series.

The crucial point of the seismic evaluation of the seismic response of the structure is the selection of ground motion intensity measure IM

Table 4.1. Intensity Measures (IM) used in the study.

IM	Description
PGA	Peak Ground Acceleration
PGV	Peak Ground Velocity
EPA	Effective Peak Acceleration
AI	Arias Intensity
CAV	Cumulative Absolute Velocity
ASI	Acceleration Spectrum Intensity
VSI	Velocity Spectrum Intensity
T_m	Mean Period
t_{eff}	Effective Duration

Peak Ground Acceleration (PGA) is among the simplest and most widely used ground motion parameters. PGA is the maximum absolute amplitude of the acceleration time history of a ground motion. PGA is sensitive to high frequency components

of the ground motion. Many attenuation relationships are readily available in literature for PGA (Douglas, 2001). Popularity of PGA originates from the relationship between the inertial forces and acceleration in seismic design. PGA does not present frequency content or duration of the ground motion.

Peak Ground Velocity (PGV) is the largest absolute value of velocity trace and, in recent years, has gained an increasing popularity. PGV is less sensitive to higher frequency components of the ground motion and may measure the damage more accurately than PGA at the intermediate frequencies. Prediction equations for PGV are also presented in the literature (Akkar and Bommer, 2007). Nonetheless, those equations do not fill too much space in literature when the prediction equations for PGA and spectral ordinates are taken into consideration. PGA and PGV are often used in fragility curves.

Effective Peak Acceleration (EPA) was first defined in ATC-3 (Applied Technology Council, 1978) report. It is calculated as the average of spectral acceleration values of elastic response spectrum between 0.1 s and 0.5 s divided by a constant value of 2.5 for 5% damping. Considering an acceleration trace with a single cycle of high amplitude and lower amplitudes in the other cycles, PGA value of that trace may not give sufficient information about the damage potential. As an alternative to PGA, EPA is computed by averaging the spectral values in the period range of 0.1-0.5 s divided by 2.5 as defined earlier to lessen the effect of local spikes. EPA is not necessarily same or proportional to PGA. Also, its relation with PGA strongly depends on the frequency content of the ground motion. EPA offers information regarding the frequency content and the amplitude of ground motion.

Arias Intensity (AI) was introduced by Arias (Arias, 1970) as ground motion intensity related to the energy content of the ground motion. Square of the acceleration is integrated over the whole length of the ground motion record (Equation 4.1). The assumption behind the formulation of AI is that the energy dissipated by the structure per unit weight is related to the damage occurred in that particular structure. AI is a cumulative representation of energy dissipated per unit weight by undamped SDOF

oscillators that have frequencies uniformly distributed between (0, ∞). Amplitude, frequency content and the duration characteristics of the ground motion are shown in AI. Empirical attenuation relationship for AI is demonstrated in Travasarou *et al.*, (2003).

$$AI = \frac{\pi}{2g} \int_0^{t_d} a(t)^2 dt \tag{4.1}$$

Cumulative Absolute Velocity (CAV) is the absolute area under the ground motion trace and was suggested in Electrical Power Research Institute (EPRI, 1998). Amplitude, frequency content and the duration characteristics of ground motion are demonstrated in CAV. This quantity is calculated by using Equation 4.2, where t_d is the total duration of the record.

$$CAV = \int_0^{t_d} |a(t)| dt \tag{4.2}$$

Acceleration Spectrum Intensity, (ASI) is defined as the area under the elastic acceleration spectrum between the periods 0.1-0.5 s (Von Thun *et al.*, 1988). This parameter was introduced to characterize strong ground motion for analysis and design of concrete dams, which usually have fundamental periods less than 0.5 s. (Von Thun *et al.*, 1988) stated that scaling design ground motions using ASI for concrete dams takes frequency content into consideration.

$$ASI = \int_{0.1}^{0.5} S_a(T, 5\%) dT \tag{4.3}$$

Formulation of *Velocity Spectrum Intensity* (VSI) is described as the in integral of the pseudospectral velocity (PSV) over the period of 0.1 to 0.25 seconds as given by the Equation. VSI can be computed by using GMPEs (Bradley *et al.*, 2009)

$$VSI = \int_{0.1}^{2.5} PSV(T, 5\%)dT \tag{4.4}$$

where PSV (T, 5%) is the 5% damped pseudospectral velocity.

Mean Period (T_m) is computed from the Fourier Amplitude Spectrum and defined as

$$T_m = \frac{\sum_i C_i^2(1/f_i)}{\sum_i C_i^2} \tag{4.5}$$

for 0.25 Hz $<$ f_i $<$ 20 Hz. Where $\mathbf{C}_i$ is the Fourier amplitudes of the entire accelerogram and fi is the discrete Fourier frequencies between 0.25 and 20 Hz. The Fourier amplitude is described as the square root of the sum of squares of the real and imaginary parts of the Fourier coefficient (Rathje *et al.*, 1998). (Rathje *et al.*, 1998) judged Tm to be the best simplified frequency content characterization parameter. Mean Period (Tm) can be estimated by using GMPE's (Rathje *et al.*, 2004).

Effective duration (t_{eff}) is based on the significant duration concept; however, both the start and end of the strong shaking phase are identified by absolute criteria.

4.3. SeismoSignal

SeismoSignal comprises an efficient and simple way to process strong-motion data, featuring a user-friendly visual interface and the capability of deriving a number of strong-motion parameters frequently required by engineer seismologists and earthquake

engineers, such as:

- Fourier and power spectra
- Elastic response spectra and pseudo spectra
- Overdamped and constant-ductility inelastic response spectra
- Arias (Ia) and characteristic (Ic) intensities
- Cumulative absolute velocity (CAV) and specific energy density (SED)
- Root-mean-square (RMS) of acceleration, velocity and displacement
- Sustained maximum acceleration (SMA) and velocity (SMV)
- Effective design acceleration (EDA)
- Acceleration (ASI) and velocity (VSI) spectrum intensity
- Predominant (Tp) and mean (Tm) periods
- Husid and energy flux plots
- Bracketed, uniform, significant and effective durations

The program can read accelerograms defined in both single- and multiple-values per line formats (the two most popular formats used by strong-motion databases), which may then be filtered and baseline-corrected. Polynomials of up to the 3rd order may be used for the latter, while three different digital filter types are accessable, all of which able to fulfill highpass, lowpass, bandpass and bandstop filtering (SeismoSignal, 2002).

4.4. Previous Studies on Strong-Ground Motion Parameters

Selected studies from the literature examining the adequacy of ground motion parameters to show the severity of ground shaking through analytical analyses as well as investigating the observed damage after earthquakes are briefly described below (Yılmaz, 2007).

Uang and Bertero, (1988) examined the adequacy of the parameters that have been used to identify the damage potential of an earthquake and reported that the destructiveness of a ground motion record at the foundation of a structure relies on the intensity, frequency content, duration and the dynamic characteristics of the structure.

They reached the conclusion that the most dependable parameter for measuring the damage potential is earthquake energy input.

Cabanas *et al.*, (1997) studied the correlation of AI and CAV with the observed damage stated through local intensity (MSK intensity) that proposes relationships for these intensity measures. A total of 25 strong motion records were picked out from the Campano Lucano, Umbria and Lazio-Abruzzo earthquakes. Damage data were assembled from more than 100 buildings in the neighborhood of the recording stations, where the maximum distance between the station and the observed building is 300 m (local intensity ranging between 5.5 and 7.5). AI and CAV are found to have an exponential relation with the local intensity. Damage data comprises three types of buildings: rural structures, ordinary brick buildings and precast concrete skeleton structures. Apart from the local intensity, correlation of both parameters with damage is investigated using the damage data gathered from different types of buildings. Amongst those aforementioned three types, rural structures show a clear exponential trend.

Sucuoglu, (1997) discussed the results of the study carried out by (Cabanas *et al.*, 1997) and concluded that PGA and PGV have stronger correlations than AI and CAV contrary to the priority given to AI and CAV.

Correlation of seven intensity parameters with surface wave magnitude (Ms) was investigated by (Sucuoglu *et al.*, 1999). Fifteen pairs of near-fault ground motion records with magnitudes ranging from 4.6 to 7.1 were employed. The aim of the selection of near-fault records is to reduce the effect of site-to-source distance and site response on magnitude. Results of the study mentioned above reveal that spectral parameters show stronger correlation with magnitude and effect of magnitude on response spectrum shows itself in the medium period range.

Wu *et al.*, (2004) examined the relationship between some ground motion parameters and earthquake loss and intensity by using 1999 Chi-Chi, Taiwan earthquake data. Earthquake loss is described in two various ways as the number of fatalities and

totally collapsed households, respectively. Among the ground motion parameters that are considered in the study, the two parameters that have the highest correlation with earthquake damage are PGA and Sa at 1 s. However, authors do not recommend using PGA as a damage assessment parameter in that a single spike with high frequency may lead to a misleading impression about the damage potential. As a second part of the study, (Wu *et al.*, 2004) investigated the correlation of ground motion parameters with intensity and declared that PGV and Sa at 1 s. are consistent parameters with intensity. (Wu *et al.*, 2004) studied on earthquake loss and intensity independently and came to the conclusion that PGV and S_a at 1 s. are more stable parameters in intensity estimation and earthquake loss assessment.

Cordova *et al.*, (2000) proposed a two-parameter seismic intensity measure which considers period softening faced in inelastic time-history analysis. Authors indicated that linear response spectrum quantities are not sufficient to reveal the inelastic behavior and corresponding period softening as the structure deforms into inelastic range. This new intensity measure is formulated as follows in Equation 4.6.

$$S^* = S_\alpha(T_1).[\frac{S_a(cT_1)}{S_a(T_1)}]^\alpha \tag{4.6}$$

Parameters c and a were determined by a calibration process as 2 and 0.5 respectively. Three six-story and one twelve-story moment frames (fundamental periods ranging from 1.3 to 2.1 s) were employed in the calibration process. Two sets of; general and near-fault records, eight ground motions were used in the study. This new intensity measure accounts for both spectral shape and spectral intensity. S* can easily be computed for a given S_a (T1) and Sa (cT1) in that there are attenuation relations available for spectral ordinates. (Elenas, 2000) examined the interdependency between seismic parameters and structural response, in terms of overall structural damage indices, by using an eight story reinforced concrete frame building (having a fundamental period of 1.18 s) that were designed in an accordance with Eurocode 8 (2003). A to-

tal number of 20 ground motions were employed in the analyses. Hysteretic behavior of the model is formed using the results of an experimental study performed on the typical members of the analyzed frame. Sa was found to be the parameter having the highest correlation with the overall structural damage. The same frame and ground motion data set were employed in (Elenas and Meskouris, 2001) so as to carry out a correlation study between the maximum interstory drift demand and floor acceleration with ground motion parameters and deduced that S_a has the highest correlation with both demand parameters. The results of (Elenas, 2000) and (Elenas and Meskouris, 2001) cannot be generalized because of the use of limited number of records and a single frame in the analyses.

Liao *et al.*, (2001) studied the response of two concrete moment resisting frames (twelve-storey and five-storey) exposed to near-fault ground motions. Liao *et al.*, using 22 near-fault ground motions, observed that maximum interstory drift increases as PGV/PGA, Sv and input energy increase for the analyzed frames. Results of this study are limited to the number of frames and records.

Having investigated the effect of PGV on SDOF response and interdependency between PGV and some ground motion features, (Akkar and Özen, 2005) highlighted PGV as a potential ground motion intensity measure for earthquake hazard analysis. 60 soil site records that have moment magnitudes between 5.5 and 7.6 with maximum source-to-site distance being 23 km are employed in the study. Records do not include pulse signals that may have notable effects on response. The study by (Akkar and Ozen, 2005) concluded that PGV has a good correlation with the earthquake magnitude, effective ground motion duration and frequency content of ground motions, and affirmed that PGV correlates better with SDOF response than PGA, PGV/PGA and S_a when different R (normalized lateral strength ratio) and constant p (ductility ratio) levels are considered.

The study of (Riddell, 2007) presents the result of a correlation study between 23 ground motion parameters and SDOF response. SDOF response was described in four distinct ways; elastic and inelastic deformation demands, input energy and hysteretic

energy respectively. Elastoplastic, bilinear and bilinear with stiffness degradation models exposed to 90 ground motions were employed in the analysis. Ground motion data was gathered such that all records have PGA larger than 0.25 g and PGV larger than 25 cm/s. (Riddell, 2007) found that none of the intensity parameters is sufficient over the three spectral regions. Ground acceleration related parameters have higher correlation in the acceleration-sensitive region, and parameters related to the ground velocity are more satisfactory in the velocity-sensitive region. Also, the same situation is valid for displacement-sensitive region. Considering average response for four distinct responses, for stiff structures PGA, AI and I_c are promising parameters, and PGV, HI and IF show higher correlation with response for intermediate periods.

5. FORMULATION OF THE NUMERICAL MODEL WITH FEA

5.1. Introduction

The well known program Plaxis was used for the finite element analysis (Brinkgreve, 2002). Plaxis is a state-of the art program, developed at the Technical University of Delft specifically for analyzing geomechanics and soil-structure interaction problems using the finite element method. Its development started in 1987, and since then the program has been extensively tested in academia and industry. Its capabilities to simulate dynamic earthquake condition and interface response between soil and other material were critical features for the application considered in this study. The newest version of Program Plaxis.2D2011 was used to conduct the finite element analysis.

The Plaxis code and its soil models have been developed to perform calculations of realistic geotechnical problems. In this respect Plaxis can be considered as a geotechnical simulation tool. The soil models can be regarded as a qualitative representation of soil behavior whereas the model parameters are used to quantify the soil characteristics. Although much care has been taken for the development of the Plaxis code and its soil models, the simulation of reality remains an approximation, which implicitly involves some inevitable numerical and modeling errors. Moreover, the accuracy at which reality is approximation depends highly on the expertise of the user regarding the modeling of the problem.

5.2. Geometric Assumptions

Two dimensional (2-D) plane strain analysis was performed. In reality, most geotechnical problems that involve earth retaining structures are three dimensional (3-D). However, computer resources for 3-D analyses are considerable and the undertaking is usually non-practical. Generally, the 2-D idealization is considered a reasonable

assumption for the central cross section of the anticipated structure (Rowe and Skinner, 2001).

In Plaxis the boundary conditions are identified as fixities. The conditions are applied to the model boundaries. The distinction can be made between horizontal fixity (u_x=0 ; horizontal displacement is zero) and vertical fixity (u_y = 0 ; vertical displacement is zero). In the geometry of our model the right and the left boundary had horizontal fixity and the bottom boundary had total fixity which means a combination of both horizontal and vertical fixites (u_y = 0 and u_x=0).

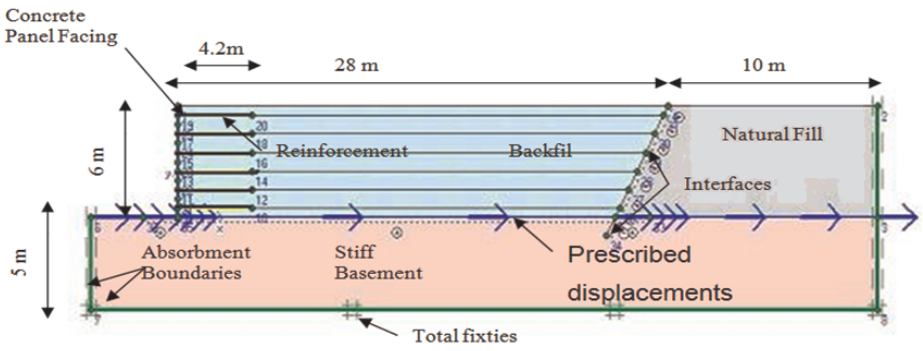

Figure 5.1. The geometry of one sided wall model.

Also in dynamic calculations the absorbent boundaries were used. The absorbent boundaries are special boundary conditions that have to define to account that in reality soil is semi infinite medium so without these special boundary conditions the waves would be reflected from the model boundaries, returning into the model and disturbing the results. To avoid these spurious reflection absorbent boundaries were specified at the bottom right and left side boundary. In order to minimize absorbent boundary effects on face deformation back to back retaining wall is the most adaptable and realistic design. It is easy to compare physical and numerical model of back to back retaining wall.

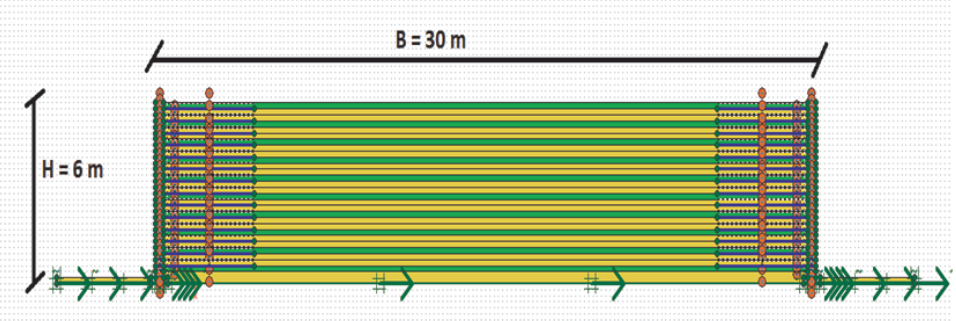

Figure 5.2. The geometry of back to back wall model (B/H=5).

5.3. Modeling of the Soil

The mechanical behavior of soils may be modeled at various degrees of accuracy. Hook e' law of linear, isotropic elasticity, involves only two input parameters, i.e. Young's modulus, E, Poisson's ratio, ν, it is generally too crude to capture essential features of soil and rock behavior. For massive structural elements and bedrock layers, however, linear elasticity tends to be appropriate.

Linear Elastic Model (LEM) is based on Hooke's law of isotropic elasticity. It involves two basic elastic parameters, Young modulus E and Poisson's ratio ν. Although the LEM is not suitable to model soil, it may be used to model stiff volumes in the soil, like concrete walls. Soil behavior is highly non-linear and irreversible. The linear elastic model is insufficient to capture the essential features of soil. Stress states in the LEM are not limited in any way, which means that the model show infinite strength.

The linear elastic perfectly-plastic Mohr-Coulomb Model (MCM) model involves five input parameters, E and ν for soil elasticity; φ and c for soil plasticity and ψ as an angle of dilatancy. This MCM represents a 'first-order' approximation of soil behavior. It is recommended to use this model for a first analysis of the problem considered. The shear modulus of the soil elements is calculated by the program in the formula of;

$$G = \frac{E}{2(1+\nu)} \tag{5.1}$$

Plaxis also support some advanced soil models such as Hardening soil, Soft soil, soft soil creep model, but in our study soil was modeled in Mohr Coloumb model. We used drained type of soil because of there is no water in our model.

Table 5.1. Material properties of soil.

Material Model	Unit Weight (γ_{dry})	Elasticity Modulus (E)	Poisson Ratio (ν)	Cohesion (c)	Internal Friction Angle (ϕ)	Dilatency Angle (ψ)
Mohr-Coulomb	18 kN/m3	30000 kN/m2	0.3	5 kN/m2	35°	0°

5.4. Modeling of the Reinforcement

The reinforcing elements could only sustain tensile forces and have no bending stiffness. These elements are used to model soil reinforcement as geotextile (woven fabric), geogrid, and metallic strips in the current analysis. The material property of reinforcement is the elastic axial stiffness (EA). In case elastoplastic behavior the maximum tension force in any direction is bound by N_p .The relationship between the force and strain is defined as:

$$N = EA_{\epsilon} \tag{5.2}$$

For geotextiles reinforcements EA=4,000 kN/m was chosen. NP=400 kN/m for 10% strain condition. This EA value was also used in many previous studies and incorporating similar parameters would provide a benchmark on the effect of reinforcement stiffness on wall static behavior and cyclic response (Bathurst and Hatami, 1998).

Reinforcement strips (made of galvanized mild steel) are modeled using line elements. The only material property that is needed to model a steel strip as a line element is the elastic normal (axial) stiffness per strip $(EA)_s$, where E is the modulus of elasticity and A is the cross sectional area of the strip. Based on the properties tabulated on Table 5.2, the cross sectional area is 0.0002 m^2, so the axial stiffness is $(EA)_S$ = 40,000 kN.

Table 5.2. Typical properties of steel strips used in reinforced soil applications.

Property	Symbol	Vale
Width (m)	b	0.05
Thickness (m)	h	0.004
Cross sectional area (m2)	A	0.0002
Modulus of elasticity (MPa)	E	200,000
Poisson's ratio (-)	V	0.3
Yield strength (MPa)	Fy	450
Ultimate tensile strength (MPa)	Fu	520

In order to model the reinforcement strips in plane strain analysis, an approximation has to be made. More specifically, discrete strips are replaced by a plate extended to the full width and breadth of the structure, i.e. strips are considered continuous in the out-of-plane direction (Figure 5.3). This assumption has been used for many years and provides reasonable results (Al-Hussaini and Johnson, 1979). The methodology for determining the equivalent properties of a continuous plate is the following:

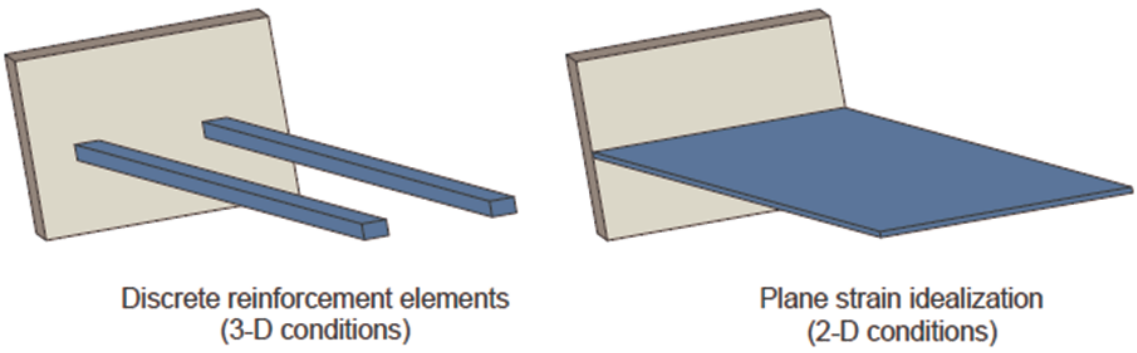

Figure 5.3. Modeling of discrete reinforcement elements in plane strain analysis.

The axial stiffness, S, of one strip is given by:

$$S = \frac{E_S A_S}{L_S} \tag{5.3}$$

where A_s, E_s, and L_s are the cross sectional area, the elasticity modulus, and the length of the strip, respectively. For N strips per linear meter, the equivalent stiffness, S_N, is given by:

$$S_N = \sum_{i=1}^{N} \frac{E_i A_i}{L_i} = N \frac{E_s A_S}{L_S} \tag{5.4}$$

where A_i , E_i, and Li are the cross sectional area, the elasticity modulus, and the length of the i^{th} strip, respectively. Replacing the N strips with one plate, the equivalent stiffness, S_{eq}, of this plate is given by:

$$S_{eq} = \frac{E_{eq} A_{eq}}{L_{eq}} \tag{5.5}$$

and the condition that must be satisfied is:

$$S_N = S_{eq} \tag{5.6}$$

Taking into account that $L_s = L_{eq}$, the above equation yields:

$$(EA)_{eq} = N.(EA)S \tag{5.7}$$

or

$$(EA)_{eq} = \frac{1}{S_h}(EA)S \tag{5.8}$$

where Sh is the horizontal spacing distance of the strips in reality. The thickness of the plate can be found using Equation 5.7 by substituting the cross sectional areas, A_{eq} and A_s, with $(b.h)_{eq}$ and $(b.h)_s$, respectively. For strips having the dimensions of Table 5.2, h_{eq} is given in mm by the following relation:

$$h_{eq} = 0.2N \tag{5.9}$$

Table 5.3. Plate characteristics in plane strain analysis.

S_h (m)	N	h_{eq} (mm)	$(EA)_{eq}$ (kN)
0.75	4/3	0.27	53.333
0.5	6/3	0.4	80.000
0.375	8/3	0.53	106.667

5.5. Modeling of the Facing Unit

In our parametric analysis modular block facing and precast concrete panel which are especially constructed with geosynhtetic reinforcing materials was used to determine the wall seismic response.

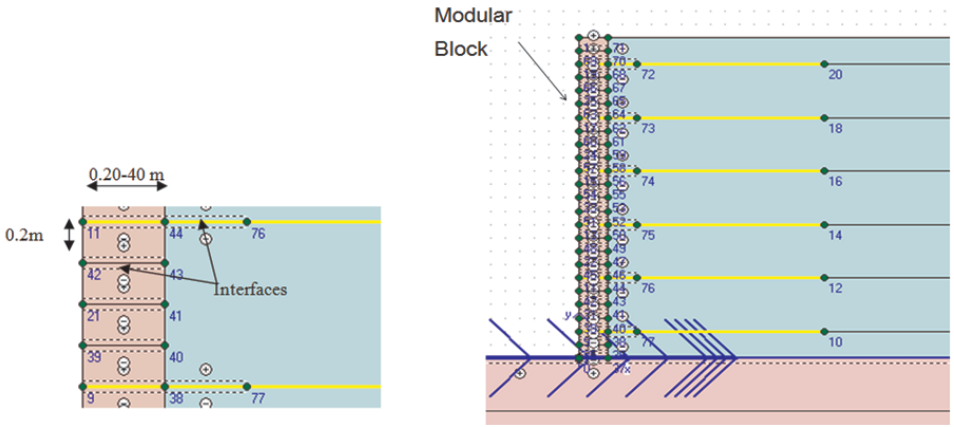

Figure 5.4. Modular block facing.

The modular block facing elements are modeled as soil element of 0.5 m width and 0.25 m in height between two modular block interfaces elements existed which will be described in the Section 5.7.

Table 5.4. Material properties of modular block facing.

Parameter	Material Model	Unit Weight (gdry)	Elasticity Modulus (E)	Poisson Ratio (ν)
Modular Block	Lineer Elastic	21 kN/m^3	4.4x106 kN/m^2	0.17

Precast facing panels are modeled using plates. These are elastic structural objects appropriate for modeling slender structures that extend in the z direction and that have a significant flexural rigidity (bending stiffness), EI and a normal (axial) stiffness, EA. Plate thickness, d_{eq}, is calculated from these two parameters as following (Brinkgreve, 2002).

$$d_{eq} = \sqrt{12\frac{EI}{EA}} \tag{5.10}$$

In 2D analysis, plates are composed of beam (line) elements. These are based on Mindlin's theory, allowing for deflection due to both shearing and bending. Typical properties of precast facing panels used in soil reinforcement applications are provided in Table 5.5.

Based on these properties, input values of EA and EI can be calculated as following: The cross sectional area A of the panels for one linear meter, perpendicular to the axial forces, is 0.20 m^2. So, the axial stiffness EA is equal to 5.000,000 kN/m. Taking into account that the thickness d of the panels is 0.20 m, the bending stiffness is found (from Equation 5.10) to be equal to $16,660.7$ kNm^2/m. Finally, for one meter height, the weight of the panels is found to be equal to 4.7 kN/m/m. Table 5.6 summarizes the properties of facing panels, as these were used as input in the analysis.

Table 5.5. Typical properties of precast concrete facing panels.

Property	Symbol	Value
Height (m)	h	0.6
Width (m)	w	0.6
Thickness (m)	d	0.2
Modulus of elasticity (MPa)	E	25.000
Poisson's ratio (-)	V	0.2
Unit weight (kN/m3)	Y	23.5
28-day compressive strength (MPa)	fc'	28

Table 5.6. Typical properties of precast concrete facing panels used in Plaxis.

Property	Symbol	Value
Axial stiffness (kN/m)	EA	5.000.000
Bending stiffness (kNm2/m)	EI	16.660.7
Thickness (m)	d	0.20
Weight (kN/m/m)	w	4.7
Poisson's ratio (-)	v	0.20

5.6. Modeling of the EPDM Bearing Pad

Modeling the EPDM (Ethylene Propylene Diene Monomer) or rubber bearing pads is often neglected in finite element analyses of reinforced soil structures (references). This is to say, the connection between facing panels is modeled by simple hinges and the compressibility that develops between them due to the presence of pads is neglected. However, this postulation does not allow for accurate assessment of the performance of facing panels, especially with respect to horizontal displacements. Since deformations are the main focus of the present study, rubber pads were modeled using the same type of elements that were used for the facing panels (elastic plates)(Zevgolis, 2007).

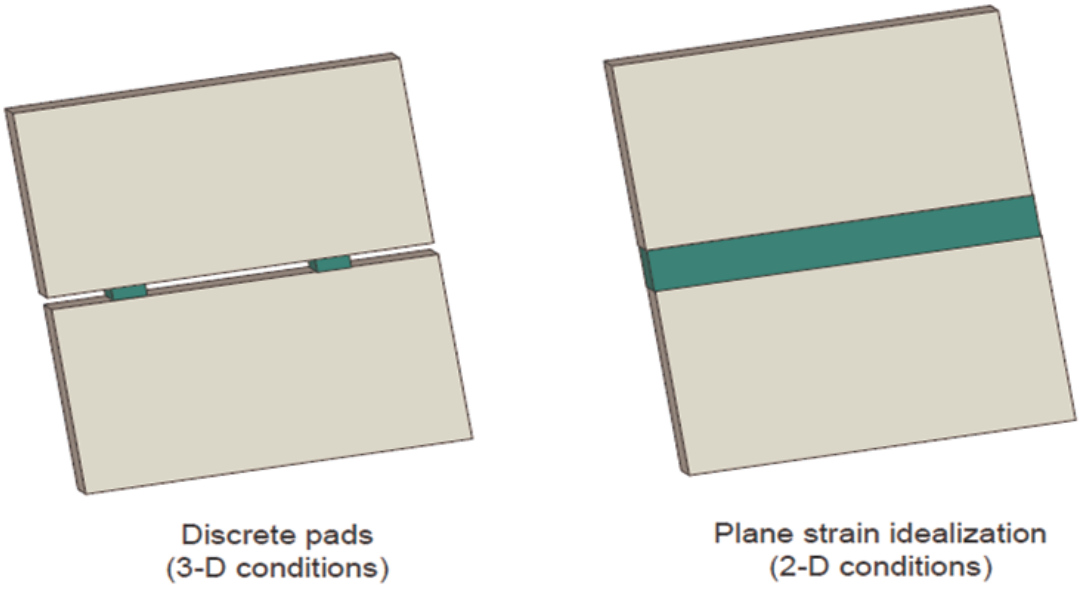

Figure 5.5. Modeling of discrete bearing pads in plane strain analysis.

Taking into account the cross sectional area of the pad, which is 0.0085 m^2, the axial stiffness is equal to 400.0 kN/m. However, this refers to one pad with dimensions 100 mm* 85 mm* 60 mm. In plane strain analysis Figure 5.5, the pad is replaced by a plate whose equivalent axial stiffness is given by:

$$(EA)_{eq} = N.EA \tag{5.11}$$

Considering two pads per panel, the number of pads per linear meter of wall is 4/3, so the equivalent axial stiffness $(EA)_{eq}$ is equal to 533.3 kN/m. Knowing the thickness of the pads (d = 0.085 m), the bending stiffness per linear meter is found equal to 0.321 kNm^2/m. Table 5.7 summarizes the properties of EPDM bearing pads as these were used as input in the analysis. Note that pads are assumed to be weightless and with a very high Poisson's ratio.

Table 5.7. Bearing pads input parameters.

Property	Symbol	Value
Axial stiffness (kN/m)	EA	533.3
Bending stiffness (kNm^2/m)	EI	0.321
Thickness (m)	d	0.085
Weight (kN/m/m)	w	0
Poisson's ratio (-)	v	0.495

5.7. Modeling of Interfaces

Interfaces are used to model the interaction between structures and soil. The roughness of the interaction is modeled by choosing a suitable value for the strength reduction factor (R_{inter}) in the interface. This factor relates the interface strength (wall friction and adhesion) to the soil strength (friction and cohesion). The strength properties of interfaces are linked to the strength properties of soil layer. The interface properties are calculated from the soil properties in the associated data set and the strength reduction factor by applying following formulation;

$$c_{inter} = R_{inter} x c_{soil} \tag{5.12}$$

$$tan\phi_{inter} = R_{inter} x tan\phi_{inter} \tag{5.13}$$

In the current finite element model, between the precast concrete panel and the backfill soil interface element existed. Nearby this, between all block elements there were interfaces. The strength reduction factor value 0.7 was taken between backfill soil and precast concrete panel and between modular blocks.

5.8. Cyclic Loading Applied to the Finite Element Model

The Finite element model was subjected to a base excitation, which is a variable amplitude harmonic motion. The frequency of the applied harmonic input base acceleration was representative of a typical predominant frequency of medium-to-high frequency content earthquake (Bathurst and Hatami, 1998). The constant frequency cyclic load was modeled by employing the prescribed displacement feature of the program at the base of the wall, which is shown in Figure 5.1 with right arrows. The cyclic load was applied at equal time intervals of 0.05 s and its variation with time is shown in Figure 5.4. This accelogram was also used by (Bathurst and Hatami, 1998) and has been accepted as a good representation of commonly encountered accelerograms. The accelogram has both increasing and decreasing peak acceleration portions and is expressed by Equation 5.14.

$$\ddot{U}(t) = \sqrt{\beta . e^{-\alpha . t} t \xi} sin(2.\pi . f . t) \tag{5.14}$$

where α= 5.5, β=55 and ξ = 12 are constant coefficients, f is frequency, and t is the time. The peak amplitude of the input acceleration was selected as 0.2, 0.4 and 0.6 g. A frequency of 3 Hz was selected to represent a typical predominant frequency of medium to high frequency content earthquake. Additionally, a frequency of 3 Hz was close to the fundamental frequency of the reference wall geometry as explained in the following section (Hatami and Bathurst, 2001).

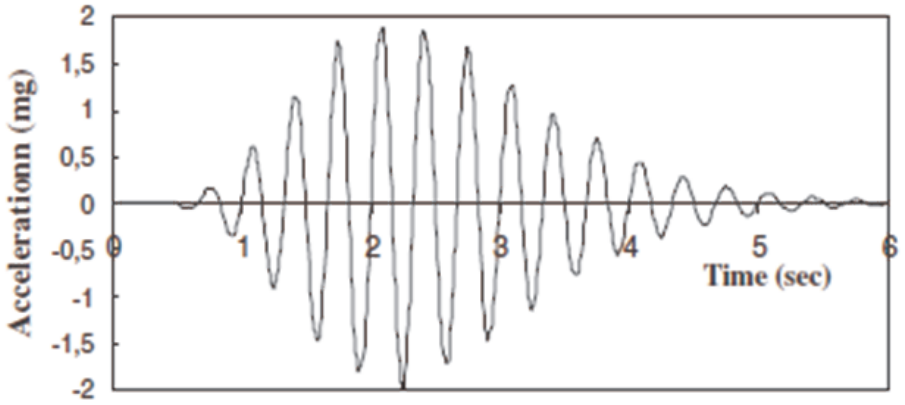

Figure 5.6. Base harmonic acceleration history used as cyclic load in the analysis (a_{peak}=0.2g).

5.9. Fundamental Frequency of the Analyzed Walls

The fundamental frequency of vibration for a two-dimensional, linear elastic medium of width 'B' and height 'H' contained between two rigid vertical boundaries and rigid base, which is subjected to horizontal base excitation, is given by (Bathurst and Hatami, 1998):

$$f = \frac{1}{4H} \cdot \sqrt{\frac{G}{\rho}} \cdot \sqrt{1 + (\frac{2}{1-\nu})(\frac{H}{B})^2} \tag{5.15}$$

where f is frequency in Hz, G is the shear modulus, p is density, and v is the Poisson ratio of the soil medium. For the present model, height of wall H was 6 m and the width B was 30 m. With a soil density (ρ) of 1.835 t/m^3, a shear modulus (G) of

11, 540kN/m^2, and a Poisson ratio (ν) of 0.3, the fundamental frequency of the wall was calculated as 3.45 Hz. This value is close to the frequency of the harmonic input acceleration record (f = 3 Hz) used in the numerical simulations (Guler, *et al.*, 2011).

A global damping term that was proportional to the mass and the stiffness of the system was used. Global damping was applied to the model using Rayleigh coefficients α and β. The Rayleigh alpha is related to the influence of the mass in damping and the Rayleigh beta is related to the influence of the stiffness in the damping of the system. This means that as the alpha value increases, the lower frequencies are damped more and as the beta value increases, the higher frequencies are damped more (Brinkgreve and Vermeer, 1998). A damping ratio of 5% was proposed for a conventional reinforced concrete cantilever wall with a height of less than 10 m and subjected to typical seismic excitation (Bathurst and Hatami, 1998). This value was believed to be conservative and therefore was used in the current study. The α and β parameters are adjusted to give this damping ratio.

6. VALIDATION ANALYSIS OF NUMERICAL MODEL

The finite element model used in the current research was validated for static conditions through a series of comparison analysis with actual test data and reported by (Guler *et al.*, 2007). The actual test data used for this purpose was a static loading test. In this paper it was shown that the model agreed well with outcomes of the actual test data.

In order to validate the finite element modeling technique under earthquake loading conditions results of a shaking test reported by (Ling *et al.*, 2005b) was used and results were compared and reported by (Guler *et al.*, 2011).

However to validate the Finite Element model under dynamic loading conditions, using the diffirent wall geometry, soil material model, reinforcement model, boundary properties etc, a new validation study was undertaken.

To check the accuracy of the Finite Element Model (FEM) used in this study, results of a 1-g shaking test reported by (Anastasopoulos *et al.*, 2010) was modeled using the same Finite Element modeling technique. Solutions obtained are compared to the results of the experiment.

6.1. Physical Model Configuration of Shaking Table Tests

As shown in Figure 6.1, the prototype refers to two reinforced earth retaining walls, both 7.5 m high, positioned back-to-back at 21.4 m distance, supporting a dry granular backfill. Each wall is reinforced with 13 rows of bar-mat grid, at 0.6 m vertical spacing. Each reinforcement row is 0.7H long (i.e. 5.12 m in prototype scale). Two types of reinforcement were selected: (i) a relatively "flexible" reinforcement grid, consisting of 8 mm bars at 20 cm spacing both in the longitudinal and the transverse direction; and (ii) a "stiff" reinforcement grid, consisting of 20 mm bars also at 20 cm spacing. In both cases, the facing panels are made of reinforced concrete, 0.2 m

in thickness, and 0.6 m in height. The models were constructed at 1:20 scale, taking account of the capabilities of the shaking table. The dimensions are given in model scale (prototype scale in parentheses).

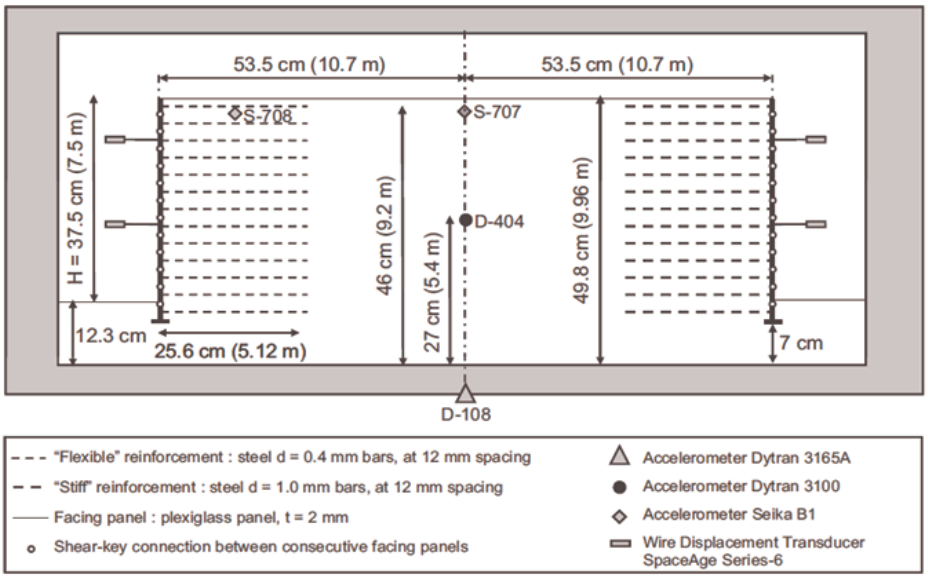

Figure 6.1. Shaking table model setup, showing geometry and instrumentation (Anastasopoulos *et al.*, 2010).

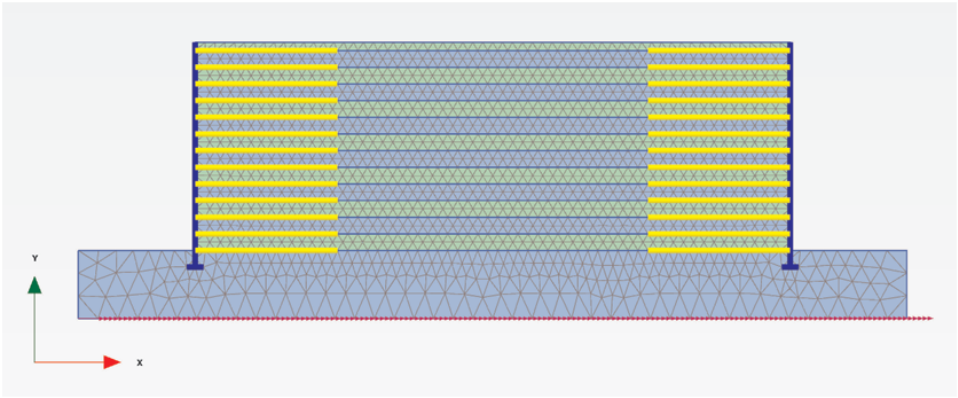

Figure 6.2. Numerical finite elements (Plaxis) model.

Taking account of the capacity of the shaking table, a N=20 scale factor was selected for the experiments, resulting to a total height of the model of 49.8 cm. The selection of model materials was conducted taking account of scaling laws (Gibson, A.D., 1997), as synopsized in Table 6.1, so that the simulation is as realistic as possible for the given prototype. The bar-mats were constructed using commercially available

steel wire mesh: d=0.4 mm at 12 mm spacing, for the "flexible" reinforcement; d=1 mm, also at 12 mm spacing, for the "stiff" reinforcement. Although the stiffness is not accurately scaled; this selection was made as a compromise between the target stiffness and the scaling in terms of the soil-reinforcement interface (which depends on geometry). The facing panels were made of t=2 mm Plexiglas strips (E=3 GPa), and were connected to each other through a customized connection, using a "shear key" configuration to block relative horizontal displacements between consecutive panels, but allowing differential rotation (as in reality).

Table 6.1. Scaling factors for 1 modelling (Anastasopoulos *et al.*, 2010).

Quantity to be scaled	1g scaling factor prototype to model ration	Cantrifugu scaling Factor prototype to Model ratio
Displacement	N	N
Time (dynamic)	$N^{0.5}$	N
Velocity	$N^{0.5}$	1
Acceleration	1	N^{-1}
Force	P^*N^3	N^2
Energy, moment	P^*N^4	N^3
Moment of inertia	N^5	N^4
Frequency	$N^{-0.5}$	N^{-1}

A series of two models were constructed and tested at the Laboratory of Soil Mechanics of the National Technical University of Athens (NTUA), utilizing a recently installed shaking table. The table, 1.3 m x 1.3 m in dimensions, is capable of shaking speci-mens of 2 tons at accelerations upto 1.6 g. Synthetic accelerograms, as well as real earthquake records can be simulated The retaining wall models were placed inside a rigid 160 x 90 x 75 cm (length x width x height) sandbox (Figure 6.3).

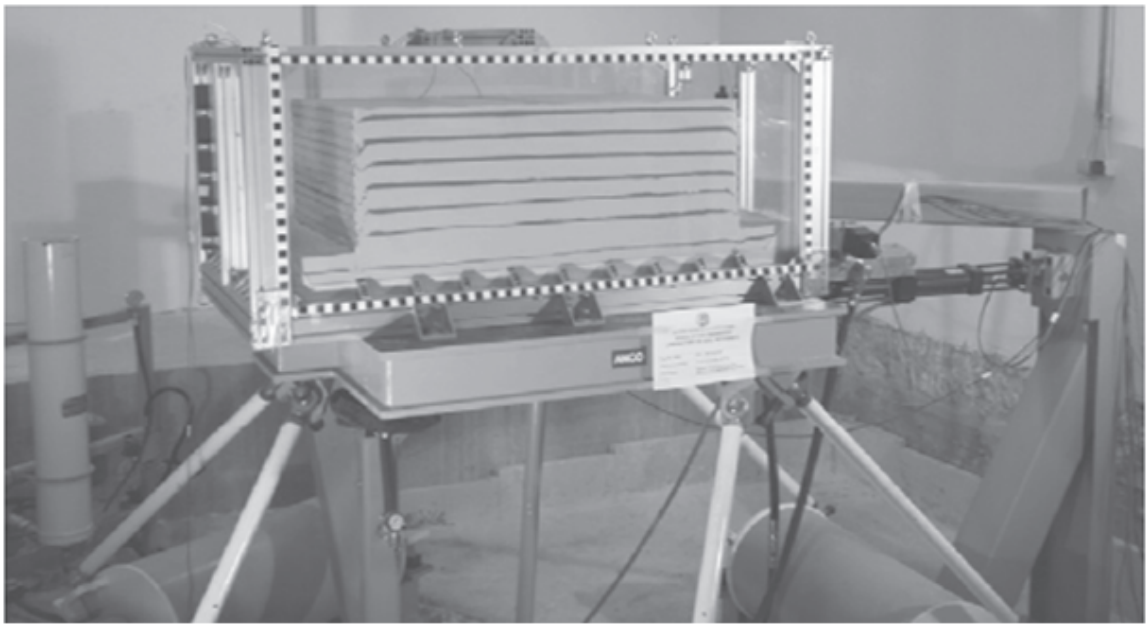

Figure 6.3. The sandbox consists of an aluminum space frame, covered with plexiglass panels to allow observation of the deformed specimen (Anastasopoulos *et al.*, 2010).

6.2. Backfill Preparation and Physical Properties

The backfill consisted of dry "longstone" sand, very fine and uniform quartz sand, industrially produced with adequate quality control. The first test model (Model-1) was constructed with D_r =44% (to represent the loose state), while the second test model (Model-2) with Dr =83% (dense state).

Direct shear tests were carried out to define peak and post- peak strength characteristics of the sand. For the dense specimens the angle of shearing resistance increases to φ=36° for higher stress levels indicating an angle of dilation ψ=6° Figure 6.4.

Table 6.2. Longstone sand index properties of validation model (Anastasopoulos *et al.*, 2010).

Spesific gravity, (G_s)	2.64
Maximum void ratio. (e_{max})	0.995
Minimum void ratio. (e_{min})	0.614
Median diameter, (D_{50})(mm)	0.15
Uniformity coefficient, (Cu)	1.42
Unit weight (kN/m^3)	18
Friction Angle(φ)	36°
Relative Density (D_r)	44%, 83%
Poission Ratio (ν)	0.3
Dilation Angle (ψ)	6°

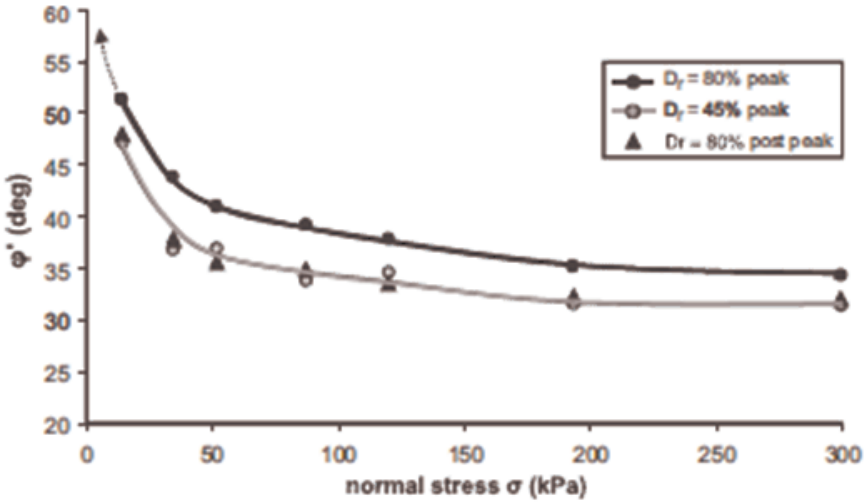

Figure 6.4. Direct shear test results: dependence of the angle of shearing resistance (Anastasopoulos *et al.*, 2010).

6.3. Testing Sequence and Seismic Excitation

As summarized in Table 6.3, two test series were conducted. In the first test series (Model 1), the backfill soil was loose (Dr = 43%) and the model was subjected to "extreme seismic shaking": a 60-cycle "cos sweep" of dominant period To=0.5 s and PGA= 1.0 g (Figure 6.4).

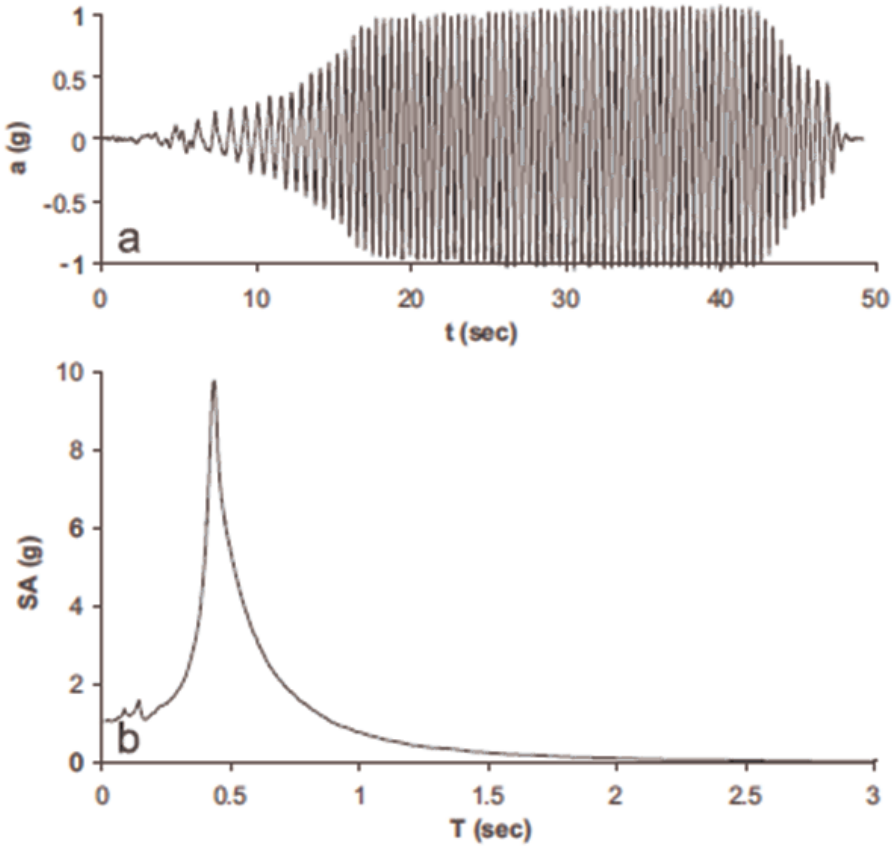

Figure 6.5. 60-cycle "extreme shaking" synthetic excitation and the corresponding elastic acceleration response spectrum (Anastasopoulos *et al.*, 2010).

Although not realistic (both in terms of retained soil density and shaking intensity), this test was conducted to derive deeper insights on the ultimate capacity of reinforced soil walls.

Table 6.3. Model configuration and shaking sequence of the two shaking table test series (Anastasopoulos *et al.*, 2010).

Model	Bacmfill	Seismic excitation	Peak acceleration (g)	Dominant Period (s)
Model 1	Loose D_r= 43%	Extreme shaking 60-cycle cos-sweep	1	0.5
Model 2	Dense D_r= 84%	Lefkada-1973	0.53	0.48
		Kalamata	0.27	0.36
		Lefkada-2003	0.42	0.35
		Rinaldi-228	0.84	0.72
		Cos swwep T= 0.4s	0.5	0.4
		Cos swwep T= 0.8s	0.5	0.8

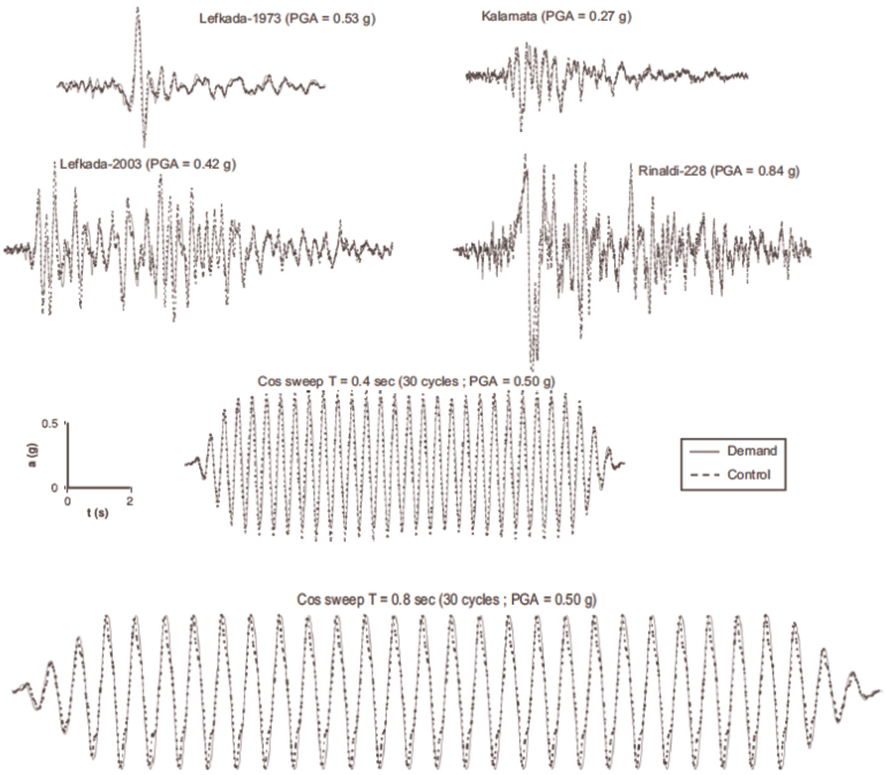

Figure 6.6. Real records and artificial multi-cycle accelerograms used as seismic excitations (Anastasopoulos *et al.*, 2010).

In the second test series (Model 2), a more realistic case of dense sand (Dr = 85%) was subjected to real earthquake records and artificial multi-cycle seismic motions Figure 6.6. The order of shaking events started with smaller intensity records, followed by the larger ones, and completed with multi-cycle artificial motions: the two 30-cycle so-called "cos sweeps" of PGA=0.5 g and To=0.4 or 0.8 s. The selected records cover a wide range from medium intensity earthquakes (Lefkada-1973, Kalamata) to stronger seismic events characterized by forward- rupture directivity effects (Rinaldi-228) or large number of significant cycles (Lefkada-2003).

6.4. Comparison of the Shaking Table Model and Numerical Model

Utilizing the finite element program Plaxis the analysis is modeled and conducted according to chapter 5.

Figure 6.7 shows to final position of the wall after 60-cycle "cos sweep" seismic excitation which has a period T0=0.5 s and PGA= 1 g.

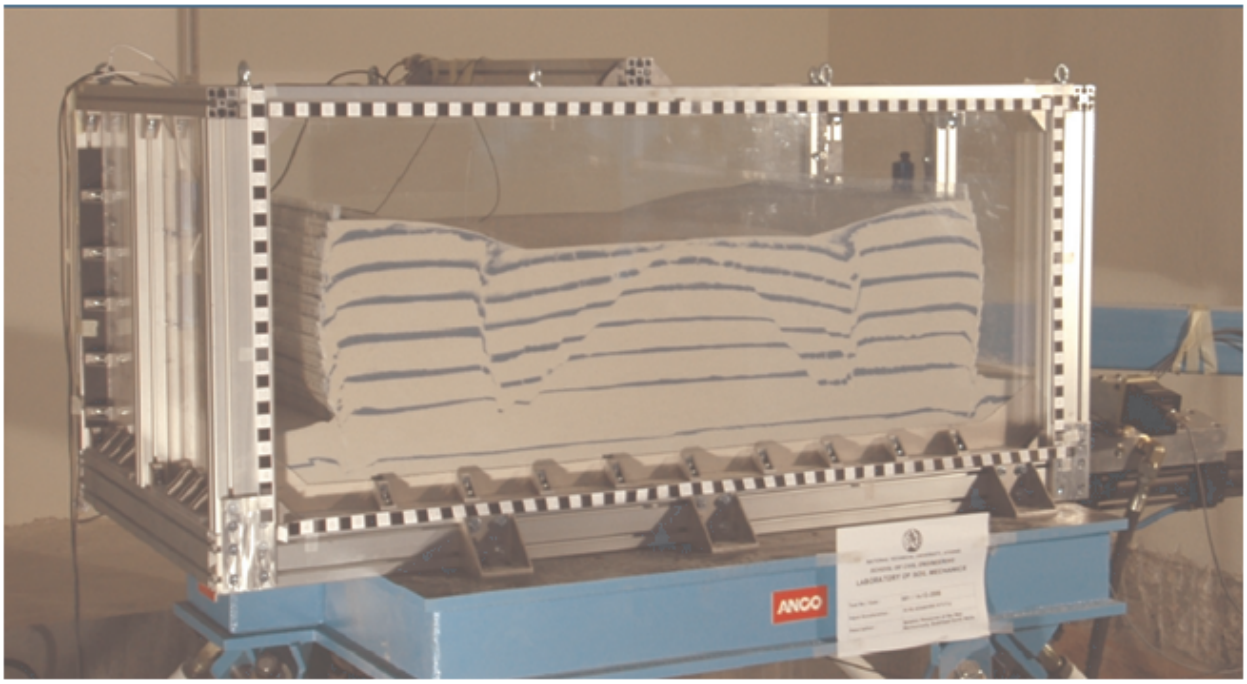

Figure 6.7. Shaking table test result after harmonic motion (60-cycle "cos sweep" of dominant period T_o=0.5 s and PGA= 1.0 g).

Figure 6.8 shows to Plaxis models final deformation position of the wall after 60-cycle "cos sweep" seismic excitation which has a period T0=0.5 s and PGA= 1 g.

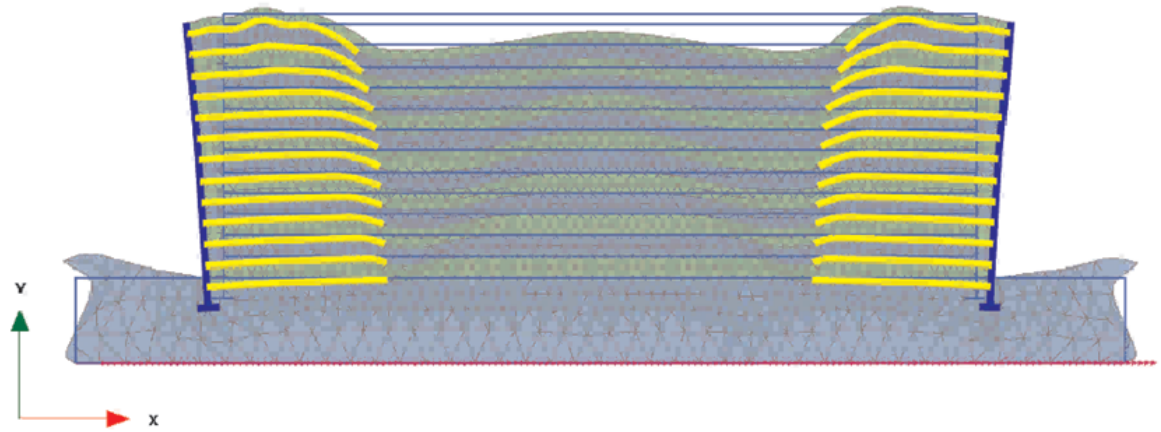

Figure 6.8. Plaxis output after harmonic motion (60-cycle "cos sweep" of dominant period T_o=0.5 s and PGA= 1.0g).

The results of the numerical analyses are summarized in Figure 6.9 and Figure 6.10. The results are shown for both sets of analysis (analysis of the shaking table test, assuming model parameters for small confining pressures; and analysis of the prototype, assuming model parameters for standard confining pressures). The first set (analysis of the shaking table model) is compared directly with shaking table test results, to serve as validation of the numerical analysis and of the Mohr Cloumb model. The second set (analysis of the prototype) is used as an indirect numerical prediction of the actual performance of the prototype.

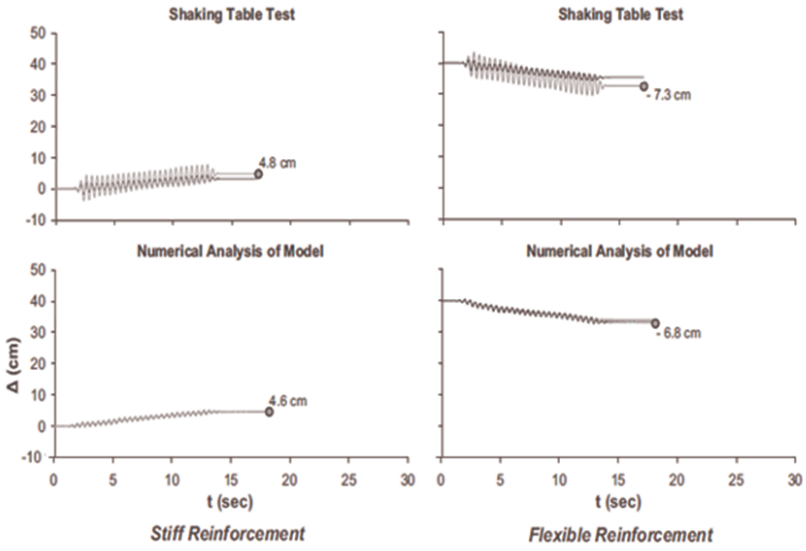

Figure 6.9. Wall displacement time histories for the multi-cycle seismic excitation of T=0.4 s.

As depicted in Figure 6.9 and Figure 6.10 the numerical prediction (analysis of shaking table model) compares well with the results of the shaking table tests for the two artificial 30-cycle cos-sweeps. The numerical analysis underestimates the cyclic component of the horizontal (lateral) wall displacement, but the examined herein (reinforcement stiffness and dominant period of residual displacement (the key performance indicator of retaining the seismic motion).

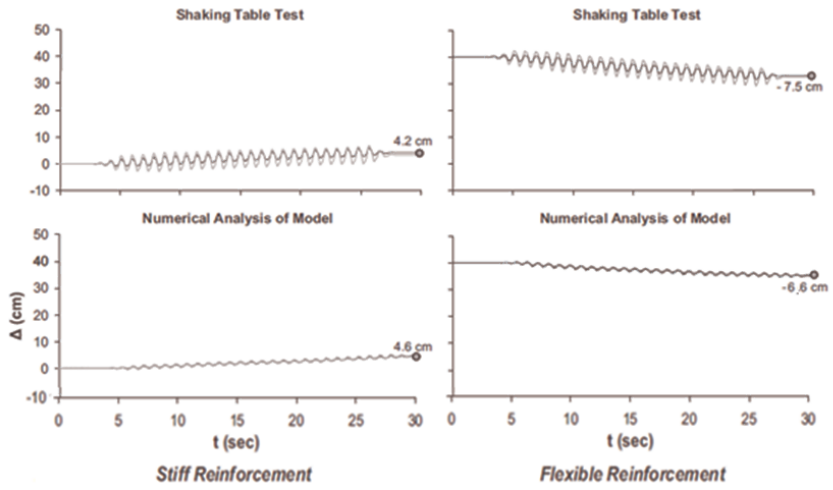

Figure 6.10. Wall displacement time histories for the multi-cycle seismic excitation of T=0.8 s.

7. RESULTS OF FINITE ELEMENT ANALYSIS

In addition to the displacements and stresses in the soil, the Output program of Plaxis can be used to view the forces in structural objects.

7.1. Permanent Lateral Displacement on Facing

Output module of Plaxis has a 3 type of demonstration for deformed mesh according to displacement. These are total displacement$|u|$, lateral displacement $|u_x|$ and vertical displacement$|u_y|$. Deformation distribution can be simulated by arrows, counter lines and shadings. Figure 7.1 shows deformed models $|u_x|$ after seismic loading by the means of shadings. Color scale on the right side of deformed model shows the displacement distributions of all systems.

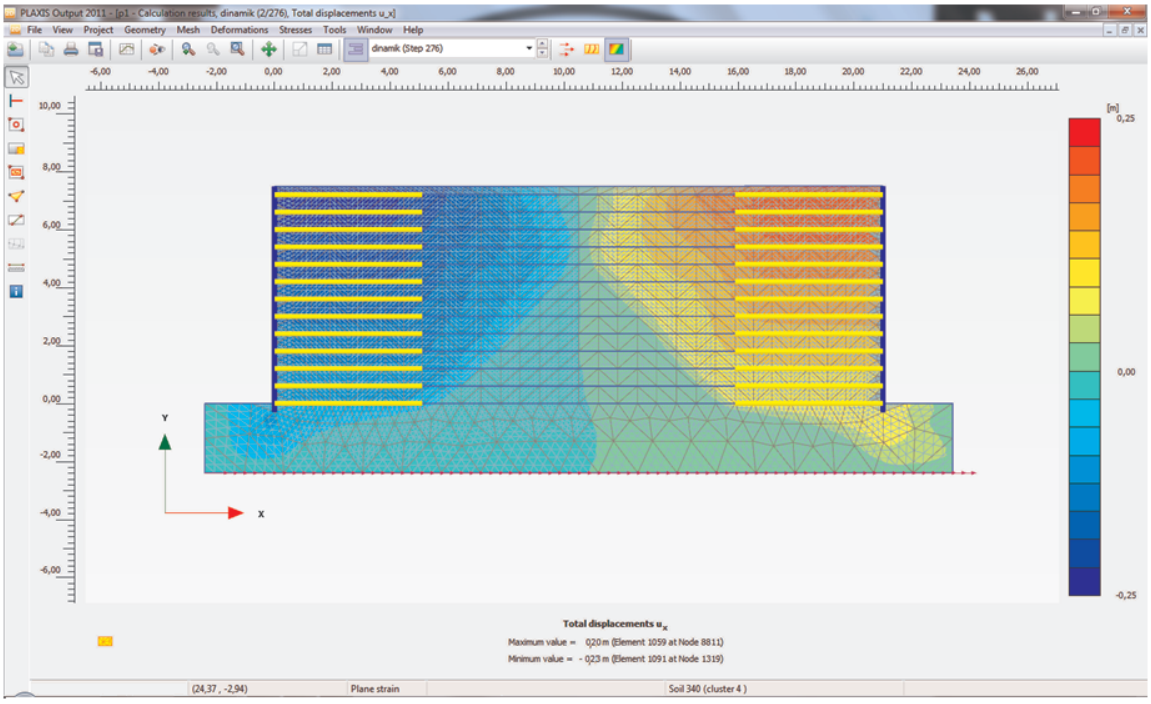

Figure 7.1. Deformed mesh after seismic loading (PGA= 0.2g).

7.1.1. Permanent Displacement According to Wall Height

Permanent displacement increases with height of wall and PGA value. Wall with modular block facing and precast concrete panel facing have different displacement increments behavior. Figure 7.2 and Figure 7.3.

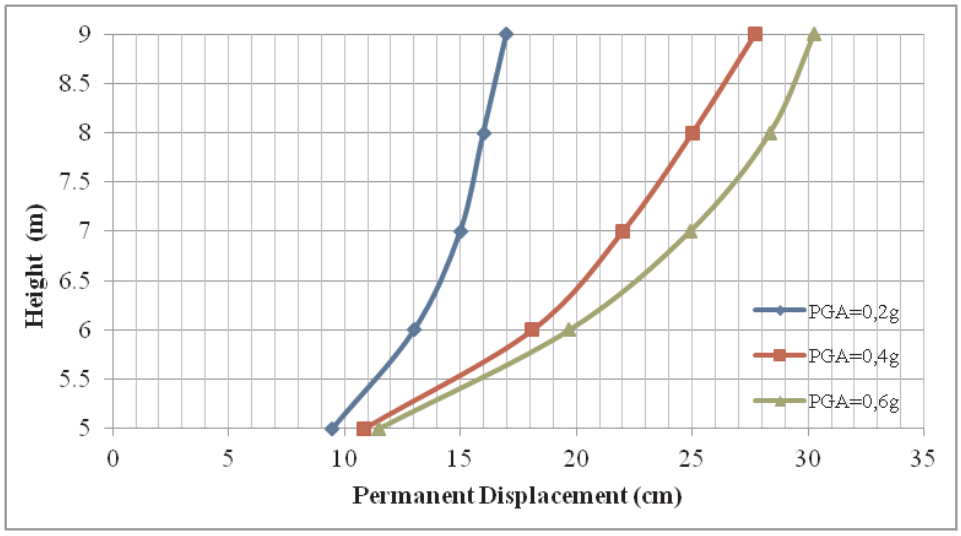

Figure 7.2. Permanent displacement according wall height (L/H= 0.7, S_v =40cm, modular block facing).

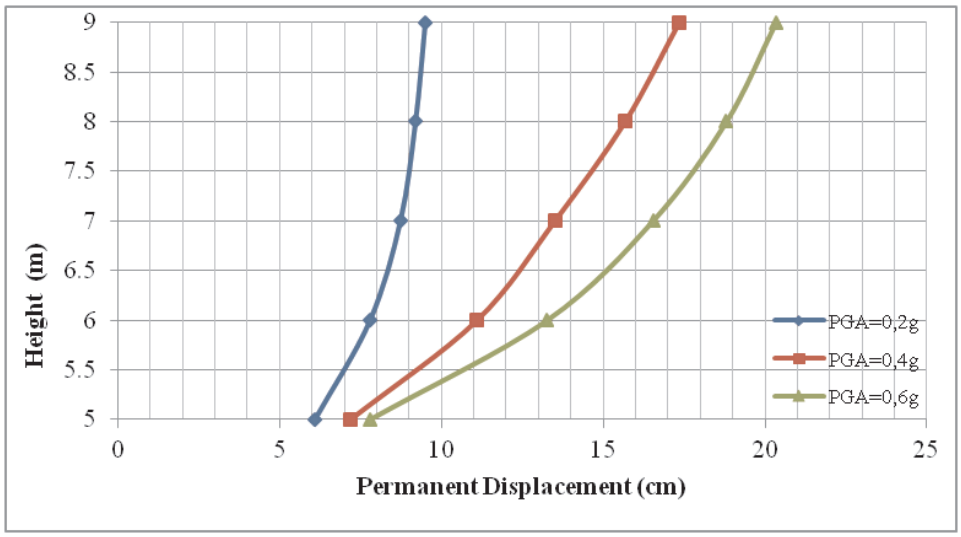

Figure 7.3. Permanent displacement according wall height (L/H= 0.7, S_v =40cm, precast concrete panel facing).

7.1.2. Permanent Displacement According to Reinforcement Length

Under the static loading condition, Figure 7.4 shows the empirical curve for estimating lateral displacement. This figure indicates that increasing the length-to-height ratio of reinforcements from its theoretical lower limit of 0.5 H to 0.7 H, decreases the deformation by 50 percent for static condition (FHWA, 2001).

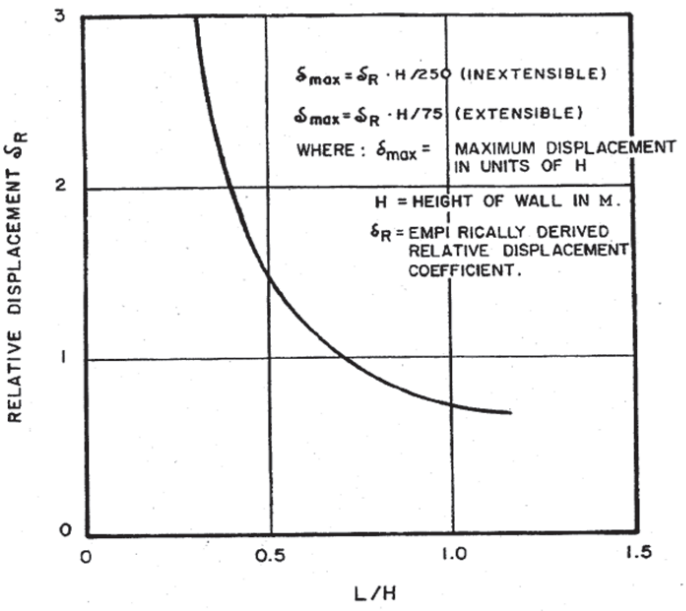

Figure 7.4. Empirical curve for estimating probable anticipated lateral displacement during construction for MSE walls (FHWA RD 89-043).

Formulation for dynamic loading condition which can be applicable for our FE models does not exist in FHWA guidelines. Relative displacements are obtained from static conditions in FHWA are compared with dynamic condition in our study. In order to obtain this r curve at Figure 7.5, formulation 7.1 is derived by using max values from Plaxis results for different L/H ratios and S_v=0.2 m.

$$\delta_{max} = \delta_r . H/50 \tag{7.1}$$

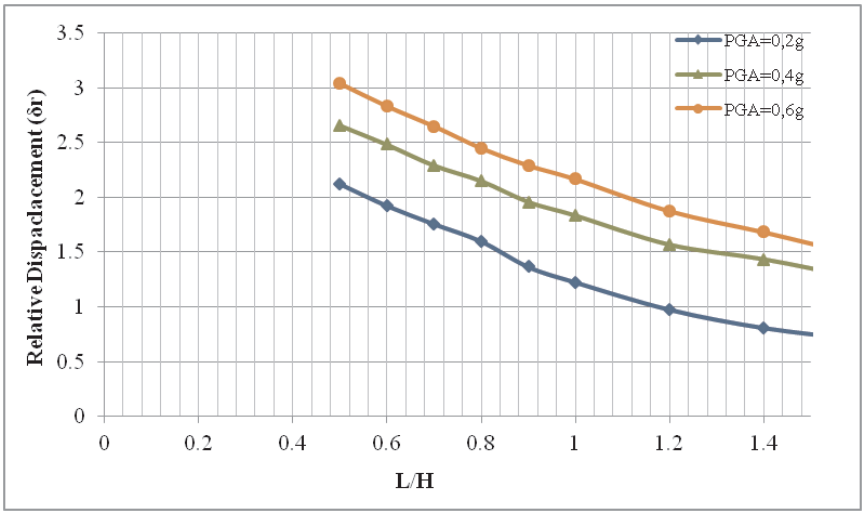

Figure 7.5. Empirical curve for estimating probable anticipated lateral displacement during construction for MSE walls (FHWA RD 89-043).

In order to obtain this r curve at Figure 7.6, formulation 7.2 is derived by using max values from Plaxis results for different L/H ratios and S_v=0.4m.

$$\delta_{max} = \delta_{r.} H/65 \tag{7.2}$$

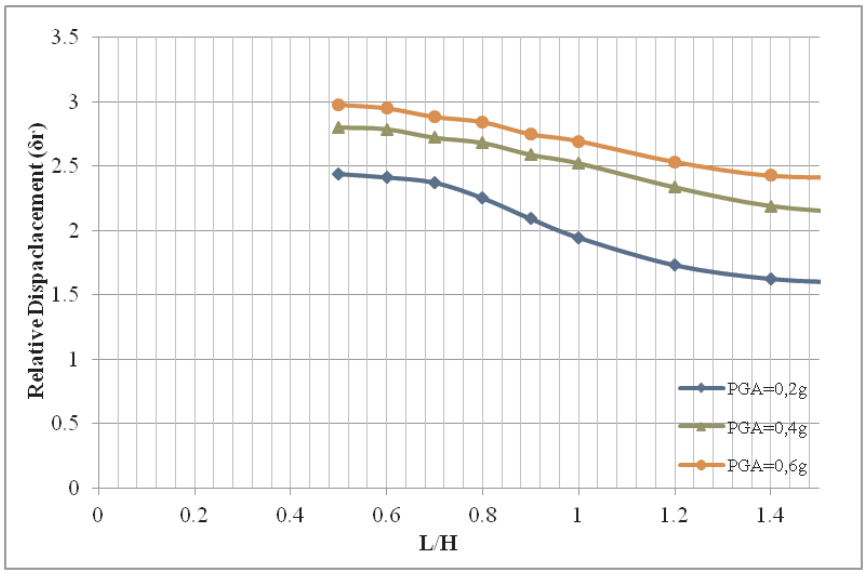

Figure 7.6. Relative displacement factors according to L/H (S_v=40 cm).

7.1.3. Permanent Displacement According to Reinforcement Vertical Spacing

As it can be seen in Figure 7.7 displacement values normalized by height are increased with increasing vertical spacing values.

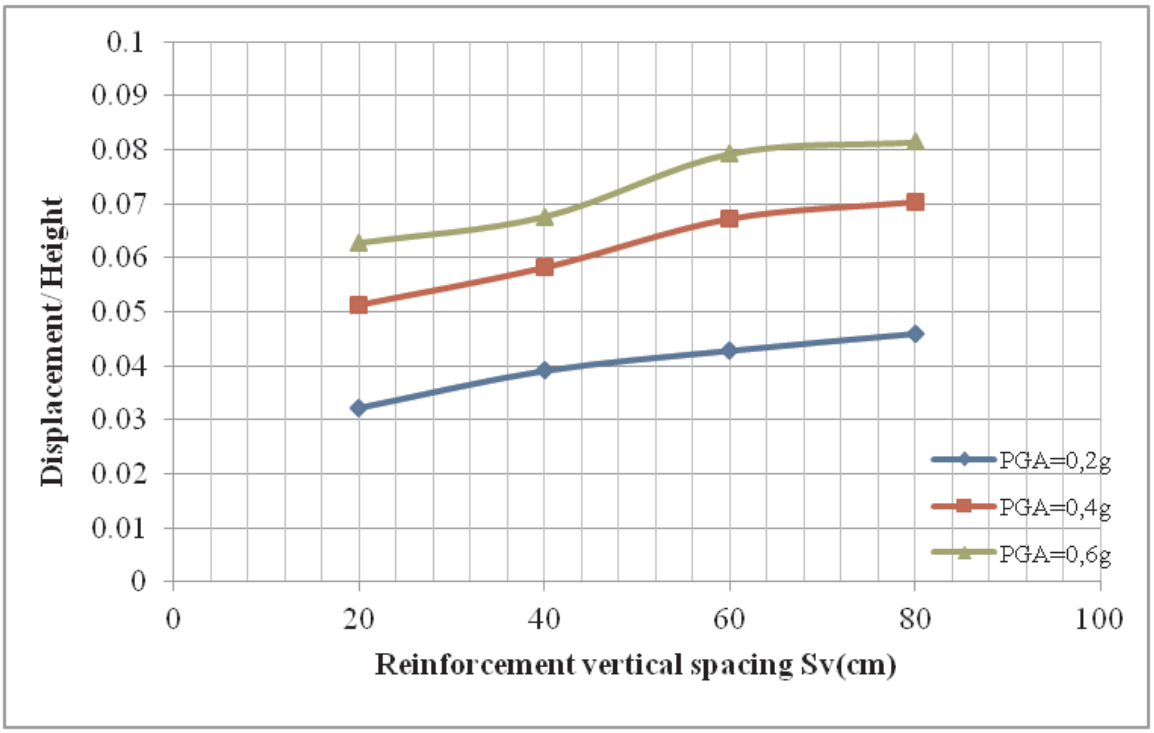

Figure 7.7. Displacement/Height according to vertical spacing S_v (L/H=0.7 H=7 m).

7.2. Maximum Tensile Stress on Reinforcement

7.2.1. Vertical Spacing (S_v) Effect on Maximum Tensile Stress on Reinforcement

Under dynamic loading condition maximum tensile forces on reinforcements are more than static condition as it is shown in Figure 7.8.

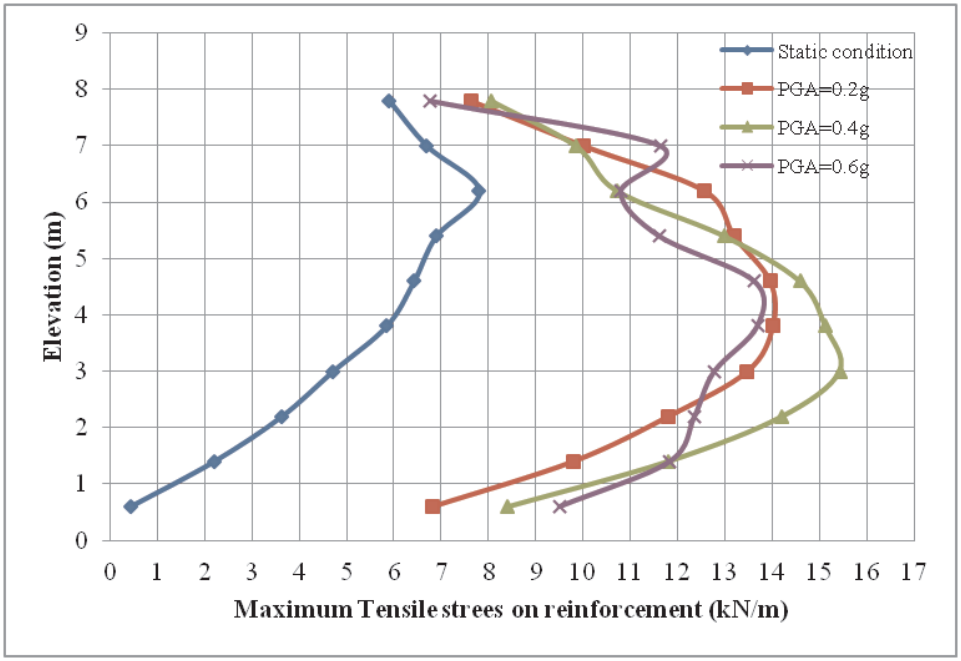

Figure 7.8. Maximum tensile stresses according to elevation for different static and dynamic loading (S_v= 80 cm, L/H=0.7).

Maximum tensile stresses on reinforcements are increased with increasing vertical spacing values as it can be seen in Figure 7.9 for static condition and PGA=0.4g.

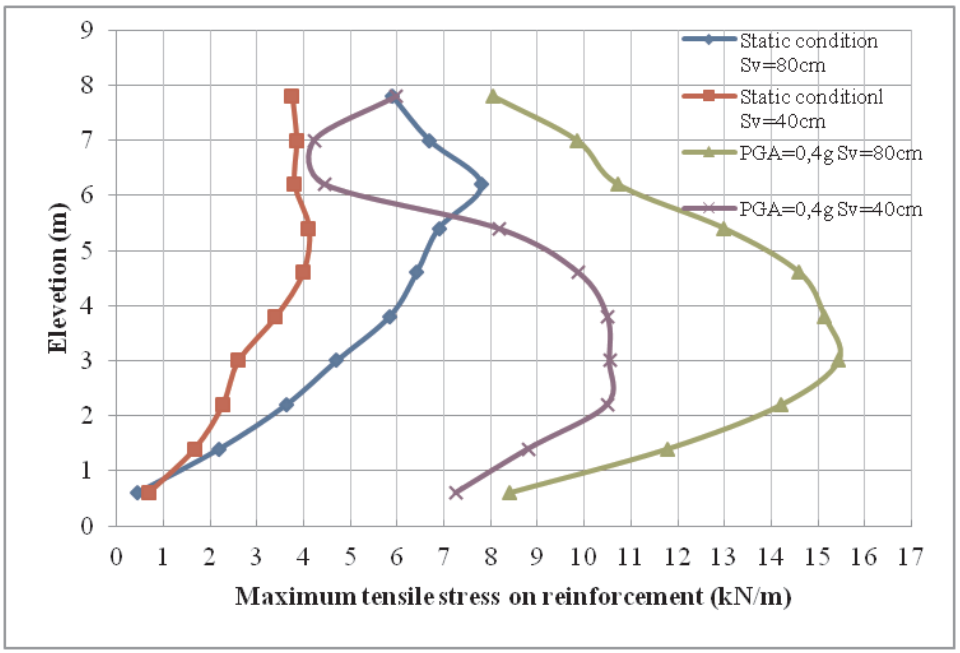

Figure 7.9. Maximum tensile stresses according to elevation for different static and dynamic loading (S_v= 80 cm, L/H=0.7).

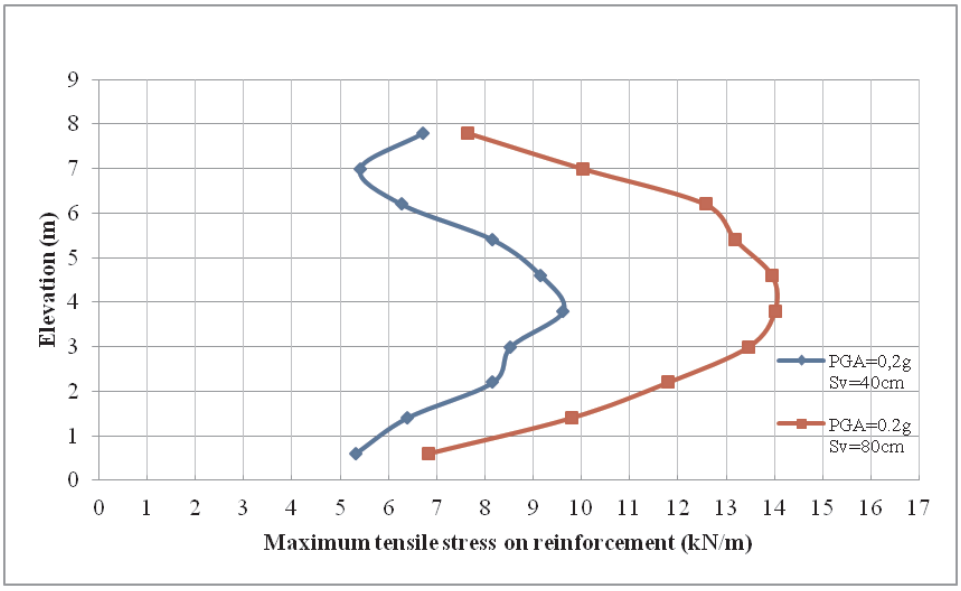

Figure 7.10. Maximum tensile stresses according to elevation (PGA = 0.2g, L/H=0.7).

Maximum tensile stresses on reinforcements are increased with increasing vertical spacing values as it can be seen in Figure 7.10 and Figure 7.11 for PGA=0.2 g and PGA=0.6 g, respectively.

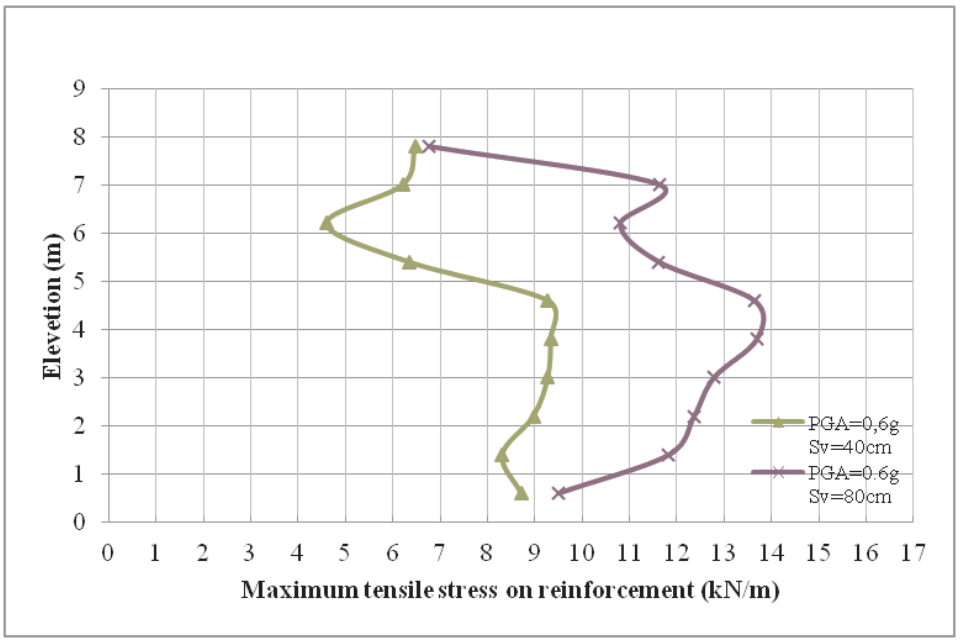

Figure 7.11. Maximum tensile stresses according to elevation (PGA = 0.6g, L/H=0.7).

7.2.2. L/H Effect on Maximum Tensile Stress on Reinforcement

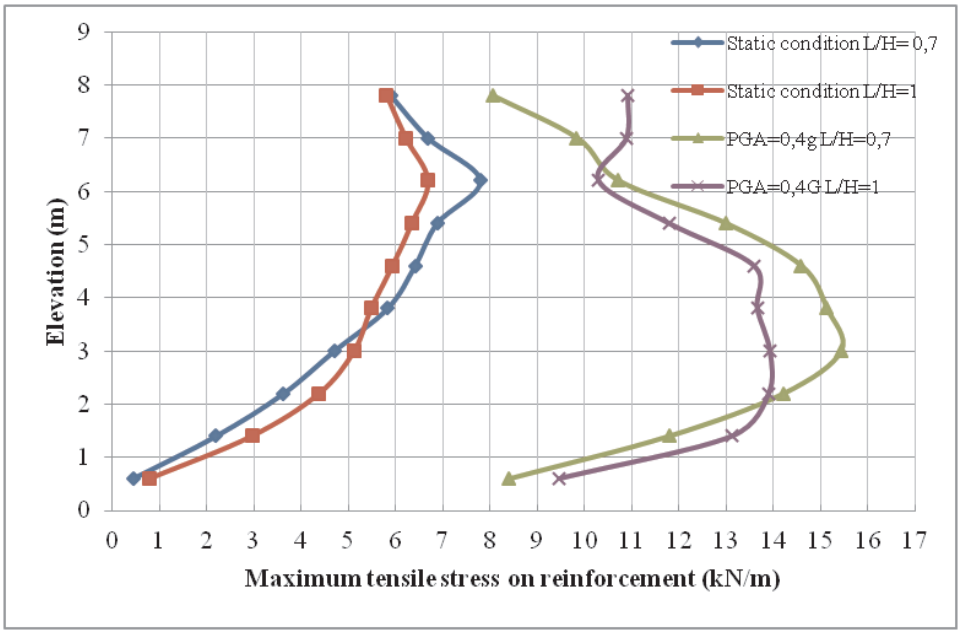

Figure 7.12. Maximum tensile stresses according to elevation (S_v=80).

Increases of reinforcement lengths decrease maximum tensile stress on reinforcement as it can be seen in Figure 7.12. The stress distribution on reinforcement is normalized with the help of this increase of reinforcement length as it is seen in Figure 7.13.

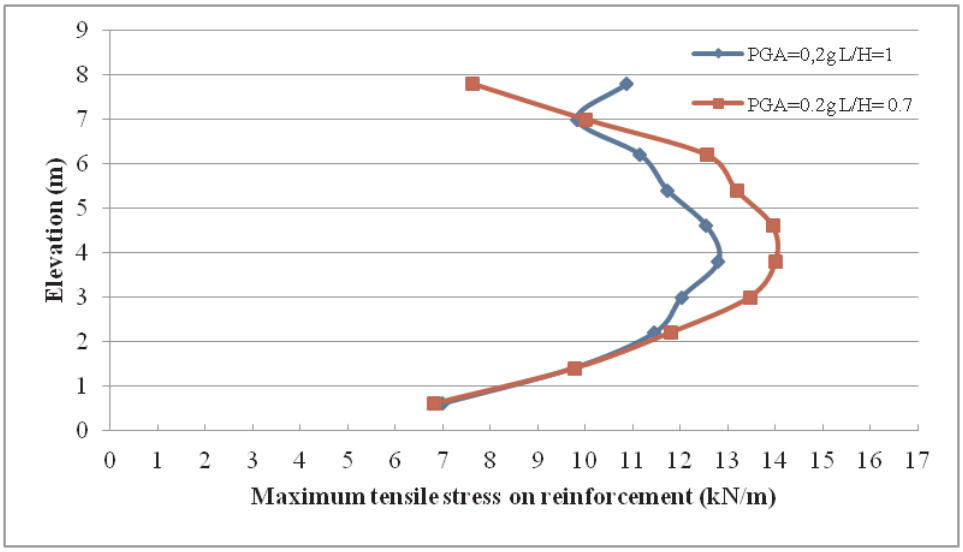

Figure 7.13. Maximum tensile stresses according to elevation (S_v=80).

7.3. Acceleration Amplification Factor

To simplify the presentation of acceleration response at different elevations of the walls, RMS acceleration amplification factors (RMSA amplification factors) are used to represent the acceleration. These factors are calculated using the root mean square (RMS) method applied to the acceleration-time history for each accelerometer device. The RMS value is calculated using Equation 7.3 (Kramer, 1996). RMSA amplification factor is the ratio of RMS acceleration record value in the soil to the corresponding base RMS acceleration value:

$$RMS = [\frac{1}{t_d}\int_0^{d_d} \alpha(t)^2 dt]^{-1/2} \tag{7.3}$$

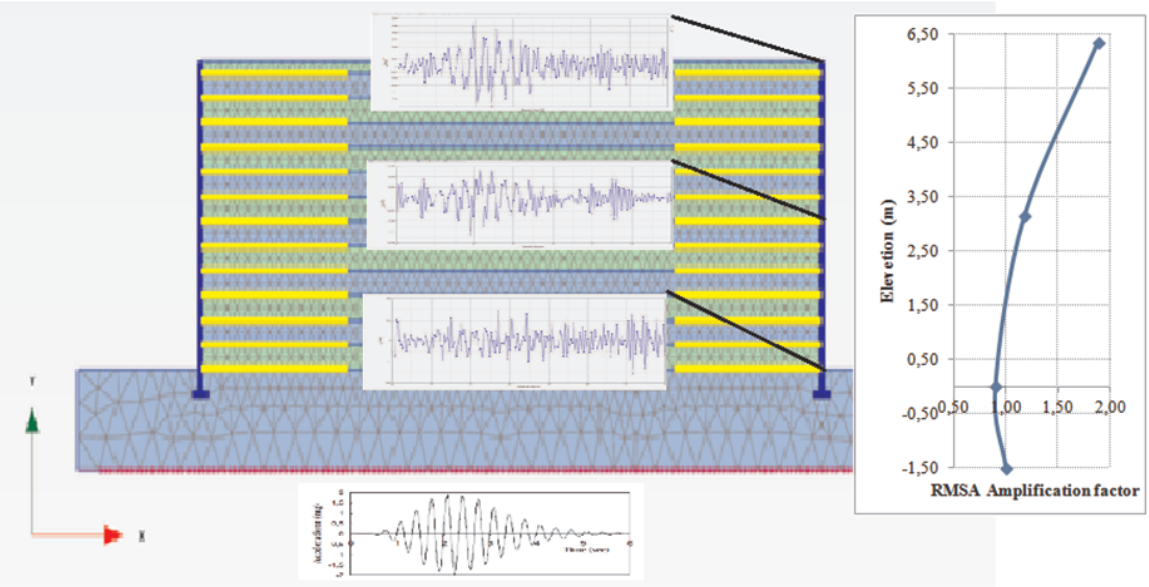

Figure 7.14. RMSA Amplification factor according to elevation of 6 m height wall.

8. ANN ANALYSIS AND RESULTS

8.1. Determination of Model Inputs

In this study there are 14 data parameters were used in order to predict permanent displacement of back to back retaining wall facing. Five of them are about wall geometry and the other nine parameters about intensity measures of dynamic loading.

8.1.1. Geometric Parameters for Model Inputs

In the study, the ANN based model was applied to predict permanent displacements and classify deformation level of back to back reinforced soil wall. Figure 8.1 shows the back to back retaining wall geometry.

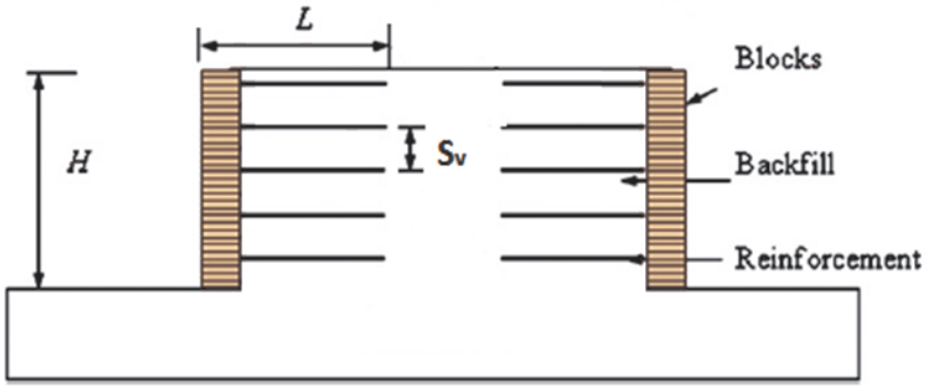

Figure 8.1. Back to back retaining wall geometry.

- H(m): Wall height (5 m-10 m),
- L(m): Reinforcement length (according to L/H),
- L/H: Length over height ratio (0.5 -2),
- S_v (m): Vertical spacing of reinforcement (0.2 m-0.8 m).
- F_{type}: Facing Type (Modular block and precast concrete panel)

8.1.2. Strong Ground Motion Parameters for Model Inputs

The program Seismosignal gives the intensity measure results for a given acceleration time history. Table 8.1 gives the results of three harmonic ground motion analyses.

- PGA(m/s^2)= Peak Ground Acceleration
- PGV(m/s= Peak Ground Velocity
- EPA(m/s^2)= Effective Peak Acceleration
- AI(m/s)= Arias Intensity
- CAV(m/s)= Cumulative Absolute Velocity
- ASI(m/s)= Acceleration Spectrum Intensity
- VSI(m)= Velocity Spectrum Intensity
- T_m(s)= Mean Period
- t_{eff}(s)= Effective Duration

Table 8.1. Sigmosignal results of harmonic motion.

Ground Motion	PGA	PGV	EPA	AI	CAV	ASI	VSI	Tm	Teff
	(m/s^2)	(m/s)	(m/s^2)	(m/s)	(m/s)	(m/s)	(m)	(s)	(s)
0.2g	1,977	0,096	1,961	0,5	2,826	2,014	0,317	0,188	2,155
0.4g	3,999	0,196	3,903	2,151	5,962	4,098	0,644	0,188	2,195
0.6g	5,93	0,288	5,882	4,505	8,48	6,041	0,950	0,188	2,150

8.2. Analysis

ANNs can efficiently be used as a tool for performing tasks such as function approximation (regression) and classification.

The basic characteristic of ANN is its architecture. Design of ANN architecture consists of determining the number of layers, the number of neurons in each layer, activation functions of the neurons and the learning algorithm for the network. The most common ANN architecture is a multi-layer feed-forward structure also known as a multi-layer perceptron (MLP) trained by Back-Propagation (BP) algorithm (Kim *et al.*, 1999). A simple MLP consisting of three layers: the input layer, the output layer

and one hidden layer can be seen in Figure 8.2.

Most commonly used transfer function is a sigmoid function because of its simple derivative, which is useful for the learning algorithm (see Figure 8.3).

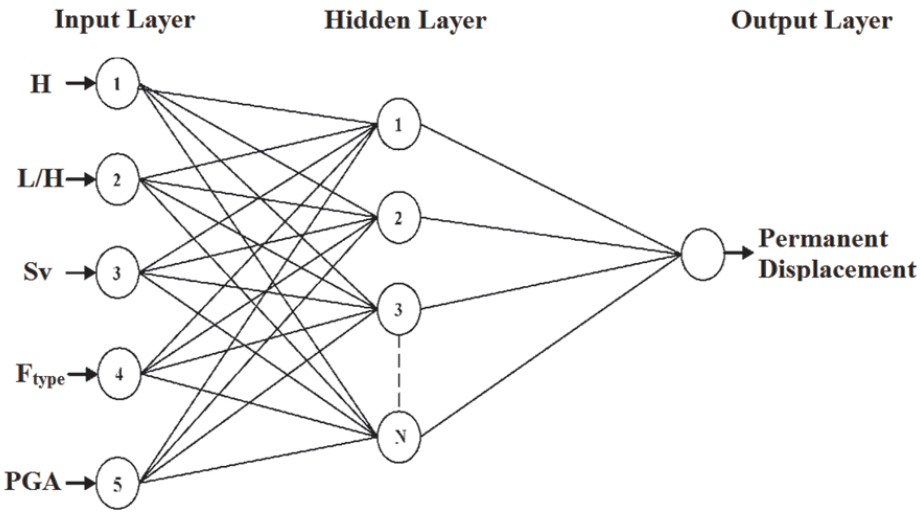

Figure 8.2. Multi-layer perceptron (MLP) with tree layers.

The mean square error (MSE) is generally used for calculating the error. For this study, the Levenberg-Marquardt (LM) algorithm is adopted for its efficiency in training MLP. The details of the BP algorithm can be found in the literature (Haykin, 1999).

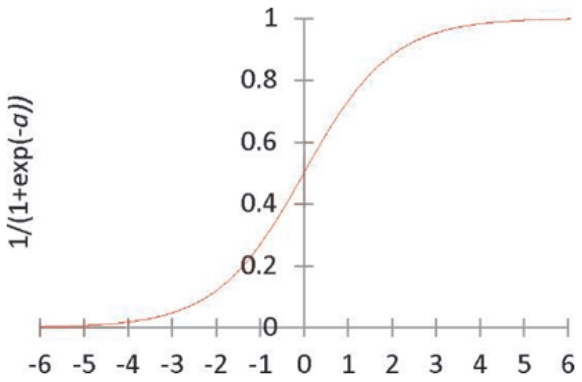

Figure 8.3. Sigmoid function.

8.3. Results

8.3.1. Regression Analysis Result

Mean Squared Error (MSE) is performance metric adopted to determine the network performance, while regressions; R is used to measure the correlation between outputs and targets. The fitting curve between targets with inputs is shown in Figure 8.4 and the best validation performance is approached at epoch 10 Figure 8.3.

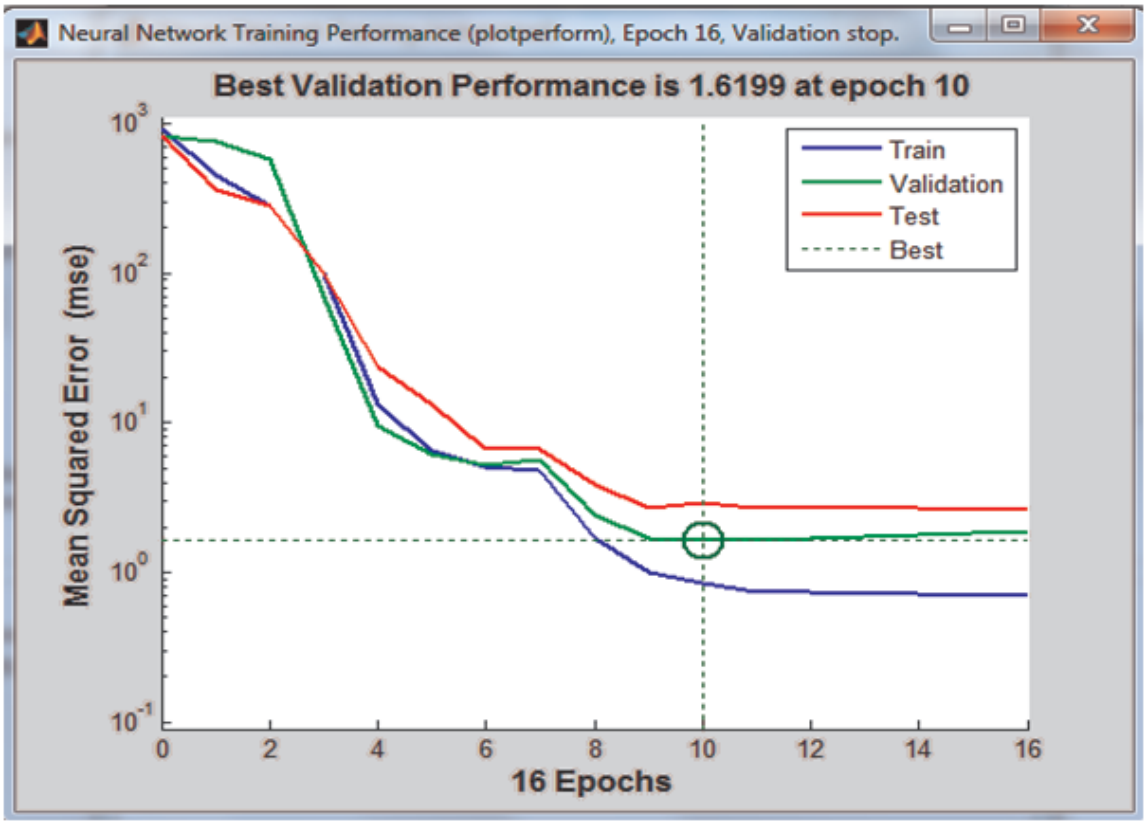

Figure 8.4. Validation performance.

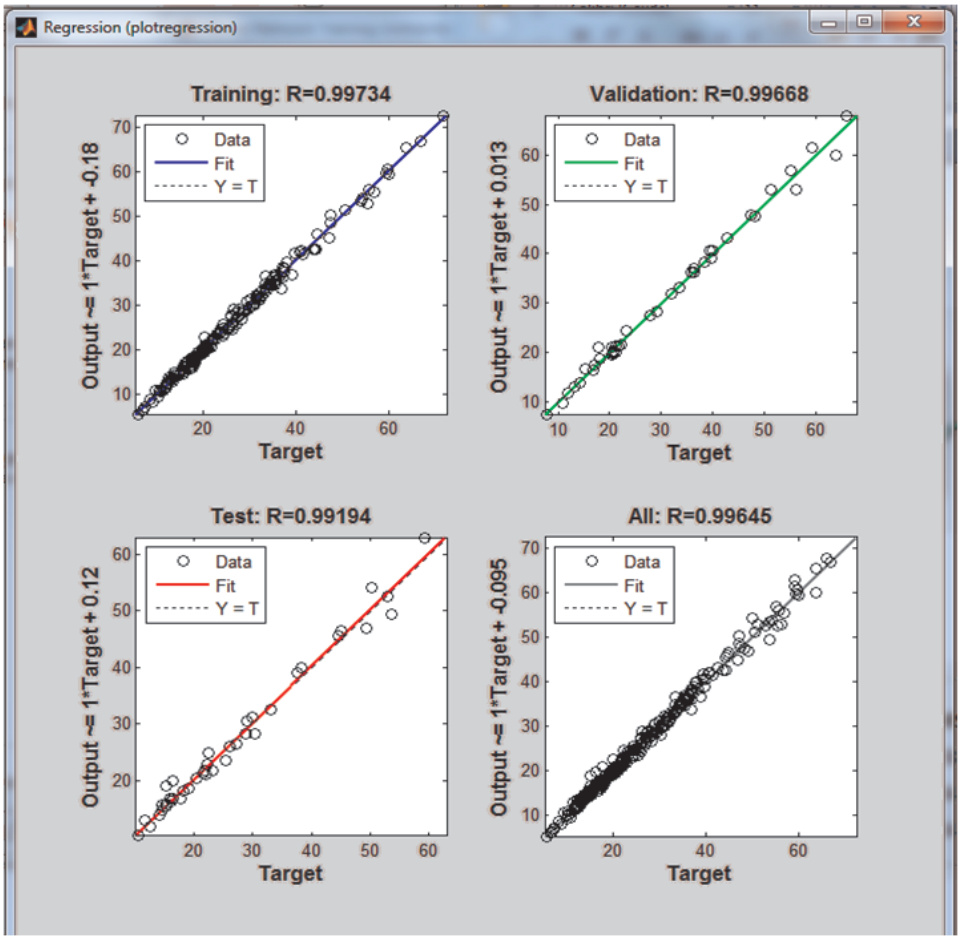

Figure 8.5. Fitting curve between targets with inputs.

The neural network is trained and validated using the first batch of 110 learning points and the performance is evaluated using 83 test points. The performance of the ANN regression model for the first 83 learning points using 10 neurons in the hidden layer can be seen in Figure 8.5. Even for a relatively low number of learning points, ANN regression performs well on the test data. Totally 276 data are distributed among to training, validating and testing in different percentage. Although distribution of the data in various proportions, no significant change about R has been seen in Table 8.2.

Table 8.2. Results for MSE and regression for different data distribution.

	Number of Samples	MSE	R
Training	110	0.8412	0.9972
Validating	83	60.033	0.9871
Testing	83	35.156	0.9902

	Number of Samples	MSE	R
Training	220	17.781	0.9951
Validating	28	22.581	0.9932
Testing	28	22.096	0.9921

For each number of features up to a total of 8 features, all possible combinations

are tested and the IM that give the best correlation coefficient are shown in the Table 8.3.

Table 8.3. Exhaustive search for the IM input features.

Number of Features	R (Testing) (%)	Intensity Measures (IM)
1	99.37	PGA
2	99.81	PGA, PGV
3	99.74	PGA, PGV, EPA
4	99.92	PGA, PGV, EPA, AI, CAV
5	99.75	PGA, PGV, EPA, AI, CAV, ASI
6	99.23	PGA, PGV, EPA, AI, CAV, ASI, VSI
7	98.87	PGA, PGV, EPA, AI, CAV, ASI, VSI, T_m
8	98.89	PGA, PGV, EPA, AI, CAV, ASI, VSI, T_m, T_{eff}

For same geometric input with each intensity measures except Tm gives high coefficients of correlation for testing data as seen in Table 8.4.

Table 8.4. Search for each IM input features.

Number of Features	R (%)	Intensity Measures (IM)
1	99.37	PGA
2	98.32	PGV
3	99.24	EPA
4	98.84	AI
5	98.75	CAV
6	99.23	ASI
7	99.42	VSI

The agreement of the neural network predicted displacements and FEA results were encouraging, as shown in Table 8.5.

Table 8.5. Comparison of neural network predictions and FEA results.

Measured wall displacement (cm)	Predicted wall displacement (cm)
31.09	29.52
27.95	26.38
24.81	23.25
20.37	18.12
16.29	14.52
11.61	9.83
8.44	7.6

8.3.2. Classification Analysis Result

The calculated permanent displacements from Plaxis analysis can be viewed properly as an index of the seismic performance of the back to back reinforced soil retaining wall. However, these calculations will always be approximations due to the complexity of the dynamic response of the wall geometry and variability of strong motion. Therefore, in order to simplify the problem at hand, deformation strain (ε) that is equal to permanent displacement at the top of wall over height of wall can be classified in to different deformation classes and the problem can be treated as a classification problem. For that reason deformation strains smaller than 3% are assigned the deformations class "Low". Deformation strain between 3% and 5% are assigned "Medium" and higher than 5% "High".

The same data set which has been consisted of 286 FEA displacements results was used to investigate the performance of the ANN model to predict the deformation class. The problem is modeled as a three class classification problem. The permanent displacement at the top of wall over height of wall gives the deformation strain strains (ε) are assigned one of the three deformation classes given in Table 8.6.

Table 8.6. Assigned deformation classes for permanent displacements.

Deformation Strain $\leq 3\%$	Low
$3\% <$ Deformation Strain $\leq 5\%$	Medium
$5\% <$ Deformation Strain	High

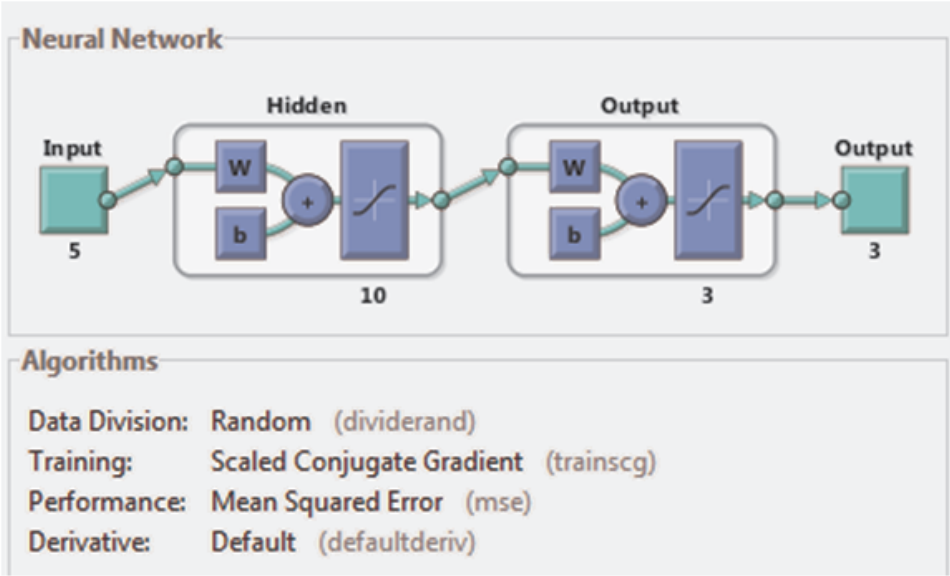

Figure 8.6. ANN algorithms detail.

The learning algorithm used Scaled Conjugate Gradient as it seen in Figure 8.5. In order to check the performance of ANN model, selected criteria was the sum of the mean square error. Lower values are better. Percent error indicates the fraction of samples which are misclassified. Table 8.7 shows results of analysis.

Table 8.7. Results for MSE and E%.

	Number of Samples	MSE	%E
Training	194	0.00711	1.03092
Validating and Testing	82	0.01199	4.89002

Table 8.8. Confusion matrixes for ANN classification model.

PREDICTED

ACTUAL		L	M	H	Prediction Accuracy
	L	41	2	0	95.30%
	M	0	98	0	100.00%
	H	0	0	53	100.00%
	Training Prediction Accuracy				99.00%

PREDICTED

ACTUAL		L	M	H	Prediction Accuracy
	L	19	1	0	95.00%
	M	1	34	0	97.10%
	H	0	2	25	92.60%
	Testing & Validation Prediction Accuracy				95.10%

PREDICTED

ACTUAL		L	M	H	Prediction Accuracy
	L	60	3	0	95.20%
	M	1	132	0	99.20%
	H	0	2	78	97.50%
	Total Prediction Accuracy				97.80%

9. CONCLUSION

This study deals with the calculation of permanent displacements of back to back geosynthetic reinforced segmental retaining walls under earthquake loading condition. A commercial finite elements software Plaxis has been used to calculate the deformations. Three harmonic motions which have PGA values 0.2 g, 0.4 g and 0.6 g respectively have been applied. The frequency of the all harmonic input acceleration record is 3 Hz.

Artificial Neural Network was used for the first time in literature to estimate the deformations of geosynthetic reinforced walls under dynamic loading conditions. The study intended to use the ANN model in order to make reliable predictions for geosynthetic reinforced wall design and to check whether the results of classical design results fall between reasonable limits. Not only regression but also classification ANN models were applied to finite element analysis results.

The parameters investigated and their chosen values were as follows: height of the wall (5 m, 6 m, 7 m, 8 m, and 9 m), type of facing (modular block and concrete panel), reinforcement length (L/H = 0.5, 0.7) and spacing of reinforcement (0.2 m, 0.4 m, 0.6 m and 0.8 m). Following results are observed.

As can be expected the permanent displacement increases with height of wall.

Permanent displacements of modular block facing back to back geosynthetic reinforced retaining walls are more than precast concrete panel facing systems for all L/H and S_v values.

Increasing reinforcement length, decreased the permanent displacements of wall facing and maximum tensile stress on reinforcement. The stress distribution on reinforcement becomes more uniform with depth as the reinforcement length incresased.

Decreases of reinforcement vertical spacing (S_v) decreased the permanent displacements of wall facing when equivalent reinforcement was used along to wall.

The peak ground acceleration had strong influence on the dynamic response of the walls. When the peak ground acceleration was 0.2 g, 0.4 g, and 0.6 g permanent displacements for 9m height wall were 17 cm, 28 cm, and 32 cm, respectively. In spite of the regular 0.2 g linear increments in peak ground acceleration, the relevant increases in permanent displacements were 19 cm and 4 cm, respectively. This indicates that the displacements of a reinforced soil wall under earthquake loading conditions are not linearly related to the peak maximum acceleration of the harmonic motion. As can be seen, the relation between various parameters is non-linear. Since it is known that such non-linear behavior in geotechnical engineering problems can be modeled successfully with ANN, we decided to conduct an ANN analysis.

The ANN was used to synthesize data derived from finite element studies on back to back geosynthetic reinforced retaining walls under seismic excitation. The input parameters used in the model were H, L, L/H, S_v, F_{type}, PGA, PGV, EPA, AI, CAV, ASI, VSI, T_m and t_{eff}. The permanent displacement of wall was chosen the only output. Using regression analysis, the scatter of the predicted ANN displacements relative to the displacements obtained using the finite element method were assessed. The results produced high coefficients of correlation for training and testing data of 0.997 and 0.989, respectively. The agreement of the ANN predicted and measured wall deflections were encouraging.

The important point of the seismic evaluation of the seismic response of the back to back MSE retaining wall is the selection of ground motion intensity measure IM for different earthquakes. In this study due to constant frequency value of harmonic motions, intensity measures; PGV, EPA, CAV, ASI, and VSI are linearly correlated with PGA values but AI is not. Therefore any of these IM is enough to approach high coefficients of correlated ANN model.

ANNs can efficiently be used as a tool for performing not only as a function approximation (regression) but also classification. Deformation strain (ε) which is equal to permanent displacement at the top of wall over height of wall was classified into different deformation classes as: High (H), Medium (M), and Low (L). ANN model inputs consisted of H, L/H, S_v, and PGA which will give outputs as H, M, or L classes according to this classification. Prediction accuracy is 99% and MSE value is 0.00711 for 194 training data. 82 validating and testing data has 95.11% prediction accuracy with 0.0112 MSE.

The agreement of the neural network predicted displacements and deformation classification with Finite Element Analyses results were encouraging by the means of correlation coefficient values of R=0.99 for ANN regression analysis and predicted accuracy value 97.8% for ANN classification analysis.

REFERENCES

Adeli, H., 2001, "Neural networks in civil engineering: 1989-2000", *Computer-Aided Civil and Infrastructure Engineering*, Vol. 16, No. 2, pp. 126-142.

Agrawal, G., J. A., Chameau, and P. L., Bourdeau, 1997, "Assessing the liquefaction susceptibility at a site based on information from penetration testing", *Artificial neural networks for civil engineers: Fundamentals and applications*, N. Kartam, I. Flood, and J. H. Garrett, eds., New York, pp. 185-214.

Agrawal, G., S., Weeraratne and K., Khilnani, 1994, "Estimating clay liner and cover permeability using computational neural networks", *Proceedings of the 1st Congress on Computing in Civil Engineering*, Washington.

Ahmad, I., H., El Naggar and A. N., Kahn, 2007, "Artificial neural network application to estimate kinematic soil pile interaction response parameters", *Soil Dynamics and Earthquake Engineering*, Vol. 27, No. 9, pp. 892-905.

Akkar, S., J.J.,Bommer, 2007, "Empirical prediction equations for peak ground velocity derived from strong-motion records from Europe and the Middle East", *Bulletin of the Seismological Society of America,* Vol. 97, No. 2, pp. 511-530.

Akkar, S., O., Ozen, 2005, "Effect of peak ground velocity on deformation demands for SDOF systems", *Earthquake Engineering and Structural Dynamics*, Vol. 34, pp. 1551-1571.

Al-Hussaini, M. M., and L. D., Johnson, 1979, "Numerical analysis of a reinforced earth wall", *Symposium on Earth Reinforcement*, ASCE, April 27, 1978, Pittsburgh, USA, pp. 98-126.

Ali, H.E. and Y.M., Najjar, 1998, "Neuronet-based approach for assessing liquefaction potential of soils", *Transportation Research Record*, No. 1633, pp. 3-8.

Anastasopoulos I., T., Georgarakos, V., Georgiannou, V., Drosos, R., Kourkoulis, 2010, "Seismic performance of bar-mat reinforced-soil retaining wall: Shaking table testing versus numerical analysis with modified kinematic hardening constitutive model", *Soil Dynamics and Earthquake Engineering*, 10.1016/j.soildyn.2010.04.020 journal homepage: www.elsevier.com/locate/soildyn

Applied Technology Council (ATC), 1978, "Tentative provisions for the development of seismic regulations for buildings", ATC-3, California.

Arias, A., 1970, "A measure of earthquake intensity", *In Seismic Design for Nuclear Power Plants*, Hansen RJ (ed.). MIT Press: Cambridge, MA, pp. 438-483.

Basheer, I.A., 1998, "Neuromechanistic-based modeling and simulation of constitutive behaviour of fine-grained soils", PhD Thesis, Kansas State University, Manhattan.

Basheer, I.A., 2000, "Selection of methodology for neural network modeling of constitutive hysteresis behavior of soils", *Computer-Aided Civil and Infrastructure Engineering*, Vol. 15, No. 6, pp. 445-463.

Basheer, I.A., 2002, "Stress-strain behavior of geomaterials in loading reversal simulated by time-delay neural networks", *Journal of Materials in Civil Engineering*, Vol. 14, No.3, pp. 270-273.

Basheer, I.A., and Y.M., Najjar, 1998, "Modeling cyclic constitutive behavior by neural networks: Theoretical and real data", *Proceedings of the 12th Engineering Mechanics Conference*, La Jolla, California, pp. 952-955.

Basheer, I.A., L.N., Reddi and Y.M., Najjar, 1996, "Site characterization by neuronets: An application to the landfill sitting problem", *Ground Water*, Vol. 34, pp. 610-617.

Bathurst R.J. and K., Hatami, 1998a, "Influence or Reinforcement Length and Base Condition on Seismic Response of Geosynthetic Reinforced Retaining Walls", *Pro-*

ceedings of the 6th International Conference on Geosynthetics, Atlanta Georgia, USA, pp. 613-616.

Bathurst R.J. and Z., Cai. 1995, "Pseudo-static Seismic Analysis Reinforced Segmental Retaining Walls", *Geosynthetics Internatinal*, Vol. 2, No. 5, pp. 787-830.

Bathurst, R.J., Hatami, K., 1998, "Seismic response analysis of a geosynthetic-reinforced soil wall", *Geosynthetics Internatinal*, Vol. 5, No. 1-2, pp. 127-166.

Bathurst, R.J., and K., Hatami, 1998b, "Seismic Response Analysis of a Reinforced Soil Retaining Wall", *Geosynthetics International* (special issue on Earthquake Engineering. Industrial Fabrics Association International (IFAI)), USA, Vol. 5, No. 1-2, pp. 127-166.

Bathurst, R.J. and M.C., Alfero, 1997, "Review of Seismic Design, Analysis and Performance of Geosynthetic Walls, Slopes, and Embankments", *Proceedings of the International Symposium on Earth Reinforcement*, Fukuoka Kyushu, Japan, Rotherdam, Balkema.

Bathurst, R.J., and K., Hatami, 1998c, "Influence of Reinforcement Properties on Seismic Response and Design of Reinforced-soil Retaining Walls", *Proceedings of the 51st Canadian Geotechnical Conference*, Edmonton, Alberta, Canada, pp. 479-486.

Bathurst, R.J. and M.C., Alfaro, 1996, "Review of Seismic Design Analysis and Performance of Geosynthetic Reinforced Walls, Slopes and Embankments", *Proceedings of the Earth Reinforcement - International Symposium on Earth Reinforcement*, Fukuoka Kyushu, Japan, pp. 887-918.

Baziar, M.H. and Ghorbani, A., 2005, "Evaluation of lateral spreading using artificial neural networks", *Soil Dynamics and Earthquake Engineering*, Vol. 25, No.1, pp. 1-9.

Bebis, G. and M., Georgiopoulos, 1994, "Feed-forward neural networks: Why network size is so important", *IEEE Potentials*, October/November, pp. 27-31.

Benardos, A.G. and D.C., Kaliampakos, 2004, "Modeling TBM performance with artificial neural networks", *Tunneling and Underground Space Technology*, Vol. 19, No. 6, pp. 597-605.

Berke, L. and P., Hajela, 1991, "Application of neural networks in structural optimization", *NATO/AGARD Advanced Study Institute*, Vol. 23, No. I-II, pp. 731-745.

Bommer, J.J. and A., Martinez-Pereira,2000, "Strong-motion parameters: definition, usefulness and predictability", *Procedings of the 12th World Conference on Earthquake Engineering*, Auckland Paper No. 206.

Bowden, G.J., H.R., Maier and G.C., Dandy, 2002. "Optimal division of data for neural network models in water resources applications", *Water Resources Research*, Vol. 38, No. 2, pp. 1-11.

Bradley, B.A., M., Cubrinovski, *et al.*, 2009, "Ground-Motion Prediction Equation for SI Based on Spectral Acceleration Equations", *Bulletin of the Seismological Society of America*, Vol. 99, No. 1, pp. 277-285.

Breiman, L., 1994, "Comment on 'Neural networks: A review from a statistical by B. Cheng and D. M. Titterington", *Statistical Science*, Vol. 9, No. 1, pp. 38-42.

Brinkgreve R.B.J., 2002, Plaxis 2D version8. A.A., Balkema Publisher, Lisse, 2002. J.T., Christian, J.M., Roesset, C.S., Desai, 1977, "Two- Dor Three-Dimensional Dynamic Analyses", *Numerical Methods in Geotechnical Engineering*, Chapter 20, pp. 683-718.

Brinkgreve R.B., J., Vermeer, 1998 "Finite element code for soil and rock analyses", Balkema, Rotterdam, p. 195.

Brinkgreve, R.B.J., and M., Yogendrakumar, 1992, "Dynamic Response Analysis of

Reinforced Soil Retaining Wall", *Journal of Geotechnical Engineerin*g, Vol. 118, No. 8, pp. 1158-1167.

Brown, M., and C.J., Harris, 1994, "Neurofuzzy adaptive modeling and control", Prentice-Hall, Englewood Cliffs, New Jersey.

Cabanas, L., B.,Benito, M., Herraiz, 1997, "An approach to the measurement of the potential structural damage of earthquake ground motions", *Earthquake Engineering and Structural Dynamics,* No. 26, pp. 79-92.

Cai, S., H., Toral, J., Qiu, and J.S., Archer, 1994, "Neural network based objective flow regime identification in air-water two phase flow", *Canadian Journal of Chemical Engineering*, No. 72, pp. 440-445.

Cai, Z. and R.J., Bathutst, 1996a, "Seismic-induced Permanent Displacement of Geosynthetic Reinforced Segmental Retaining Walls", *Canadian Geotechnical Journal*, No. 31, pp. 937-955.

Cai, Z. and R.J., Bathurst, 1996b, "Deterministic Sliding Block Methods for Estimating Seismic Displacements of Earth Structures", *Soil Dynamics and Earthquake Engineering*, No. 15, pp. 255-268.

Cal, Y., 1995, "Soil classification by neural-network", *Advances in Engineering Software*, Vol. 22, No. 2, pp. 95-97.

Castellano, G., A.M., Fanelli and M., Pelillo, 1997, "An iterative pruning algorithm for feed-forward neural networks", *IEEE Transactions on Neural Networks*, Vol. 8, No. 3, pp. 519-531.

Celik, S., and O., Tan, 2005, "Determination of pre-consolidation pressure with artificial neural network", *Civil Engineering and Environmental Systems*, Vol. 22, No. 4, pp. 217-231.

Chan, W.T., Y.K., Chow, and L.F., Liu, 1995, "Neural network: An alternative to pile

driving formulas", *Computers and Geotechnics*, No. 17, pp. 135-156.

Cho, S.E., 2009, "Probabilistic stability analyses of slopes using the ANN-based response surface", *Computers and Geotechnics*, Vol. 36, No. 5, pp. 787-797.

Chugh, A.K., 1995, "Dynamic displacement analysis of embankment dams", *Geotechnique*, Vol. 45, No. 2, pp. 295-299.

Collin, J.G., C., Chourery and R.R., Berg, 1992, "Field Observation of Reinforced Soil Structures Under Seismic Loading", *Proceedings of International Symposium on Earth Reinforcement*, pp. 223-228, Rotherdam, Balkema.

Cordova, P.P., G.G., Deierleing, S.S., Mehanny and C.A., Cornell, 2000, "Development of a two-parameter seismic intensity measure and probabilistic assessment procedure", *Proceedings of the 2nd U.S.-Japan Workshop on Performance- Based Earthquake Engineering for Reinforced Concrete Building Structures*, Sapparo, Japan.

Das, B.M., 1994, *Principles of Foundation Engineering*, BWS-KEN Publishing Company, Boston.

Das, S.K. and P.K., Basudhar, 2006, "Undrained lateral load capacity of piles in clay using artificial neural network", *Computers and Geotechnics*, Vol. 33, No. 8, pp. 454-459.

Douglas, J., 2001, A comprehensive worldwide summary of strong-motion attenuation relationships for peak ground acceleration and spectral ordinates (1969 to 2000), *ESEE Report* No. 01.1, Imperial College of Science, Technology and Medicine.

El-Emam, M. and R.J., Bathurst, 2004, "Experimental Design, Instrumentation and Interpretation of Reinforced Soil Wall Response using a Shaking Table", *International Journal of Physical Modelling in Geotechnics*, Vol. 4, No. 4, pp. 13-32.

Elenas, A., 2000, Correlation between seismic acceleration parameters and overall structural damage indices of buildings, *Soil Dynamics and Earthquake Engineering*, No.

20, pp. 93-100.

Elenas, A., and K., Meskouris, 2001, "Correlation study between seismic acceleration parameters and damage indices of structure", *Engineering Structures*, No. 23, pp. 698-704.

Ellis, G.W., C., Yao, and R., Zhao, 1992, "Neural network modeling of the mechanical behavior of sand", *Proceedings of the Engineering Mechanics*, pp. 421-424.

Ellis, G.W., C., Yao, R., Zhao and D., Penumadu, 1995, "Stress-strain modeling of sands using artificial neural networks", *Journal of Geotechnical Engineering*, ASCE, Vol. 121, No. 5, pp. 429-435.

Elms, D.G. and R, Richards, 1990, "Seismic Design of Retaining Walls ASCE Specially Conference Design and Performance of Earth Retaining Structures", Cornell University, Ithaca, New York, USA, pp. 854-871, ASCE *Geotecnical Special Publication*, No. 25.

Electrical Power Research Institute (EPRI), 1998, "A criterion for determining exceedence of the operating basis earthquake", EPRINP-5930, Palo Alto, CA.

Erzin, Y., 2007, "Artificial neural networks approach for swell pressure versus soil suction behavior", *Canadian Geotechnical Journal*, Vol. 44, No. 10, pp. 1215-1223.

European Committee for Standardization 2003, Eurocode 8: Design of structures for earthquake resistance Part 3: Strengthening and repair of buildings - Draft No:4 *Eurocode 8*, Brussels.

Fahlman, S.E., and C., Lebiere, 1990, "The cascade-correlation learning architecture", Advances in Neural Information Processing Systems 2, D. S. Touretzky, ed., Morgan Kaufmann, San Mateo, California, pp. 524-532.

Faraway, J., and C., Chatfield, 1998, "Time series forecasting with neural networks: A

comparative study using the airline data", *Applied Statistics*, Vol. 47, No. 2, pp. 231-250.

Fausett, L.V. 1994, "Fundamentals neural networks: Architecture, algorithms, and applications", Prentice-Hall, Englewood Cliffs, New Jersey.

Federal Highway Administration (FHWA), 1996, *Mechanically Stabilized Earth Wails and Reinforced Soil Slopes Design and Construction Guideline*, FHWA Demonstration Project 82 (V. Elias and B. R. Christopher), Washington, DC. USA.

Federal Highway Administration (FHWA), 2001, *Mechanically Stabilized Earth Wails and Reinforced Soil Slopes Design and Construction Guideline*, FHWA Demonstration Project 82 (V. Elias and B. R. Christopher), Washington, DC. USA.

Flood, I. 1991, "A Gaussian-based neural network architecture and complementary training algorithm", *Proceedings of the International Joint Conference on Neural Networks*, New York, pp. 171-176.

Frankenberger, P.C., R. A. Bloomfield and P. L. Anderson, 1996, "Reinforced Earth walls withstand Northridge Earthquake", *Proceedings of International Symposium on Earth Earth Reinforcement*, pp. 345-350, Rotherdam, Balkema.

Franklin, A.G. and Chang. F.K., 1977, "Permanent Displacement of Earth Embankments by Newmark Sliding Block Analysis", Misc. Paper S-71-17, Soil and Pavements Laboratory, US Army Eng. Waterways Expt. Station., Vicksburg, Mississippi, USA.

Fu, Q., Y.M.A., Hashash, S., Hung and Ghaboussi, J., 2007, "Integration of laboratory testing and constitutive modeling of soils." *Computers and Geotechnics*, Vol. 34, No. 5, pp. 330-345.

Fujii, T., J., Izawa, J., Kuwano, M., Ishihara and J., Nakane 2006, "Prediction of deformation of retaining walls of geosynthetic-reinforced soil under large earthquakes",

Proceeding of the 8^{th} International Conference on Geosynthetic, Yokohoma, Japon.

Ghaboussi, J., and D.E., Sidarta, 1998, "New nested adaptive neural networks (NANN) for constitutive modeling", *Computers and Geotechnics*, Vol. 22, No. 1, pp. 29-52.

Gibson, A.D. 1997, "Physical scale modeling of geotechnical structures at One-G", Report no. SML 97-01. Pasadena, CA: California Institute of Technology;. pp. 413.

Goh, A.T., 2002, "Probabilistic neural network for evaluating seismic liquefaction potential", *Canadian Geotechnical Journal*, Vol. 39, No. 1, pp. 219-232.

Goh, A.T.C., 1994a, "Nonlinear modeling in geotechnical engineering using neural networks" *Australian Civil Engineering Transactions*, Vol. 36, No. 4, pp. 293-297.

Goh, A.T.C., 1994b, "Seismic liquefaction potential assessed by neural network", *Journal of Geotechnical and Geoenvironmental Engineering*, ASCE, Vol. 120, No. 9, pp. 1467-1480.

Goh, A.T.C., 1995a, "Empirical design in geotechnics using neural networks", *Geotechnique*, Vol. 45, No. 4, pp. 709-714.

Goh, A.T.C., 1995b, "Modeling soil correlations using neural networks", *Journal of Computing in Civil Engineering*, ASCE, Vol. 9, No. 4, pp. 275-278.

Goh, A.T.C., 1996a, "Neural-network modeling of CPT seismic liquefaction data", *Journal of Geotechnical Engineering*, ASCE, Vol. 122, No. 1, pp. 70-73.

Goh, A.T.C., 1996b, "Pile driving records reanalyzed using neural networks", *Journal of Geotechnical Engineering*, ASCE, Vol. 122, No. 6, pp. 492-495.

Goh, A.T.C. and F.H., Kulhawy, 2003, "Neural network approach to model the limit state surface for reliability analysis", *Canadian Geotechnical Journal*, No. 40, pp.

1235-1244.

Goh, A.T.C., K.S., Wong and B.B., Broms, 1995, "Estimation of lateral wall movements in braced excavation using neural networks", *Canadian Geotechnical Journal*, No. 32, pp. 1059-1064.

Goh, A.T. and S.H., Goh, 2007, "Support vector machines: Their use in geotechnical engineering as illustrated using seismic liquefaction data", *Computers and Geotechnics*, Vol. 34, No. 5, pp. 410-421.

Goh, A.T., F.H., Kulhawy and C.G., Chua, 2005, "Bayesian neural network analysis of undrained side resistance of drilled shafts", *Journal of Geotechnical and Geoenvironmental Engineering*, Vol. 131, No. 1, pp. 84-93.

Gokceoglu, C., E., Yesilnacar, H., Sonmez and A., Kayabasi, 2004, "A neuro-fuzzy model for modulus of deformation of jointed rock masses", *Computers and Geotechncis*, Vol. 31, No. 5, pp. 375-383.

Gribb, M.M. and G.W., Gribb, 1994, "Use of neural networks for hydraulic conductivity determination in unsaturated soil", *Proceedings of the 2nd International Conference on Ground Water Ecology*, Bethesda, pp. 155-163.

Guler, E., E.,Çiçek M., Hamderi, M.M., Demirkan, 2007, "Numerical analysis of reinforced soil walls with granular and cohesive backfills under cyclic loads", *Bull Earthquake Eng.* DOI 10.1007/s10518-011-9322-y.

Guler. E., M., Hamderi, M.M., Demirkan, 2007, "Numerical analysis of reinforced soil-retaining wall structures with cohesive and granular backfills", *Geosynth International*, Vol. 14, No. 6, pp. 330-345.

Habibagahi, G. and A., Bamdad, 2003, "A neural network framework for mechanical behavior of unsaturated soils." *Canadian Geotechnical Journal*, Vol. 40, No. 3, pp. 684-693.

Hanna, A.M., G., Morcous and M., Helmy, 2004, "Efficiency of pile groups installed in cohesionless soil using artificial neural networks", *Canadian Geotechnical Journal*, Vol. 41, No. 6, pp. 1241-1249.

Hanna, A.M., D., Ural and G., Saygili, 2007, "Neural network model for liquefaction potential in soil deposits using Turkey and Taiwan earthquake data", *Soil Dynamics and Earthquake Engineering*, Vol. 27, No. 6, pp. 521-540.

Hassoun, M.H., 1995, *Fundamentals of artificial neural networks*, MIT Press, Cambridge.

Haykin, S.S., 1999, *Neural networks : a comprehensive foundation*, Upper Saddle River, N.J., Prentice Hall.

Hecht-Nielsen, R., 1989, "Theory of the back-propagation neural network", *Proceedings of the International Joint Conference on Neural Networks*, Washington, DC, pp. 593-605.

Hush, D.R. and B.G., Horne, 1993, "Progress in supervised neural networks", *IEEE SP Magazine*, Vol. 10, No. 1, pp. 8-39.

Ingold, T. S., 1982, *Reinforced Earth*, Thomas Telford Ltd., London.

Javadi, A., M., Rezania and N.M., Mousavi, 2006, "Evaluation of liquefaction induced lateral displacements using genetic programming", *Computers and Geotechnics*, Vol. 33, No. 4-5, pp. 222-233.

Kavli, T., 1993 "ASMOD - An algorithm for adaptive spline modeling of observation data", *International Journal of Control*, Vol. 58, No. 4, pp. 947-967.

Kim, D.H., D.J., Kim, *et al.*, 1999, "The application of neural networks and statistical methods to process design in metal forming processes", *International Journal of Advanced Manufacturing Technology*, Vol. 15, No. 12, pp. 886-894.

Kim, Y. and B., Kim, 2008, "Prediction of relative crest settlement of concrete-faced rockfill dams analyzed using an artificial neural network model", *Computers and Geotechnics*, Vol. 35, No. 3, pp. 313-322.

Kingston, G.B., H.R., Maier and M.F., Lambert, 2005b, "Calibration and validation of neural networks to ensure physically plausible hydrological modeling", *Journal of Hydrology*, No. 314, pp. 158-176.

Kingston, G.B., H.R., Maier and M.F., Lambert, 2008, "Bayesian model selection applied to artificial neural networks used for water resources modeling", *Water Resources Research*, 44(W04419), doi:10.1029/2007WR006155.

Kocjancic, R. and J., Zupan, 2000, "Modeling of the river flow rate: The influence of the training set selection", *Chemometric and Intelligent Laboratory Systems*, No. 54, pp. 21-34.

Kramer, S.L., 1996, *Geotechnical Earthquake Engineering*, Prentice Hall, New Jersey.

Kung, G.T., E.C., Hsiao, M., Schuster and C.H., Juang, 2007, "A neural network approach to estimating deflection of diaphram walls caused by excavation in clays" *Computers and Geotechnics*, Vol. 34, No. 5, pp. 385-396.

Kurup, P. U., and Dudani, N. K. 2002, "Neural network for profiling stress history of clays from PCPT data", Vol. 128, No. 7, pp. 569-579.

Lachtermacher, G. and J.D., Fuller, 1994, "Back-propagation in hydrological time series forecasting", *Stochastic and Statistical Methods in Hydrology and Environmental Engineering*, K. W. Hipel, A. I. McLeod, U. S. Panu, and V. P. Singh, eds., Kluwer Academic, Dordrecht.

Lee, C. and R., Sterling, 1992, "Identifying probable failure modes for underground openings using a neural network", *International Journal of Rock Mechanics and Mining Science and Geomechanics Abstracts*, Vol. 29, No. 1, pp. 49-67.

Lee, I.M. and J.H., Lee, 1996, "Prediction of pile bearing capacity using artificial neural networks", Computers and Geotechnics, Vol. 18, No. 3, pp. 189-200.

Lee, S.J., S.R., Lee and Y.S., Kim, 2003, "An approach to estimate unsaturated shear strength using artificial neural network and hyperbolic formulation", *Computers and Geotechnics*, Vol. 30, No. 6, pp. 489-503.

Liao, W., C., Loh, S., Wan, 2001, Earthquake responses of RC moment frames subjected to near-fault ground motions, *Structural Design of Tall Buildings*, No. 10, pp. 219-229.

Ling, H.I., Y., Mohri, D., Leshchinsky, C., Burke, K., Matsushima, H., Liu, 2005b "Large-scale shaking table tests on modular-block reinforced soil retaining walls", *J Geotech Geoenviron Eng*, ASCE Vol. 131, No. 4, pp. 465-476.

Ling, H.I., D., Leshchirsky and N.N.S., Chou, 2001, "Post-Earthquake Investigation on Several Geosynthetic-Reinforced Soil Retaining walls and Slopes During Ji-Ji Earthquake of Taiwan", *Soil Dynamics and Earthuake Engineering*, Vol 21, pp. 297-313.

Lu, Y. 2005, "Underground blast induced ground shock and its modeling using artificial neural network", *Computers and Geotechnics*, Vol. 32, No. 3, pp. 164-178.

Maier, H.R. and G.C., Dandy, 2000, "Neural networks for the prediction and forecasting of water resources variables: A review of modeling issues and applications", *Environmental Modeling and Software*, No. 15, pp. 101-124.

Maren, A., C., Harston and R., Pap, 1990, *Handbook of neural computing applications*, Academic Press, San Diego, California.

Masters, T. 1993, Practical neural network recipes in C++, Academic Press, San Diego, California.

Miller, G.F., P.M., Todd and S.U., Hedge, 1989, "Designing neural networks using

genetic algorithms", *Proceedings of the 3rd International Conference on Genetic Algorithms*, Arlington, pp. 379-384.

Minns, A.W. and M.J., Hall, 1996, "Artificial neural networks as rainfall-runoff models", *Hydrological Sciences Journal*, Vol. 41, No. 3, pp. 399-417.

Moon, H.K., S.M., Na and C.W., Lee, 1995, "Artificial neural-network integrated with expert-system for preliminary design of tunnels and slopes", *Proceedings of the 8th International Congress on Rock Mechanics*, Rotterdam: Balkema, pp. 901-905.

Najjar, Y.M. and I.A., Basheer, 1996, "Neural network approach for site characterization and uncertainty prediction", *ASCE Geotechnical Special Publication*, Vol. 58, No. 1, pp. 134-148.

Najjar, Y.M., I.A., Basheer and R., McReynolds, 1996a, "Neural modeling of Kansan soil swelling", *Transportation Research Record*, No. 1526, pp. 14-19.

Najjar, Y.M., I.A., Basheer and W.A., Naouss, 1996b, "On the identification of compaction characteristics by neuronets", *Computers and Geotechnics*, Vol. 18, No. 3, pp. 167-187.

Nawari, N.O., R., Liang and J., Nusairat, 1999, "Artificial intelligence techniques for the design and analysis of deep foundations", *Electronic Journal of Geotechnical Engineering*, http://geotech.civeng.okstate.edu/ejge/ppr9909.

Neaupane, K. and S., Achet, 2004 "Some applications of a back-propagation neural network in geo-engineering", *Environmental Geology*, Vol. 45, No. 4, pp. 567-575.

Newmark N.M., 1965, "Effect of Earthquakes on Dams and Embankments", *Géotechnique*, Vol. 15, No. 2, pp. 139-159.

Nishimura, J., H., Shintani and H., Yamamoto, 1996, "Earthquake Resistance og Geogrid Reinforced Soil Walls Based on a Study Conducted Following the Southern Hyogo Earthquake", *Proceedings of International Symposium on Earth Reinforce-*

ment, pp. 439-444, Rotherdam, Balkema.

Okabe S., 1924, "General Theory on Earth Pressure and Seismic Stability of Retaining Wall and Dam Doboku Gakkai", *Journal of the Japan Society of Civil Engineers*, Vol. 10, No. 6, pp. 1277-1323.

Olden, J.D., M.K., Joy and R.G., Death, 2004, "An accurate comparison of methods for quantifying variable importance in artificial neural networks using simulated data", *Ecological Modeling*, Vol. 178, No. 3-4, pp. 389-397.

Olgun, C.G. and J.R., Martin, 2002, "Performance of Analysis of Arifiye Overpass Reinforced Earthwalls During the 1999 Kocaeli (Turkey)", *Earthquake Reinforced Soil Engineering: Advances in Research and Practice*, Edited by H.I. Ling and D. Leshchinsky, in Progress expected to be published in 2002.

Penumadu, D., Jin-Nan, L., Chameau, J.-L., and Arumugam, S., 1994. "Rate dependent behavior of clays using neural networks." *Proceedings of the 13th Conference of the International Society of Soil Mechanics and Foundation Engineering*, New Delhi, pp. 1445-1448.

Rahman, M.S., J., Wang, W., Deng and J.P., Carter, 2001, "A neural network model for the uplift capacity of suction cassions", *Computers and Geotechnics*, Vol. 28, No. 4, pp. 269-287.

Rankine, R. and N., Sivakugan, 2005, "Prediction of paste backfill performance using artificial neural networks", *Proceedings of the 16th International Society for Soil Mechanics and Foundation Engineering*, Osaka, Japan, pp. 1107-1110.

Rathje, E.M. and N.A., Abrahamson, 1998, "Simplified frequency content estimates of earthquake ground motions", *Journal of Geotechnicaland Geoenvironmental Engineering*, Vol. 124, No. 2, pp. 150-159.

Richardson, G.N. and K.L., Lee, 1975, "Seismic Design of Reinforced Earth Walls",

Journal Goetechnical Engineering Division, Vol. 101., GT2, pp. 167-18.

Riddell, R., 2007, "On Ground Motion Intensity Indices", *Earthquake Spectra*, Vol. 23, No. 1, pp. 147-173.

Rimoldi, P., 2002, *Reinforced Soil Retaining Walls*, http: // www.tenax.net / geosynthetics/ techdoc.htm.

Rizzo, D.M. and D.E., Dougherty, 1994, "Application of artificial neural networks for site characterization using hard and soft information", *Proceedings of the 10th International Conference on Computational Methods in Water Resources*, Dordrecht: Kluwer Academic, pp. 793-799.

Rizzo, D.M., T.P., Lillys and D.E., Dougherty, 1996, "Comparisons of site characterization methods using mixed data", *ASCE Geotechnical Special Publication*, Vol. 58, No. 1, pp. 157-179.

Rogers, L.L. and F.U., Dowla, 1994, "Optimization of groundwater remediation using artificial neural networks with parallel solute transport modeling", *Water Resources Research*, Vol. 30, No. 2, pp. 457-481.

Rowe, R.K. and S.K., Ho, 1997, "Continuous Panel Reinforced Soil Walls on Rigid Foundations", *Journal of Geotechnical and Geoenvironmental Engineering*, Vol. 123, No. 10, pp. 912-920.

Rowe, R.K. and G.D., Skinner, 2001, "Numerical analysis of geosynthetic reinforced retaining wall constructed on a layered soil foundation", *Geotextiles and Geomembranes*, Vol. 19, No. 7, pp. 387-412.

Salchenberger, L.M., E.M., Cinar and N.A., Lash, 1992, "Neural networks: A new tool for predicting thrift failures", *Decision Science*, No. 23, pp. 899-916.

Sarma S. K., 1975, "Seismic Stability of Earth Dams and Embankments", *Géotechique*, Vol. 25, No. 4, pp. 473-761.

Seed, H.B. and R.V., Whitman, 1970, "Design of Earth Remaining Structures for Dynamic Loads", *Proceedings of the ASCE Specialty Conference. Lateral Stresses in the Ground and Design of Earth Retaining Structures*, Ithaca, New York, pp. 103-147.

Segrestin, P. and M.J., Bastick, 1988, "Seismic Design of Reinforced Earth Retaining Walls - the Contribution of Finite Element Analysis, *Theory and Practice of Earth Reinforcement:", Proceedings of the International Geotechnical Symposium on Theory and Practice of Earth Reinforcemen,. IS-Kyushu* '88. Fukuoka, Japan, Balkema, Rotterdam, pp. 577-582.

SeismoSignal, 2002, developed by Stelios Antoniou and Rui Pinho, SeismoSoftCompany.

Shahin, M.A. 2008, "Modeling axial capacity of pile foundations by intelligent computing", *Proceedings of the BGA International Conference on Foundations*, Dundee (Scotland), in press.

Shahin, M.A. and B., Indraratna, 2006, "Modeling the mechanical behavior of railway ballast using artificial neural networks", *Canadian Geotechnical Journal*, Vol. 43, No. 1, pp. 1144-1152.

Shahin, M.A. and M.B., Jaksa, 2004, "Probabilistic assessment of the uncertainty associated with the pullout capacity of marquee ground anchors", *Proceedings of the 9th Australia New Zealand Conference on Geomechanics*, Auckland, In Press.

Shahin, M.A. and M.B., Jaksa, 2005a, "Modeling the pullout capacity of marquee ground anchors using neurofuzzy technique", *Proceedings of the International Journal of Modeling and Simulation*, MODSIM 2005, Melbourne, Australia, pp. 66-72.

Shahin, M.A. and M.B., Jaksa, 2006, "Pullout capacity of small ground anchors by direct cone penetration test methods and neural methods", *Canadian Geotechnical*

Journal, Vol. 43, No. 6, pp. 626-637.

Shahin, M.A., H.R., Maier and M.B., Jaksa, 2004b, "Data division for developing neural networks applied to geotechnical engineering", *Journal of Computing in Civil Engineering, ASCE*, Vol. 18, No. 2, pp. 105-114.

Shahin, M.A., H.R., Maier and M.B., Jaksa, 2005c "Investigation into the robustness of artificial neural network models for a case study in civil engineering", *Proceedings of the International Congress on Modeling and Simulation*, MODSIM 2005, Melbourne (Australia), pp. 79-83.

Shang, J.Q., W., Ding, R.K., Rowe and L., Josic, 2004, "Detecting heavy metal contamination in soil using complex permittivity and artificial neural networks", *Canadian Geotechnical Journal*, Vol. 41, No. 6, pp. 1054-1067.

Shi, J.J., 2000, "Reducing prediction error by transforming input data for neural networks", *Journal of Computing in Civil Engineering*, ASCE, Vol. 14, No. 2, pp. 109-116.

Shi, J., J.A.R., Ortigao and J., Bai, 1998, "Modular neural networks for predicting settlement during tunneling", *Journal of Geotechnical and Geoenvironmental Engineering*, ASCE, Vol. 124, No. 5, pp. 389-395.

Sidarta, D.E. and J., Ghaboussi, 1998, "Constitutive modeling of geomaterials from non-uniform material tests", *Computers and Geomechanics*, Vol. 22, No. 10, pp. 53-71.

Singh, T.N. and V., Singh, 2005, "An intelligent approach to prediction and control ground vibration in mines", *Geotechnical and Geological Engineering*, Vol. 23, No. 3, pp. 249-262.

Sinha, S.K. and M.C., Wang, 2008, "Artificial neural network prediction models for soil compaction and permeability", *Geotechnical Engineering Journal*, Vol. 26 No.

1, pp. 47-64.

Smith, G.N. 1986, *Probability and statistics in civil engineering: An introduction*, Collins, London.

Smith, G.N. and E.L., Pole, 1980, *Elements of Foundation Design, Granada Publishing*, London.

Stone, M., 1974, "Cross-validatory choice and assessment of statistical predictions", *Journal of Royal Statistical Society*, No. 36, pp. 111-147.

Sucuoglu, H., 1997, Discussion of "An approach to the measurement of the potential structural damage of earthquake ground motions", *Earthquake Engineering and Structural Dynamics*, No. 26, pp. 1283-1285.

Sucuoğlu, H., P., Gülkan, A., Erberik and S., Akkar, 1999, Measures of ground motion intensity in seismic design, *Proceedings of the Uğur Ersoy Symposium on Structural Engineering*, Ankara, pp. 105-119.

Tatsuoka, F. and M., Tateyama, 1995, "Performance of Geogrid Reinforced Soil Retaining Walls During the Great Hanshin-Auagi Earthquake, January 17, 1995", *Proceedings of International Symposium on Earth Reinforcement*, pp. 55-62, Rotherdam, Balkema.

Tatsuoka, F., J., Koseki and M., Takeyama, 1997, "Performance of Reinforced Soil Structures During the 1995 Hyokogan Nanbu Earthquake", *Proceedings of International Symposium on Earth Reinforcement*, pp. 973-1007, Rotherdam, Balkema

Tokar, S.A. and P.A., Johnson, 1999, "Rainfall-runoff modeling using artificial neural networks." *Journal of Hydrologic Engineering*, Vol. 4, No. 3, pp. 232-239.

Travasarou, T., J.D., Bray and N.A., Abrahamson, 2003, Empirical attenuation relationship for Arias Intensity, *Earthquake Engineering and Structural Dynamics*, No. 32, pp. 1133-1155.

Tutumluer, E. and U., Seyhan, 1998, "Neural network modeling of anisotropic aggregate behavior from repeated load triaxial tests", *Transportation Research Record 1615*, National Research Council, Washington, DC.

Twomey, J.M. and A.E., Smith, 1997, "Validation and verification", *Artificial neural networks for civil engineers: Fundamentals and applications*, N. Kartam, I. Flood, and J. H. Garrett, eds., ASCE, New York, pp. 44-64.

Uang, C.H. and V.V., Bertero, 1988, Implications of recorded earthquake ground motions on seismic design of buildings structures, *UCB/EERC*-88/13, California.

Ural, D.N. and H., Saka, 1998, "Liquefaction assessment by neural networks", *Electronic Journal of Geotechnical Engineering*, http://www.ejge.com/Ppr9803/ Ppr9803.htm

Von Thun J.L., L.H., Roehim, G.A., Scott and J.A., Wilson, 1988, "Earthquake ground motions for design and analysis of dams, Earthquake Engineering and Soil Dynamics II-Recent Advances in Ground Motion Evaluation", *Geotechnical Special Publication*, No. 20, pp. 463-481.

White, D.M. and R.R., Holtz, 1997, "Performance of Geosynthetic Reinforced Soils and Walls During the Northridge, California Earthquake of January 17, 1994", *Earth Reinforcement*, Balkema, No. 2, pp. 965-972.

White, H., 1989, "Learning in artificial neural networks: A statistical perspective", *Neural Computation*, No. 1, pp. 425-464.

Wolfe, W.E., K.L., Lee, D., Rea and A.M., Yourman, 1978, "The Effect of Vertical Motion on the Seismic Stability of Reinforced Earth Walls", *Proceedings of the ASCE Symposium on Earth Reinforcement.* Pittsburgh, Pennsylvania, USA, pp. 856-879.

Wu, Y.M., N.C., Hsiao and T.L., Teng, 2004, "Relationship between strong motion peak values and seismic loss during the 1999 Chi-Chi, Taiwan earthquake", *Natural*

Hazards, No. 32, pp. 357-373.

Yang, Y. and M.S., Rosenbaum, 2002, "The artificial neural network as a tool for assessing geotechnical properties", *Geotechnical Engineering Journal*, Vol. 20, No. 2, pp. 149-168

Yılmaz, H., 2007, *Correlation of deformation demands with ground motion intensity*, PhD Thesis, Middle East Technical University.

Yoo, C. and J., Kim, 2007, "Tunneling performance prediction using an integrated GIS and neural network", *Computers and Geotechnics*, Vol. 34, No. 1, pp. 19-30.

Young-Su, K. and K., Byung-Tak, 2006, "Use of artificial neural networks in the prediction of liquefaction resistance of sands", *Journal of Geotechnical and Geoenvironmental Engineering*, Vol. 132, No. 11, pp. 1502-1504.

Zarrabi K., 1979, *Sliding of Gravity Retaining Wall During Earthquakes Considering Vertical Acceleration and Changing Inclination of Failure Surface*, MSc thesis, Department of Civil Engineering, Massachusetts Institute of Technology, Cambridge, Massachusetts, USA.

Zevgolis, I., 2007, *Numerical and Probabilistic Analysis of Reinforced Soil Structures*, PhD Thesis, Purdue University.

Zhou, Y. and X., Wu, 1994, "Use of neural networks in the analysis and interpretation of site investigation data", *Computer and Geotechnics*, No. 16, pp. 105-122.

Zhu, J.H., M.M., Zaman and S.A., Anderson, 1998a, "Modeling of soil behavior with a recurrent neural network", *Canadian Geotechnical Journal*, Vol. 35, No. 5, pp. 858-872.

Zhu, J.H., M.M., Zaman and S.A., Anderson, 1998b, "Modeling of shearing behaviour of a residual soil with recurrent neural network", *International Journal of Numerical and Analytical Methods in Geomechanics*, Vol. 22, No. 8, pp. 671-687.

Zhu, J.H., M.M., Zaman and T.B., Trafalis, 1996, "Prediction of shear stress-strain behavior of soil with recurrent neural network", *Intelligent Engineering Systems Through Artificial Neural Networks*, No. 6, pp. 809-814.

Zurada, J.M., 1992, Introduction to artificial neural systems, West Publishing Company, St. Paul.

Zurada, J.M., 1992, Introduction to artificial neural systems, West Publishing Company, St. Paul.

APPENDIX A: FEA RESULTS FOR ANN REGRESSION MODEL

Table A.1. Appendix A

INPUT											OUTPUT
Wall Geometry				IM							
H (m)	Sv (m)	L (m)	L/H	PGA (m/s2)	PGV (m/s)	Aeff (m/s2)	Ia (m/s)	CAV (m/s)	ASI (m/s)	VSI (m)	Displacement (cm)
6	0.6	3	0.5	1.977	0.096	1.961	0.5	2.83	2.01	0.32	29.1
6	0.6	3.6	0.6	1.977	0.096	1.961	0.5	2.83	2.01	0.32	28.5
6	0.6	4.2	0.7	1.977	0.096	1.961	0.5	2.83	2.01	0.32	27.8
6	0.6	4.8	0.8	1.977	0.096	1.961	0.5	2.83	2.01	0.32	26.5
6	0.6	5.4	0.9	1.977	0.096	1.961	0.5	2.83	2.01	0.32	25
6	0.6	6	1	1.977	0.096	1.961	0.5	2.83	2.01	0.32	23.4
6	0.6	7.2	1.2	1.977	0.096	1.961	0.5	2.83	2.01	0.32	20.3
6	0.6	8.4	1.4	1.977	0.096	1.961	0.5	2.83	2.01	0.32	18
6	0.6	9.6	1.6	1.977	0.096	1.961	0.5	2.83	2.01	0.32	16.1
6	0.6	11	1.8	1.977	0.096	1.961	0.5	2.83	2.01	0.32	14.7
6	0.6	12	2	1.977	0.096	1.961	0.5	2.83	2.01	0.32	13.1
6	0.6	3	0.5	3.999	0.196	3.903	2.15	5.96	4.1	0.64	38.4
6	0.6	3.6	0.6	3.999	0.196	3.903	2.15	5.96	4.1	0.64	37.3
6	0.6	4.2	0.7	3.999	0.196	3.903	2.15	5.96	4.1	0.64	35.2
6	0.6	4.8	0.8	3.999	0.196	3.903	2.15	5.96	4.1	0.64	34.5
6	0.6	5.4	0.9	3.999	0.196	3.903	2.15	5.96	4.1	0.64	34.3
6	0.6	6	1	3.999	0.196	3.903	2.15	5.96	4.1	0.64	33.7
6	0.6	7.2	1.2	3.999	0.196	3.903	2.15	5.96	4.1	0.64	32
6	0.6	8.4	1.4	3.999	0.196	3.903	2.15	5.96	4.1	0.64	30.4
6	0.6	9.6	1.6	3.999	0.196	3.903	2.15	5.96	4.1	0.64	28.4
6	0.6	11	1.8	3.999	0.196	3.903	2.15	5.96	4.1	0.64	26.7
6	0.6	12	2	3.999	0.196	3.903	2.15	5.96	4.1	0.64	25.3
6	0.6	3	0.5	5.930	0.288	5.882	4.51	8.48	6.04	0.95	41.5
6	0.6	3.6	0.6	5.930	0.288	5.882	4.51	8.48	6.04	0.95	39.6
6	0.6	4.2	0.7	5.930	0.288	5.882	4.51	8.48	6.04	0.95	37.9
6	0.6	4.8	0.8	5.930	0.288	5.882	4.51	8.48	6.04	0.95	37.6
6	0.6	5.4	0.9	5.930	0.288	5.882	4.51	8.48	6.04	0.95	37.3
6	0.6	6	1	5.930	0.288	5.882	4.51	8.48	6.04	0.95	37.1
6	0.6	7.2	1.2	5.930	0.288	5.882	4.51	8.48	6.04	0.95	35.9
6	0.6	8.4	1.4	5.930	0.288	5.882	4.51	8.48	6.04	0.95	35

INPUT											OUTPUT
Wall Geometry				IM							
H (m)	Sv (m)	L (m)	L/H	PGA (m/s2)	PGV (m/s)	Aeff (m/s2)	Ia (m/s)	CAV (m/s)	ASI (m/s)	VSI (m)	Displacement (cm)
6	0.6	9.6	1.6	5.930	0.288	5.882	4.51	8.48	6.04	0.95	32.8
6	0.6	11	1.8	5.930	0.288	5.882	4.51	8.48	6.04	0.95	31.6
6	0.6	12	2	5.930	0.288	5.882	4.51	8.48	6.04	0.95	31.2
6	0.4	3	0.5	1.977	0.096	1.961	0.5	2.83	2.01	0.32	28.7
6	0.4	3.6	0.6	1.977	0.096	1.961	0.5	2.83	2.01	0.32	27.2
6	0.4	4.2	0.7	1.977	0.096	1.961	0.5	2.83	2.01	0.32	25.7
6	0.4	4.8	0.8	1.977	0.096	1.961	0.5	2.83	2.01	0.32	24.1
6	0.4	5.4	0.9	1.977	0.096	1.961	0.5	2.83	2.01	0.32	21.6
6	0.4	6	1	1.977	0.096	1.961	0.5	2.83	2.01	0.32	19.8
6	0.4	7.2	1.2	1.977	0.096	1.961	0.5	2.83	2.01	0.32	16.7
6	0.4	8.4	1.4	1.977	0.096	1.961	0.5	2.83	2.01	0.32	14.2
6	0.4	9.6	1.6	1.977	0.096	1.961	0.5	2.83	2.01	0.32	11.9
6	0.4	11	1.8	1.977	0.096	1.961	0.5	2.83	2.01	0.32	10.7
6	0.4	12	2	1.977	0.096	1.961	0.5	2.83	2.01	0.32	10.1
6	0.4	3	0.5	3.999	0.196	3.903	2.15	5.96	4.1	0.64	37
6	0.4	3.6	0.6	3.999	0.196	3.903	2.15	5.96	4.1	0.64	35.5
6	0.4	4.2	0.7	3.999	0.196	3.903	2.15	5.96	4.1	0.64	33.2
6	0.4	4.8	0.8	3.999	0.196	3.903	2.15	5.96	4.1	0.64	32.1
6	0.4	5.4	0.9	3.999	0.196	3.903	2.15	5.96	4.1	0.64	30.8
6	0.4	6	1	3.999	0.196	3.903	2.15	5.96	4.1	0.64	29.3
6	0.4	7.2	1.2	3.999	0.196	3.903	2.15	5.96	4.1	0.64	27.1
6	0.4	8.4	1.4	3.999	0.196	3.903	2.15	5.96	4.1	0.64	24.6
6	0.4	9.6	1.6	3.999	0.196	3.903	2.15	5.96	4.1	0.64	21.9
6	0.4	11	1.8	3.999	0.196	3.903	2.15	5.96	4.1	0.64	20.4
6	0.4	12	2	3.999	0.196	3.903	2.15	5.96	4.1	0.64	19.2
6	0.4	3	0.5	5.930	0.288	5.882	4.51	8.48	6.04	0.95	38.2
6	0.4	3.6	0.6	5.930	0.288	5.882	4.51	8.48	6.04	0.95	37
6	0.4	4.2	0.7	5.930	0.288	5.882	4.51	8.48	6.04	0.95	36.3
6	0.4	4.8	0.8	5.930	0.288	5.882	4.51	8.48	6.04	0.95	35.7
6	0.4	5.4	0.9	5.930	0.288	5.882	4.51	8.48	6.04	0.95	34.6
6	0.4	6	1	5.930	0.288	5.882	4.51	8.48	6.04	0.95	33.6
6	0.4	7.2	1.2	5.930	0.288	5.882	4.51	8.48	6.04	0.95	32
6	0.4	8.4	1.4	5.930	0.288	5.882	4.51	8.48	6.04	0.95	29.7
6	0.4	9.6	1.6	5.930	0.288	5.882	4.51	8.48	6.04	0.95	27.4
6	0.4	11	1.8	5.930	0.288	5.882	4.51	8.48	6.04	0.95	26.1
6	0.4	12	2	5.930	0.288	5.882	4.51	8.48	6.04	0.95	24.3
6	0.2	3	0.5	1.977	0.096	1.961	0.5	2.83	2.01	0.32	25.5
6	0.2	3.6	0.6	1.977	0.096	1.961	0.5	2.83	2.01	0.32	23.1
6	0.2	4.2	0.7	1.977	0.096	1.961	0.5	2.83	2.01	0.32	21.1
6	0.2	4.8	0.8	1.977	0.096	1.961	0.5	2.83	2.01	0.32	19.2

INPUT											OUTPUT
Wall Geometry				IM							
H (m)	Sv (m)	L (m)	L/H	PGA (m/s2)	PGV (m/s)	Aeff (m/s2)	Ia (m/s)	CAV (m/s)	ASI (m/s)	VSI (m)	Displacement (cm)
6	0.2	5.4	0.9	1.977	0.096	1.961	0.5	2.83	2.01	0.32	16.4
6	0.2	6	1	1.977	0.096	1.961	0.5	2.83	2.01	0.32	14.7
6	0.2	7.2	1.2	1.977	0.096	1.961	0.5	2.83	2.01	0.32	11.7
6	0.2	8.4	1.4	1.977	0.096	1.961	0.5	2.83	2.01	0.32	9.7
6	0.2	9.6	1.6	1.977	0.096	1.961	0.5	2.83	2.01	0.32	8.5
6	0.2	11	1.8	1.977	0.096	1.961	0.5	2.83	2.01	0.32	7.7
6	0.2	12	2	1.977	0.096	1.961	0.5	2.83	2.01	0.32	7.1
6	0.2	3	0.5	3.999	0.196	3.903	2.15	5.96	4.1	0.64	31.9
6	0.2	3.6	0.6	3.999	0.196	3.903	2.15	5.96	4.1	0.64	29.8
6	0.2	4.2	0.7	3.999	0.196	3.903	2.15	5.96	4.1	0.64	27.5
6	0.2	4.8	0.8	3.999	0.196	3.903	2.15	5.96	4.1	0.64	25.8
6	0.2	5.4	0.9	3.999	0.196	3.903	2.15	5.96	4.1	0.64	23.5
6	0.2	6	1	3.999	0.196	3.903	2.15	5.96	4.1	0.64	22
6	0.2	7.2	1.2	3.999	0.196	3.903	2.15	5.96	4.1	0.64	18.8
6	0.2	8.4	1.4	3.999	0.196	3.903	2.15	5.96	4.1	0.64	17.2
6	0.2	9.6	1.6	3.999	0.196	3.903	2.15	5.96	4.1	0.64	15.2
6	0.2	11	1.8	3.999	0.196	3.903	2.15	5.96	4.1	0.64	13.6
6	0.2	12	2	3.999	0.196	3.903	2.15	5.96	4.1	0.64	12.5
6	0.2	3	0.5	5.930	0.288	5.882	4.51	8.48	6.04	0.95	36.5
6	0.2	3.6	0.6	5.930	0.288	5.882	4.51	8.48	6.04	0.95	34
6	0.2	4.2	0.7	5.930	0.288	5.882	4.51	8.48	6.04	0.95	33
6	0.2	4.8	0.8	5.930	0.288	5.882	4.51	8.48	6.04	0.95	29.4
6	0.2	5.4	0.9	5.930	0.288	5.882	4.51	8.48	6.04	0.95	27.5
6	0.2	6	1	5.930	0.288	5.882	4.51	8.48	6.04	0.95	26
6	0.2	7.2	1.2	5.930	0.288	5.882	4.51	8.48	6.04	0.95	22.5
6	0.2	8.4	1.4	5.930	0.288	5.882	4.51	8.48	6.04	0.95	20.2
6	0.2	9.6	1.6	5.930	0.288	5.882	4.51	8.48	6.04	0.95	17.8
6	0.2	11	1.8	5.930	0.288	5.882	4.51	8.48	6.04	0.95	16.3
6	0.2	12	2	5.930	0.288	5.882	4.51	8.48	6.04	0.95	15.3
5	0.6	2.5	0.5	1.977	0.096	1.961	0.5	2.83	2.01	0.32	18.5
5	0.6	3	0.6	1.977	0.096	1.961	0.5	2.83	2.01	0.32	18.3
5	0.6	3.5	0.7	1.977	0.096	1.961	0.5	2.83	2.01	0.32	17.6
5	0.6	4	0.8	1.977	0.096	1.961	0.5	2.83	2.01	0.32	17.6
5	0.6	4.5	0.9	1.977	0.096	1.961	0.5	2.83	2.01	0.32	17.6
5	0.6	5	1	1.977	0.096	1.961	0.5	2.83	2.01	0.32	17.1
5	0.6	6	1.2	1.977	0.096	1.961	0.5	2.83	2.01	0.32	15.5
5	0.6	7	1.4	1.977	0.096	1.961	0.5	2.83	2.01	0.32	14.2
5	0.6	8	1.6	1.977	0.096	1.961	0.5	2.83	2.01	0.32	13.2
5	0.6	9	1.8	1.977	0.096	1.961	0.5	2.83	2.01	0.32	12.5
5	0.6	10	2	1.977	0.096	1.961	0.5	2.83	2.01	0.32	12.3
5	0.6	2.5	0.5	3.999	0.196	3.903	2.15	5.96	4.1	0.64	22

INPUT											OUTPUT
Wall Geometry				IM							
H (m)	Sv (m)	L (m)	L/H	PGA (m/s2)	PGV (m/s)	Aeff (m/s2)	Ia (m/s)	CAV (m/s)	ASI (m/s)	VSI (m)	Displacement (cm)
5	0.6	3	0.6	3.999	0.196	3.903	2.15	5.96	4.1	0.64	21.2
5	0.6	3.5	0.7	3.999	0.196	3.903	2.15	5.96	4.1	0.64	20.9
5	0.6	4	0.8	3.999	0.196	3.903	2.15	5.96	4.1	0.64	20.8
5	0.6	4.5	0.9	3.999	0.196	3.903	2.15	5.96	4.1	0.64	20.6
5	0.6	5	1	3.999	0.196	3.903	2.15	5.96	4.1	0.64	20.3
5	0.6	6	1.2	3.999	0.196	3.903	2.15	5.96	4.1	0.64	19.7
5	0.6	7	1.4	3.999	0.196	3.903	2.15	5.96	4.1	0.64	18.8
5	0.6	8	1.6	3.999	0.196	3.903	2.15	5.96	4.1	0.64	17.9
5	0.6	9	1.8	3.999	0.196	3.903	2.15	5.96	4.1	0.64	17.4
5	0.6	10	2	3.999	0.196	3.903	2.15	5.96	4.1	0.64	17.2
5	0.6	2.5	0.5	5.930	0.288	5.882	4.51	8.48	6.04	0.95	23.2
5	0.6	3	0.6	5.930	0.288	5.882	4.51	8.48	6.04	0.95	22.7
5	0.6	3.5	0.7	5.930	0.288	5.882	4.51	8.48	6.04	0.95	22.2
5	0.6	4	0.8	5.930	0.288	5.882	4.51	8.48	6.04	0.95	22
5	0.6	4.5	0.9	5.930	0.288	5.882	4.51	8.48	6.04	0.95	21.8
5	0.6	5	1	5.930	0.288	5.882	4.51	8.48	6.04	0.95	21.6
5	0.6	6	1.2	5.930	0.288	5.882	4.51	8.48	6.04	0.95	21.2
5	0.6	7	1.4	5.930	0.288	5.882	4.51	8.48	6.04	0.95	20.3
5	0.6	8	1.6	5.930	0.288	5.882	4.51	8.48	6.04	0.95	19.6
5	0.6	9	1.8	5.930	0.288	5.882	4.51	8.48	6.04	0.95	19.5
5	0.6	10	2	5.930	0.288	5.882	4.51	8.48	6.04	0.95	19.2
5	0.4	2.5	0.5	1.977	0.096	1.961	0.5	2.83	2.01	0.32	18.3
5	0.4	3	0.6	1.977	0.096	1.961	0.5	2.83	2.01	0.32	18.1
5	0.4	3.5	0.7	1.977	0.096	1.961	0.5	2.83	2.01	0.32	17.8
5	0.4	4	0.8	1.977	0.096	1.961	0.5	2.83	2.01	0.32	16.9
5	0.4	4.5	0.9	1.977	0.096	1.961	0.5	2.83	2.01	0.32	15.7
5	0.4	5	1	1.977	0.096	1.961	0.5	2.83	2.01	0.32	14.6
5	0.4	6	1.2	1.977	0.096	1.961	0.5	2.83	2.01	0.32	13
5	0.4	7	1.4	1.977	0.096	1.961	0.5	2.83	2.01	0.32	12.2
5	0.4	8	1.6	1.977	0.096	1.961	0.5	2.83	2.01	0.32	11.9
5	0.4	9	1.8	1.977	0.096	1.961	0.5	2.83	2.01	0.32	11.3
5	0.4	10	2	1.977	0.096	1.961	0.5	2.83	2.01	0.32	10.5
5	0.4	2.5	0.5	3.999	0.196	3.903	2.15	5.96	4.1	0.64	21
5	0.4	3	0.6	3.999	0.196	3.903	2.15	5.96	4.1	0.64	20.9
5	0.4	3.5	0.7	3.999	0.196	3.903	2.15	5.96	4.1	0.64	20.4
5	0.4	4	0.8	3.999	0.196	3.903	2.15	5.96	4.1	0.64	20.1
5	0.4	4.5	0.9	3.999	0.196	3.903	2.15	5.96	4.1	0.64	19.4
5	0.4	5	1	3.999	0.196	3.903	2.15	5.96	4.1	0.64	18.9
5	0.4	6	1.2	3.999	0.196	3.903	2.15	5.96	4.1	0.64	17.5
5	0.4	7	1.4	3.999	0.196	3.903	2.15	5.96	4.1	0.64	16.4
5	0.4	8	1.6	3.999	0.196	3.903	2.15	5.96	4.1	0.64	16

INPUT											OUTPUT
Wall Geometry				IM							
H (m)	Sv (m)	L (m)	L/H	PGA (m/s2)	PGV (m/s)	Aeff (m/s2)	Ia (m/s)	CAV (m/s)	ASI (m/s)	VSI (m)	Displacement (cm)
5	0.4	9	1.8	3.999	0.196	3.903	2.15	5.96	4.1	0.64	16
5	0.4	10	2	3.999	0.196	3.903	2.15	5.96	4.1	0.64	15.8
5	0.4	2.5	0.5	5.930	0.288	5.882	4.51	8.48	6.04	0.95	22.3
5	0.4	3	0.6	5.930	0.288	5.882	4.51	8.48	6.04	0.95	22.1
5	0.4	3.5	0.7	5.930	0.288	5.882	4.51	8.48	6.04	0.95	21.6
5	0.4	4	0.8	5.930	0.288	5.882	4.51	8.48	6.04	0.95	21.3
5	0.4	4.5	0.9	5.930	0.288	5.882	4.51	8.48	6.04	0.95	20.6
5	0.4	5	1	5.930	0.288	5.882	4.51	8.48	6.04	0.95	20.2
5	0.4	6	1.2	5.930	0.288	5.882	4.51	8.48	6.04	0.95	19
5	0.4	7	1.4	5.930	0.288	5.882	4.51	8.48	6.04	0.95	18.2
5	0.4	8	1.6	5.930	0.288	5.882	4.51	8.48	6.04	0.95	18.1
5	0.4	9	1.8	5.930	0.288	5.882	4.51	8.48	6.04	0.95	18.1
5	0.4	10	2	5.930	0.288	5.882	4.51	8.48	6.04	0.95	18.1
5	0.2	2.5	0.5	1.977	0.096	1.961	0.5	2.83	2.01	0.32	17.1
5	0.2	3	0.6	1.977	0.096	1.961	0.5	2.83	2.01	0.32	15.8
5	0.2	3.5	0.7	1.977	0.096	1.961	0.5	2.83	2.01	0.32	14
5	0.2	4	0.8	1.977	0.096	1.961	0.5	2.83	2.01	0.32	12.8
5	0.2	4.5	0.9	1.977	0.096	1.961	0.5	2.83	2.01	0.32	12
5	0.2	5	1	1.977	0.096	1.961	0.5	2.83	2.01	0.32	11.8
5	0.2	6	1.2	1.977	0.096	1.961	0.5	2.83	2.01	0.32	11
5	0.2	7	1.4	1.977	0.096	1.961	0.5	2.83	2.01	0.32	9.1
5	0.2	8	1.6	1.977	0.096	1.961	0.5	2.83	2.01	0.32	7.4
5	0.2	9	1.8	1.977	0.096	1.961	0.5	2.83	2.01	0.32	6.6
5	0.2	10	2	1.977	0.096	1.961	0.5	2.83	2.01	0.32	5.8
5	0.2	2.5	0.5	3.999	0.196	3.903	2.15	5.96	4.1	0.64	19.9
5	0.2	3	0.6	3.999	0.196	3.903	2.15	5.96	4.1	0.64	18.8
5	0.2	3.5	0.7	3.999	0.196	3.903	2.15	5.96	4.1	0.64	17.5
5	0.2	4	0.8	3.999	0.196	3.903	2.15	5.96	4.1	0.64	16.5
5	0.2	4.5	0.9	3.999	0.196	3.903	2.15	5.96	4.1	0.64	15.3
5	0.2	5	1	3.999	0.196	3.903	2.15	5.96	4.1	0.64	14.9
5	0.2	6	1.2	3.999	0.196	3.903	2.15	5.96	4.1	0.64	14.1
5	0.2	7	1.4	3.999	0.196	3.903	2.15	5.96	4.1	0.64	13.4
5	0.2	8	1.6	3.999	0.196	3.903	2.15	5.96	4.1	0.64	12.6
5	0.2	9	1.8	3.999	0.196	3.903	2.15	5.96	4.1	0.64	11.6
5	0.2	10	2	3.999	0.196	3.903	2.15	5.96	4.1	0.64	10.4
5	0.2	2.5	0.5	5.930	0.288	5.882	4.51	8.48	6.04	0.95	20.8
5	0.2	3	0.6	5.930	0.288	5.882	4.51	8.48	6.04	0.95	19.3
5	0.2	3.5	0.7	5.930	0.288	5.882	4.51	8.48	6.04	0.95	18.1
5	0.2	4	0.8	5.930	0.288	5.882	4.51	8.48	6.04	0.95	17.2
5	0.2	4.5	0.9	5.930	0.288	5.882	4.51	8.48	6.04	0.95	16.4

INPUT											OUTPUT
Wall Geometry				IM							
H (m)	Sv (m)	L (m)	L/H	PGA (m/s2)	PGV (m/s)	Aeff (m/s2)	Ia (m/s)	CAV (m/s)	ASI (m/s)	VSI (m)	Displacement (cm)
5	0.2	5	1	5.930	0.288	5.882	4.51	8.48	6.04	0.95	16
5	0.2	4	0.8	5.930	0.288	5.882	4.51	8.48	6.04	0.95	17.2
5	0.2	4.5	0.9	5.930	0.288	5.882	4.51	8.48	6.04	0.95	16.4
5	0.2	5	1	5.930	0.288	5.882	4.51	8.48	6.04	0.95	16
5	0.2	6	1.2	5.930	0.288	5.882	4.51	8.48	6.04	0.95	15.3
5	0.2	7	1.4	5.930	0.288	5.882	4.51	8.48	6.04	0.95	15.1
5	0.2	8	1.6	5.930	0.288	5.882	4.51	8.48	6.04	0.95	14.7
5	0.2	9	1.8	5.930	0.288	5.882	4.51	8.48	6.04	0.95	13.7
5	0.2	10	2	5.930	0.288	5.882	4.51	8.48	6.04	0.95	12.8
7	0.2	4.9	0.7	1.977	0.096	1.961	0.5	2.83	2.01	0.32	22.6
7	0.2	7	1	1.977	0.096	1.961	0.5	2.83	2.01	0.32	17.5
7	0.2	11	1.5	1.977	0.096	1.961	0.5	2.83	2.01	0.32	13.7
7	0.4	4.9	0.7	1.977	0.096	1.961	0.5	2.83	2.01	0.32	27.4
7	0.4	7	1	1.977	0.096	1.961	0.5	2.83	2.01	0.32	20.5
7	0.4	11	1.5	1.977	0.096	1.961	0.5	2.83	2.01	0.32	15.3
7	0.6	4.9	0.7	1.977	0.096	1.961	0.5	2.83	2.01	0.32	30
7	0.6	7	1	1.977	0.096	1.961	0.5	2.83	2.01	0.32	23.7
7	0.6	11	1.5	1.977	0.096	1.961	0.5	2.83	2.01	0.32	18.5
7	0.8	4.9	0.7	1.977	0.096	1.961	0.5	2.83	2.01	0.32	32.2
7	0.8	7	1	1.977	0.096	1.961	0.5	2.83	2.01	0.32	26
7	0.8	11	1.5	1.977	0.096	1.961	0.5	2.83	2.01	0.32	20.9
7	0.2	4.9	0.7	3.999	0.196	3.903	2.15	5.96	4.1	0.64	35.8
7	0.2	7	1	3.999	0.196	3.903	2.15	5.96	4.1	0.64	31.1
7	0.2	11	1.5	3.999	0.196	3.903	2.15	5.96	4.1	0.64	28.3
7	0.4	4.9	0.7	3.999	0.196	3.903	2.15	5.96	4.1	0.64	40.7
7	0.4	7	1	3.999	0.196	3.903	2.15	5.96	4.1	0.64	33.4
7	0.4	11	1.5	3.999	0.196	3.903	2.15	5.96	4.1	0.64	26.5
7	0.6	4.9	0.7	3.999	0.196	3.903	2.15	5.96	4.1	0.64	47.1
7	0.6	7	1	3.999	0.196	3.903	2.15	5.96	4.1	0.64	39.7
7	0.6	11	1.5	3.999	0.196	3.903	2.15	5.96	4.1	0.64	32.6
7	0.8	4.9	0.7	3.999	0.196	3.903	2.15	5.96	4.1	0.64	49.3
7	0.8	7	1	3.999	0.196	3.903	2.15	5.96	4.1	0.64	42.8
7	0.8	11	1.5	3.999	0.196	3.903	2.15	5.96	4.1	0.64	36.5
7	0.2	4.9	0.7	5.930	0.288	5.882	4.51	8.48	6.04	0.95	43.9
7	0.2	7	1	5.930	0.288	5.882	4.51	8.48	6.04	0.95	39
7	0.2	11	1.5	5.930	0.288	5.882	4.51	8.48	6.04	0.95	36.9
7	0.4	4.9	0.7	5.930	0.288	5.882	4.51	8.48	6.04	0.95	47.3
7	0.4	7	1	5.930	0.288	5.882	4.51	8.48	6.04	0.95	41
7	0.4	11	1.5	5.930	0.288	5.882	4.51	8.48	6.04	0.95	33.5
7	0.6	4.9	0.7	5.930	0.288	5.882	4.51	8.48	6.04	0.95	55.5

INPUT											OUTPUT
Wall Geometry				IM							
H (m)	Sv (m)	L (m)	L/H	PGA (m/s2)	PGV (m/s)	Aeff (m/s2)	Ia (m/s)	CAV (m/s)	ASI (m/s)	VSI (m)	Displacement (cm)
7	0.6	7	1	5.930	0.288	5.882	4.51	8.48	6.04	0.95	47.4
7	0.6	11	1.5	5.930	0.288	5.882	4.51	8.48	6.04	0.95	40
7	0.8	4.9	0.7	5.930	0.288	5.882	4.51	8.48	6.04	0.95	57
7	0.8	7	1	5.930	0.288	5.882	4.51	8.48	6.04	0.95	51.3
7	0.8	11	1.5	5.930	0.288	5.882	4.51	8.48	6.04	0.95	44.5
8	0.2	5.6	0.7	1.977	0.096	1.961	0.5	2.83	2.01	0.32	25.6
8	0.2	8	1	1.977	0.096	1.961	0.5	2.83	2.01	0.32	20.2
8	0.4	5.6	0.7	1.977	0.096	1.961	0.5	2.83	2.01	0.32	28.9
8	0.4	8	1	1.977	0.096	1.961	0.5	2.83	2.01	0.32	21.7
8	0.6	5.6	0.7	1.977	0.096	1.961	0.5	2.83	2.01	0.32	31.3
8	0.6	8	1	1.977	0.096	1.961	0.5	2.83	2.01	0.32	26.1
8	0.8	5.6	0.7	1.977	0.096	1.961	0.5	2.83	2.01	0.32	34.6
8	0.8	8	1	1.977	0.096	1.961	0.5	2.83	2.01	0.32	30.4
8	0.2	5.6	0.7	3.999	0.196	3.903	2.15	5.96	4.1	0.64	44.4
8	0.2	8	1	3.999	0.196	3.903	2.15	5.96	4.1	0.64	35.5
8	0.4	5.6	0.7	3.999	0.196	3.903	2.15	5.96	4.1	0.64	47.3
8	0.4	8	1	3.999	0.196	3.903	2.15	5.96	4.1	0.64	43.8
8	0.6	5.6	0.7	3.999	0.196	3.903	2.15	5.96	4.1	0.64	50.2
8	0.6	8	1	3.999	0.196	3.903	2.15	5.96	4.1	0.64	44.6
8	0.8	5.6	0.7	3.999	0.196	3.903	2.15	5.96	4.1	0.64	53.9
8	0.8	8	1	3.999	0.196	3.903	2.15	5.96	4.1	0.64	48.3
8	0.2	5.6	0.7	5.930	0.288	5.882	4.51	8.48	6.04	0.95	48.3
8	0.2	8	1	5.930	0.288	5.882	4.51	8.48	6.04	0.95	39.6
8	0.4	5.6	0.7	5.930	0.288	5.882	4.51	8.48	6.04	0.95	55.1
8	0.4	8	1	5.930	0.288	5.882	4.51	8.48	6.04	0.95	53.7
8	0.6	5.6	0.7	5.930	0.288	5.882	4.51	8.48	6.04	0.95	59.2
8	0.6	8	1	5.930	0.288	5.882	4.51	8.48	6.04	0.95	55.8
8	0.8	5.6	0.7	5.930	0.288	5.882	4.51	8.48	6.04	0.95	63.8
8	0.8	8	1	5.930	0.288	5.882	4.51	8.48	6.04	0.95	59.2
9	0.4	6.3	0.7	1.977	0.096	1.961	0.5	2.83	2.01	0.32	30.2
9	0.4	9	1	1.977	0.096	1.961	0.5	2.83	2.01	0.32	23.2
9	0.6	6.3	0.7	1.977	0.096	1.961	0.5	2.83	2.01	0.32	33.5
9	0.6	9	1	1.977	0.096	1.961	0.5	2.83	2.01	0.32	24.3
9	0.8	6.3	0.7	1.977	0.096	1.961	0.5	2.83	2.01	0.32	35.3
9	0.8	9	1	1.977	0.096	1.961	0.5	2.83	2.01	0.32	27.2
9	0.4	6.3	0.7	3.999	0.196	3.903	2.15	5.96	4.1	0.64	54.4
9	0.4	9	1	3.999	0.196	3.903	2.15	5.96	4.1	0.64	45
9	0.6	6.3	0.7	3.999	0.196	3.903	2.15	5.96	4.1	0.64	60.1
9	0.6	9	1	3.999	0.196	3.903	2.15	5.96	4.1	0.64	50.7

INPUT											OUTPUT
Wall Geometry				IM							
H (m)	Sv (m)	L (m)	L/H	PGA (m/s2)	PGV (m/s)	Aeff (m/s2)	Ia (m/s)	CAV (m/s)	ASI (m/s)	VSI (m)	Displacement (cm)
9	0.8	6.3	0.7	3.999	0.196	3.903	2.15	5.96	4.1	0.64	63.9
9	0.8	9	1	3.999	0.196	3.903	2.15	5.96	4.1	0.64	56.3
9	0.4	6.3	0.7	5.930	0.288	5.882	4.51	8.48	6.04	0.95	59.5
9	0.4	9	1	5.930	0.288	5.882	4.51	8.48	6.04	0.95	52.9
9	0.6	6.3	0.7	5.930	0.288	5.882	4.51	8.48	6.04	0.95	66
9	0.6	9	1	5.930	0.288	5.882	4.51	8.48	6.04	0.95	59.8
9	0.8	6.3	0.7	5.930	0.288	5.882	4.51	8.48	6.04	0.95	71.7
9	0.8	9	1	5.930	0.288	5.882	4.51	8.48	6.04	0.95	66.9

APPENDIX B: FEA RESULTS FOR ANN CLASSIFICATION MODEL

Table B.1. Appendix B

INPUT				OUTPUT
A	B	C	D	E
H (m)	Sv (m)	L/H	PGA (m/s2)	Deformation level
5	0.2	2	1.977	L
5	0.2	1.8	1.977	L
5	0.2	1.6	1.977	L
5	0.2	1.4	1.977	L
5	0.2	2	3.999	L
5	0.4	2	1.977	L
5	0.2	1.2	1.977	L
5	0.4	1.8	1.977	L
5	0.2	1.8	3.999	L
5	0.2	1	1.977	L
5	0.4	1.6	1.977	L
5	0.2	0.9	1.977	L
5	0.4	1.4	1.977	L
5	0.6	2	1.977	L
5	0.6	1.8	1.977	L
5	0.2	1.6	3.999	L
5	0.2	0.8	1.977	L
5	0.2	2	5.930	L
5	0.4	1.2	1.977	L
5	0.6	1.6	1.977	L
5	0.2	1.4	3.999	L
5	0.2	1.8	5.930	L
5	0.2	0.7	1.977	L
5	0.2	1.2	3.999	L
5	0.6	1.4	1.977	L
5	0.4	1	1.977	L

INPUT				OUTPUT
A	**B**	**C**	**D**	**E**
H (m)	**Sv (m)**	**L/H**	**PGA (m/s2)**	**Deformation level**
5	0.2	1.6	5.930	L
5	0.2	1	3.999	L
5	0.2	1.4	5.930	M
5	0.2	0.9	3.999	M
5	0.2	1.2	5.930	M
5	0.6	1.2	1.977	M
5	0.4	0.9	1.977	M
5	0.4	2	3.999	M
5	0.2	0.6	1.977	M
5	0.4	1.6	3.999	M
5	0.4	1.8	3.999	M
5	0.2	1	5.930	M
5	0.4	1.4	3.999	M
5	0.2	0.9	5.930	M
5	0.2	0.8	3.999	M
5	0.4	0.8	1.977	M
5	0.6	1	1.977	M
5	0.2	0.5	1.977	M
5	0.6	2	3.999	M
5	0.2	0.8	5.930	M
5	0.6	1.8	3.999	M
5	0.4	1.2	3.999	M
5	0.2	0.7	3.999	M
5	0.6	0.7	1.977	M
5	0.6	0.8	1.977	M
5	0.6	0.9	1.977	M
5	0.4	0.7	1.977	M
5	0.6	1.6	3.999	M
5	0.4	0.6	1.977	M
5	0.4	1.6	5.930	M
5	0.4	1.8	5.930	M
5	0.4	2	5.930	M
5	0.2	0.7	5.930	M
5	0.4	1.4	5.930	M
5	0.6	0.6	1.977	M
5	0.4	0.5	1.977	M
5	0.6	0.5	1.977	M
5	0.6	1.4	3.999	M
5	0.2	0.6	3.999	M
5	0.4	1	3.999	M
5	0.4	1.2	5.930	M
5	0.6	2	5.930	M
5	0.2	0.6	5.930	M

INPUT				OUTPUT
A	**B**	**C**	**D**	**E**
H (m)	**Sv (m)**	**L/H**	**PGA (m/s2)**	**Deformation level**
5	0.4	0.9	3.999	M
5	0.6	1.8	5.930	M
5	0.6	1.6	5.930	M
5	0.6	1.2	3.999	M
5	0.2	0.5	3.999	M
5	0.4	0.8	3.999	M
5	0.4	1	5.930	M
5	0.6	1	3.999	M
5	0.6	1.4	5.930	M
5	0.4	0.7	3.999	M
5	0.6	0.9	3.999	M
5	0.4	0.9	5.930	M
5	0.6	0.8	3.999	M
5	0.2	0.5	5.930	M
5	0.6	0.7	3.999	M
5	0.4	0.6	3.999	M
5	0.4	0.5	3.999	M
5	0.6	0.6	3.999	M
5	0.6	1.2	5.930	M
5	0.4	0.8	5.930	M
5	0.6	1	5.930	M
5	0.4	0.7	5.930	M
5	0.6	0.9	5.930	M
5	0.6	0.5	3.999	M
5	0.6	0.8	5.930	M
5	0.4	0.6	5.930	M
5	0.6	0.7	5.930	M
5	0.4	0.5	5.930	M
5	0.6	0.6	5.930	M
5	0.6	0.5	5.930	M
6	0.2	2	1.977	L
6	0.2	1.8	1.977	L
6	0.2	1.6	1.977	L
6	0.2	1.4	1.977	L
6	0.4	2	1.977	L
6	0.4	1.8	1.977	L
6	0.2	1.2	1.977	L
6	0.4	1.6	1.977	L
6	0.2	2	3.999	L
6	0.6	2	1.977	L
6	0.2	1.8	3.999	L
6	0.4	1.4	1.977	L
6	0.6	1.8	1.977	L

INPUT				OUTPUT
A	**B**	**C**	**D**	**E**
H (m)	**Sv (m)**	**L/H**	**PGA (m/s2)**	**Deformation level**
6	0.2	1	1.977	L
6	0.2	1.6	3.999	L
6	0.2	2	5.930	L
6	0.6	1.6	1.977	L
6	0.2	1.8	5.930	L
6	0.2	0.9	1.977	L
6	0.4	1.2	1.977	L
6	0.2	1.4	3.999	L
6	0.2	1.6	5.930	L
6	0.6	1.4	1.977	L
6	0.2	1.2	3.999	M
6	0.4	2	3.999	M
6	0.2	0.8	1.977	M
6	0.4	1	1.977	M
6	0.2	1.4	5.930	M
6	0.6	1.2	1.977	M
6	0.4	1.8	3.999	M
6	0.2	0.7	1.977	M
6	0.4	0.9	1.977	M
6	0.4	1.6	3.999	M
6	0.2	1	3.999	M
6	0.2	1.2	5.930	M
6	0.2	0.6	1.977	M
6	0.6	1	1.977	M
6	0.2	0.9	3.999	M
6	0.4	0.8	1.977	M
6	0.4	2	5.930	M
6	0.4	1.4	3.999	M
6	0.6	0.9	1.977	M
6	0.6	2	3.999	M
6	0.2	0.5	1.977	M
6	0.4	0.7	1.977	M
6	0.2	0.8	3.999	M
6	0.2	1	5.930	M
6	0.4	1.8	5.930	M
6	0.6	0.8	1.977	M
6	0.6	1.8	3.999	M
6	0.4	1.2	3.999	M
6	0.4	0.6	1.977	M
6	0.4	1.6	5.930	M
6	0.2	0.7	3.999	M
6	0.2	0.9	5.930	M
6	0.6	0.7	1.977	M
6	0.6	1.6	3.999	M

INPUT				OUTPUT
A	**B**	**C**	**D**	**E**
H (m)	**Sv (m)**	**L/H**	**PGA (m/s2)**	**Deformation level**
6	0.6	0.6	1.977	M
6	0.4	0.5	1.977	M
6	0.6	0.5	1.977	M
6	0.4	1	3.999	M
6	0.2	0.8	5.930	M
6	0.4	1.4	5.930	M
6	0.2	0.6	3.999	M
6	0.6	1.4	3.999	H
6	0.4	0.9	3.999	H
6	0.6	2	5.930	H
6	0.6	1.8	5.930	H
6	0.2	0.5	3.999	H
6	0.6	1.2	3.999	H
6	0.4	1.2	5.930	H
6	0.4	0.8	3.999	H
6	0.6	1.6	5.930	H
6	0.2	0.7	5.930	H
6	0.4	0.7	3.999	H
6	0.4	1	5.930	H
6	0.6	1	3.999	H
6	0.2	0.6	5.930	H
6	0.6	0.9	3.999	H
6	0.6	0.8	3.999	H
6	0.4	0.9	5.930	H
6	0.6	1.4	5.930	H
6	0.6	0.7	3.999	H
6	0.4	0.6	3.999	H
6	0.4	0.8	5.930	H
6	0.6	1.2	5.930	H
6	0.4	0.7	5.930	H
6	0.2	0.5	5.930	H
6	0.4	0.5	3.999	H
6	0.4	0.6	5.930	H
6	0.6	1	5.930	H
6	0.6	0.6	3.999	H
6	0.6	0.9	5.930	H
6	0.6	0.8	5.930	H
6	0.6	0.7	5.930	H
6	0.4	0.5	5.930	H
6	0.6	0.5	3.999	H
6	0.6	0.6	5.930	H
6	0.6	0.5	5.930	H
7	0.2	1.5	1.977	L
7	0.4	1.5	1.977	L
7	0.2	1	1.977	L

INPUT				OUTPUT
A	**B**	**C**	**D**	**E**
H (m)	**Sv (m)**	**L/H**	**PGA (m/s2)**	**Deformation level**
7	0.6	1.5	1.977	L
7	0.4	1	1.977	L
7	0.8	1.5	1.977	L
7	0.2	0.7	1.977	M
7	0.6	1	1.977	M
7	0.8	1	1.977	M
7	0.4	1.5	3.999	M
7	0.4	0.7	1.977	M
7	0.2	1.5	3.999	M
7	0.6	0.7	1.977	M
7	0.2	1	3.999	M
7	0.8	0.7	1.977	M
7	0.6	1.5	3.999	M
7	0.4	1	3.999	M
7	0.4	1.5	5.930	M
7	0.2	0.7	3.999	H
7	0.8	1.5	3.999	H
7	0.2	1.5	5.930	H
7	0.2	1	5.930	H
7	0.6	1	3.999	H
7	0.6	1.5	5.930	H
7	0.4	0.7	3.999	H
7	0.4	1	5.930	H
7	0.8	1	3.999	H
7	0.2	0.7	5.930	H
7	0.8	1.5	5.930	H
7	0.6	0.7	3.999	H
7	0.4	0.7	5.930	H
7	0.6	1	5.930	H
7	0.8	0.7	3.999	H
7	0.8	1	5.930	H
7	0.6	0.7	5.930	H
7	0.8	0.7	5.930	H
8	0.2	1	1.977	L
8	0.4	1	1.977	L
8	0.2	0.7	1.977	M
8	0.6	1	1.977	M
8	0.4	0.7	1.977	M
8	0.8	1	1.977	M
8	0.6	0.7	1.977	M
8	0.8	0.7	1.977	M
8	0.2	1	3.999	M
8	0.2	1	5.930	M
8	0.4	1	3.999	H

INPUT				OUTPUT
A	**B**	**C**	**D**	**E**
H (m)	**Sv (m)**	**L/H**	**PGA (m/s2)**	**Deformation level**
8	0.2	0.7	3.999	H
8	0.6	1	3.999	H
8	0.4	0.7	3.999	H
8	0.8	1	3.999	H
8	0.2	0.7	5.930	H
8	0.6	0.7	3.999	H
8	0.4	1	5.930	H
8	0.8	0.7	3.999	H
8	0.4	0.7	5.930	H
8	0.6	1	5.930	H
8	0.6	0.7	5.930	H
8	0.8	1	5.930	H
8	0.8	0.7	5.930	H
9	0.4	1	1.977	L
9	0.6	1	1.977	L
9	0.8	1	1.977	M
9	0.4	0.7	1.977	M
9	0.6	0.7	1.977	M
9	0.8	0.7	1.977	M
9	0.4	1	3.999	M
9	0.6	1	3.999	H
9	0.4	1	5.930	H
9	0.4	0.7	3.999	H
9	0.8	1	3.999	H
9	0.4	0.7	5.930	H
9	0.6	1	5.930	H
9	0.6	0.7	3.999	H
9	0.8	0.7	3.999	H
9	0.6	0.7	5.930	H
9	0.8	1	5.930	H
9	0.8	0.7	5.930	H